UNIVERSIDADE DE LISBOA

FACULDADE DE MEDICINA

Characterization of glycinergic transmission in an *in vitro* model of Epilepsy

Catarina Pais Gomes Luís

MSc Neuroscience

Lisboa, 2012

UNIVERSIDADE DE LISBOA

FACULDADE DE MEDICINA

Master Thesis

Characterization of glycinergic transmission in an *in vitro* model of Epilepsy

Catarina Pais Gomes Luís

Supervisor:
Cláudia Valente de Castro, PhD (IMM/FMUL)

MSc Neuroscience

Lisboa, 2012

Esta dissertação foi aprovada pelo Conselho Científico da Faculdade de Medicina da Universidade de Lisboa em reunião de 17/07/2012.

O trabalho experimental constante da presente tese foi realizado no Instituto de Farmacologia e Neurociências, Faculdade de Medicina e Unidade de Neurociências, Instituto de Medicina Molecular, sob orientação da Drª Cláudia Valente de Castro, PhD.

The experimental work contained in this thesis was performed at the Institute of Pharmacology and Neuroscience, Faculty of Medicine and Unit of Neurosciences, Institute of Molecular Medicine, under the supervision of Dr. Cláudia Valente de Castro, PhD.

Para os meus avós,

Resumo

A epilepsia consiste numa condição neurológica crónica caracterizada pela propensão prolongada para gerar ataques epilépticos. É uma das doenças do foro neurológico com maior prevalência a nível mundial, tendo não só consequências neurológicas mas também cognitivas, psicológicas e sociais. A epilepsia do lobo temporal, em particular, é um dos síndromes epilépticos mais comuns. Esta patologia afecta predominantemente uma estrutura, o hipocampo, tendo como um dos principais traços característicos a esclerose do hipocampo. Esta condição envolve morte celular de diversas subpopulações neuronais da formação hipocampal.

Os ataques epilépticos, característica primária de todos os síndromes epilépticos, constituem "um acontecimento transiente de sinais ou sintomas devido a actividade anormal excessiva ou síncrona no cérebro". A nível celular caracterizam-se por despolarizações e disparos consecutivos de potenciais de acção em grandes populações neuronais. A hiperexcitabilidade e o sincronismo são características conspícuas dos ataques epilépticos, sendo que a primeira está associada a uma desregulação do balanço entre inibição e excitação na rede neuronal. Assim, muitos fármacos anticonvulsivantes actuam de forma a restaurar este balanço a fim de suprimir os ataques epilépticos e a sua propagação.

O principal neurotransmissor inibitório no cérebro, GABA (ácido γ-aminobutírico), é um dos principais alvos farmacológicos dos compostos anticonvulsivantes. Um dos mecanismos primários de acção destes fármacos assenta na potenciação da transmissão GABAérgica, que se sabe estar alterada em situações de epilepsia.

Apesar da eficácia comprovada destes compostos no tratamento de síndromes epilépticos humanos, estes também provocam efeitos secundários adversos, como sonolência, tonturas, descoordenação motora e alteração da memória a curto prazo. O uso crónico pode, em alguns casos (e.g. benzodiazepinas), causar tolerância e dependência. Acima de tudo, 20 a 25% dos doentes são refratários à terapêutica tornando a procura e o desenvolvimento de novas estratégias e alvos terapêuticos essencial e imperativa no contexto do tratamento da epilepsia.

A glicina é o principal neurotransmissor inibitório na espinal medula e no tronco cerebral, tendo sido identificado pela primeira vez há cerca de 50 anos. A glicina exerce a sua acção inibitória através dos receptores da glicina (GlyR). Estes são canais pentaméricos de cloro, ião cuja entrada provoca a hiperpolarização da membrana neuronal, diminuindo a probabilidade de disparo de potenciais de acção. O mecanismo de recaptação exercido pelos transportadores da glicina 1 e 2 (GlyT1 e 2) permite a finalização das acções inibitórias mediadas pela glicina. Apenas recentemente o papel da glicina no cérebro tem sido alvo de estudos mais aprofundados. Estes revelam a presença de receptores da glicina funcionais no hipocampo, com uma localização

preferencialmente extrasináptica. Registos electrofisiológicos comprovam que a transmissão glicinérgica no hipocampo é responsável principalmente por inibição tónica.

Os efeitos anticonvulsivantes mediados pelos receptores da glicina são conhecidos desde a década de 1980. Em particular, a administração de agonistas dos receptores da glicina, tais como a glicina e a taurina, provoca uma diminuição da hyperexcitabilidade, não só em preparações *in vitro* mas também em modelos animais.

O presente estudo tem como principal objectivo a caracterização do padrão de expressão de marcadores da transmissão glicinérgica num modelo *in vitro* de epilepsia. Para tal recorreu-se a um modelo *in vitro* de actividade epileptiforme em fatias combinadas de hipocampo-cortex entorrinal. A omissão de magnésio da solução encéfalo-raquidiana artificial provoca o aparecimento de diferentes tipos de actividade epileptiforme. Esta actividade depende essencialmente da remoção do bloqueio do magnésio nos receptores NMDA. As descargas de alta frequência e curta duração, denominadas *late recurrent discharges* (LRDs), são registadas no córtex entorrinal, e têm como principal particularidade o facto de serem resistentes aos anticonvulsivantes convencionais. Fatias que apresentaram este tipo de actividade foram recolhidas e utilizadas para análise por PCR quantitativo e por *western blot*, para avaliação da expressão de RNA mensageiro (mRNA) e de proteína, respectivamente.

A análise da expressão relativa dos transcritos das subunidades do receptor da glicina revelou um aumento das subunidades GlyR α2 e α3 associado à ocorrência de descargas epilépticas. Este padrão transcricional foi descrito em doentes com epilepsia do lobo temporal. Uma diminuição do transcrito do transportador da glicina 2 (GlyT2) foi igualmente observada, sendo que mutações no gene deste transportador estão descritas em patologias associadas a hiperexcitabilidade.

Por outro lado, foram detectadas alterações relativas a marcadores da transmissão excitatória, nomeadamente na subunidade NR1 dos receptores NMDA, cuja expressão se encontra diminuída em fatias com actividade LRD. Estudos realizados em hipocampos removidos cirurgicamente a doentes com epilepsia do lobo temporal, com esclerose hipocampal, revelaram igualmente níveis reduzidos do mRNA desta subunidade.

Assim sendo, algumas das características patofisiológicas encontradas em modelos crónicos de epilepsia são mimetizadas neste modelo em fatias agudas. É então possível inferir que os mecanismos responsáveis pela ocorrência e propagação de actividade epileptiforme *in vitro* podem, em parte, ser idênticos. Daí decorre a relevância prática e biológica do modelo explorado neste trabalho e que constitui seguramente uma ferramenta indispensável na compreensão da função da transmissão glicinérgica no hipocampo, tanto em condições fisiológicas como patológicas.

Tarefas futuras incluem o estudo da localização subcelular dos marcadores da transmissão glicinérgica, bem como a avaliação de marcadores de actividade epileptiforme (*epilepsy hallmarks*), através de imuno-histoquímica.

Palavras-chave: Epilepsia, glicina, transmissão glicinérgica, fatias combinadas de hipocampo-cortex entorrinal, actividade epileptiforme.

Abstract

Epilepsy is one of the most prevalent neurologic disorders worldwide. The International League Against Epilepsy (ILAE) defines epilepsy as "a chronic condition of the brain characterized by an enduring propensity to generate epileptic seizures, and by the neurobiological, cognitive, psychological, and social consequences". At the cellular level seizures are characterised by synchronous and paroxymal depolarisations and fire burst of action potentials in large neuronal populations. Despite the numerous antiepileptic drugs (AEDs) available, 20-25% of patients are still refractory to these therapies encouraging the research of novel pharmacological approaches. Glycine is the primary inhibitory neurotransmitter in spinal cord and brainstem, acting on strychnine-sensitive chloride channels, glycine receptors (GlyR). Glycine has been shown to decrease hyperexcitability in the hippocampus and taurine, a GlyR agonist, to significantly depress epileptiform activity *in vitro.*

The present study aims to characterize the expression pattern of glycinergic transmission markers associated with the onset of epileptiform activity in an *in vitro* model of epileptiform activity induced by lowering extracellular [Mg^{2+}].

The model was established in hippocampus-entorhinal cortex (Hip-EC) combined slices obtained from 5-7 weeks-old Wistar rats. Electrophysiological recordings showed that late recurrent discharges (LRDs) developed after 2h-exposure to free Mg^{2+} artificial cerebrospinal fluid in the medial EC with a frequency of 14 ± 3 *per* min. Hip-EC slices were subsequently used for molecular-based approaches, namely western blot and quantitative real-time PCR (qPCR). Western blot analysis of inhibitory transmission-related markers showed a slight increase in $GABA_A$ receptor β2 and β3 subunits and GlyR α2 subunit. qPCR revealed that GlyR α2 and α3 transcripts increase in the epileptiform activity-induced conditions. This pattern has been reported in temporal lobe epilepsy (TLE) patients. These data suggest that this model mimics *in vivo* TLE*,* making it a useful experimental tool to investigate the molecular mechanisms underlying epileptic disorders. Evidence further indicates that a compensatory mechanism might occur during epileptiform activity involving glycinergic transmission effectors.

Keywords: Epilepsy, glycine, glycinergic transmission, hippocampus-entorhinal cortex combined slices, late recurrent discharges.

Table of Contents

Figure index

Table index

List of abbreviations

ACSF	Artificial cerebrospinal fluid
AE	Acquired epilepsy
AEDs	Antiepileptic drugs
AMPA	α-amino-3-hydroxy-5-methyl-4-isoxazol-propionic acid
APS	Ammonium persulfate
BSA	Bovine serum albumin
CA	Cornu ammonis
cDNA	Complementary DNA
CNS	Central nervous system
DAPI	4'-6-diamidino-2-phenylindole
DG	Dentate gyrus
DIC	Days in culture
DMEM	Dulbecco's modified eagle medium
DNA	Deoxyribonucleic acid
dNTP	Deoxyribonucleotide thriphosphate
DTT	Dithiothreitol
e.g.	*exempli gratia*
E17-E18	Embrionic 17-18 day old rat
EDTA	Ethylenediamine tetraacetic acid
EEG	Electroencephalogram
EPSC	Excitatory postsynaptic current
et al.	*et alia*
FBS	Fetal bovine serum
GABA	γ-aminobutyric acid
$GABA_AR$	$GABA_A$ receptor
GlyR	Glycine receptor
GlyT	Glycine transporter
HBSS	Hank's Buffered Salt Solution
HCL	Hydrochloride acid
HEPES	*N*-2-Hydroxyethylpiperazin-*N'*2-ethansulphonic acid
i.e.	*id est*
IHC	Immunohistochemistry
LRDs	Late recurrent discharges

MEC	Medial entorhinal cortex
MEM	Minimum essential medium
MF	Mossy fibers
Mg^{2+}	Magnesium ion
NaCl	Sodium chloride
NB	Neurobasal medium
NB-B27	Neurobasal medium supplemented with B27-Supplement
NMDA	*N*-methyl-*D*-aspartic acid
NMDAR	NMDA receptor
NP-40	Nonyl phenoxylpolyethoxylethanol
ON	Over night
P0-P3	Postnatal 0-3 day old rat
PBS	Phosphate buffered saline
PBSTw	Phosphate buffered saline with 0,1 Tween-20
PCR	Polymerase chain reaction
PDL	Poly-D-lysine
PFA	Paraformaldahyde
pSpike	Population spike
RNA	Ribonucleic acid
RT	Reverse transcriptase
RT-qPCR	Real-time, reverse transcriptase quantitative PCR
SDS	Sodium dodecyl sulfate
SDS-PAGE	SDS polyacrylamide gel electrophoresis
SE	*Status epilepticus*
SEM	Standard error of the mean
SREDs	Spontaneous recurrent epileptiform discharges
TAE	Tris-acetate-EDTA
TEMED	Tetramethylethylenediamine
TLE	Temporal lobe epilepsy
TM	Transmembrane domain
Tris	Tris-hydroxymethyl-aminomethane
U	Unit, enzyme
VIAAT	Vesicular inhibitory amino acid transporter
WHO	World Health Organization

1 INTRODUCTION

The interdisciplinary term neuroscience was introduced in the mid-1960's. It marked the beginning of a period in which "*each discipline would work together cooperatively, sharing a common language common concepts and common goal*" – to uncover the structure and understand the function of the normal and abnormal brain (Squire 2003).

The central nervous system (CNS) has been extensively studied since the first anatomists, due to its intricate structure and complex functions, which continue to mesmerize and engage researchers to this day.

1.1 Parahippocampal-hippocampal network

One the most comprehensively studied structures in the CNS is the hippocampal formation. The hippocampus has a distinctive, curved structure that has captivated the first Alexandrian anatomists, who named it cornu ammonis, due to its resemblance to the ram's horn of the Egyptian god Amun. This nomenclature still persists in the hippocampal subfields CA1 (cornu ammonis), CA2, and CA3. Though, it was not until the middle 1500s that Giulio Cesare Aranzi first suggested the term hippocampus after the iconic marine teleost, the seahorse (Andersen, et al. 2007).

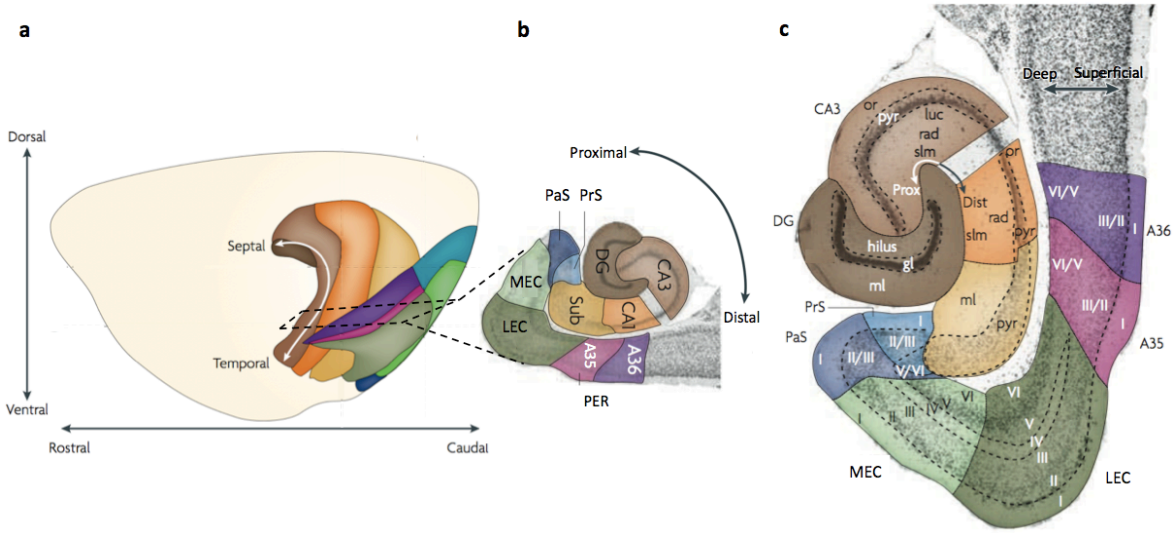

Figure 1 Schematic representation of the overall organization of the entorhinal cortex and its connectivity. (a) Position of the entorhinal cortex and surrounding cortices and hippocampus in the rat left hemisphere. The hippocampal formation consists of the dentate gyrus (DG; dark brown), CA3 (medium brown), CA2 (not indicated), CA1 (orange) and the subiculum (Sub; yellow). The parahippocampal region includes the entorhinal cortex, which has a lateral (LEC; dark green) and a medial (MEC; light green) area, postrhinal cortex (POR; blue-green) and perirhinal cortex (PER - Brodmann areas A35 in pink and A36 in purple). The dashed lines indicate a horizontal section illustrate in b. (b) Horizontal section illustrating hippocampal-parahippcampal anatomical organization. Additionally, detail of the

presubiculum (PrS; medium blue) and parasubiculum (PaS; dark blue). (c) A Nissl-stained horizontal enlarged of (b) in which the cortical layers and three-dimensional axes are represented. The Roman numerals indicate cortical layers. DG - dentate gyrus; gl - granule cell layer; luc - stratum lucidum; ml - molecular layer; or, stratum oriens; CA - cornu ammonis; pyr - pyramidal cell layer; rad - stratum radiatum; slm - stratum lacunosum-moleculare; (Adapted from van Strien, et al.2009, Canto, et al. 2008).

The hippocampal formation, which is situated in the caudal part of the brain (**Figure 1**a), is formed by two C- shaped interlocking cell layers: the granular cell layer of the dentate gyrus (DG) and the pyramidal cell layer of the hippocampus proper (or CA) and the Subiculum (reviewed in Lopes da Silva, et al. 1990), as shown in **Figure 1**b.

According to Ramón y Cajal (1909), the hippocampus proper is subdivided into CA1, CA2 and CA3 areas, which can be structured depthwise, in seven clearly defined layers or strata (**Figure 1**c): *stratum moleculare; stratum lacunosum; stratum radiatum; stratum pyramidale* (the principal cell layer); *stratum oriens; alveus* and *epithelium*. In the dentate gyrus three layers are typically considered: *stratum moleculare; stratum granulosum* (principal cell layer) and *stratum* polymorphum (or CA4 area or hilar region) (Lopes da Silva, et al. 1990).

Of all the components of the limbic cortex, the entorhinal cortex (EC) gives rise to the most prominent input to the hippocampus. The EC is most frequently divided, on the basis of cytoarchitectonic criteria, into a lateral and medial area (MEC and LEC) – Brodmann's areas 28a and 28b respectively (Canto, et al. 2008). The EC, like the presubiculum and parasubiculum, is characterized by the presence of a marked cell-sparse layer, or lamina dissecans, which results in a more or less clearcut separation of superficial layers I, II, and III from deeper positioned layers V and VI (Witter, et al. 2000) – see in detail in **Figure 1**c.

The EC-Hippocampus circuitry, known as the perforant pathway, constitutes a loop, in which most external input originates from the entorhinal cortex. Entorhinal layer II projects to the DG and to the *stratum lacunosum-moleculare* of CA3 and CA2, whereas layer III of both MEC and LEC projects to CA1 and the subiculum. The polysynaptic pathway is an extended version of the traditional trisynaptic pathway (Andersen, et al. 1971b), which describes a unidirectional route that connects all subregions of the hippocampus sequentially (van Strien, et al. 2009). Briefly, the DG granule cells' efferent fibers send information through the mossy fibre pathway, which targets CA3. The CA3 Schaffer collaterals project to CA1 and, lastly, CA1 projects to the Subiculum. Output from the hippocampus arises in CA1 and the subiculum and is directed to the parahippocampal formation, in particular to the deep layers of the EC (Lopes da Silva, et al. 1990).

Besides the essential trisynaptic glutamatergic circuit initially described by Andersen and colleagues (1971), the hippocampus proper comprises also several local inhibitory circuits, mediated by different kinds of GABAergic interneurons. These are concentrated around the soma

and axonal initial segment of many neurons, although can also be found on dendrites, and exert a prominent regulation of overall excitability, despite representing less than 10% of the neuronal hippocampal population (Freund and Buzsáki 1996, Anderson, et al. 2007).

Entorhinal fibers, as described above, synapse most often onto the dendrites of principal cells, where they form asymmetrical, excitatory synapses. But also terminate on inhibitory interneurons, forming both putative excitatory as well as inhibitory synapses with the dendrites of these interneurons (Canto, et al. 2008).

In addition to the topology along the transverse axis, the hippocampal formation shows a topographical organization along the longitudinal axis, so that a lateral-to-medial gradient in the EC corresponds to a septal-to-temporal gradient in the hippocampal formation. As so, the dorsolateral parts of the LEC and the MEC project to the septal hippocampus, the intermediate part of the EC projects to intermediate septotemporal levels, and the ventromedial EC projects to the temporal hippocampal formation (see Witter, et al. 2000, van Strien, et al. 2009).

This complex three-dimensional matrix, along with the intrinsic connectivity of the EC, points to the role of the EC as more than an input and an output interface station mediating cortico-hippocampal interplay. It has rather an "online monitor" function, able to differentiate incoming stimulus and coordinate them with the net outcome of hippocampal processing (Witter, et al. 2000).

For the past decades, the parahippocampal-hippocampal network has been implicated in various disorders, such as epilepsy, since the hippocampus is a very seizure-prone structure, due to its inherent circuitry and physiology.

1.2 Epilepsy

Epilepsy is one of the earliest recognized disorders in medicine, mistakenly considered a "sacred disease", it was first identified as a brain syndrome by Aristotle in 400 BC.

It is one of the most prevalent neurologic disorders worldwide. According to World Health Organization (WHO), epilepsy affects 50 million people and it accounts for 1% of global burden of disease, comparable to breast cancer in woman and lung cancer in man (Engel, et al. 2008; World Health Organization, 2009). The risk of epilepsy from birth through age 20 is 1% and reaches 3% by age 75 (Browne and Holmes 2003). In Europe the prevalence of epilepsy per 1000 population is 8.23 (World Health Organization 2005).

Epilepsy does not refer to a singular disease, instead it includes a complex and broad symptomatology that reflects a multiplicity of causes. The International League Against Epilepsy (ILAE) defines epilepsy as "a chronic condition of the brain characterized by an enduring

propensity to generate epileptic seizures, and by the neurobiological, cognitive, psychological, and social consequences".

Epilepsy syndromes can be classified according to the underlying etiology as idiopathic, if associated with genetic conditions without structural abnormalities, or symptomatic, which result from acquired brain disorders (e.g. trauma, CNS infection, metabolic disturbances and tumors). The term cryptogenic refers to epilepsies whose cause is unknown (Engel, et al. 2008).

A primary characteristic of epilepsy syndromes is recurrent, typically unprovoked, epileptic seizures, which can be defined as "a transient occurrence of sings and/or symptoms due to abnormal excessive or synchronous neuronal activity in the brain" (Fisher, et al. 2005). At cellular level seizures are characterized by synchronous and paroxymal depolarisations and fire burst of action potentials in large neuronal populations (Böhme and Lüddens, 2001).

Seizures are broadly classified into two major categories (see **Table 1**), partial and generalized seizures, based on seizure type and EEG characteristics.

Table 1 International Classification of Epileptic Seizures

I. Partial (focal, local) seizures
A. Simple partial seizures
1. With motor signs
2. With somatosensory or special sensory symptoms
3. With autonomic symptoms or signs
4. With psychic symptoms
B. Complex partial seizures
1. Simple partial onset followed by impairment of consciousness
2. With impairment of consciousness at onset
C. Partial seizures evolving to secondarily generalized seizures
1. Simple partial seizures evolving to generalized seizures
2. Complex partial seizures evolving to generalized seizures
3. Simple partial seizures evolving to complex partial seizures evolving to generalized seizures
II. Generalized seizures (convulsive or nonconvulsive)
A. Absence seizures
1. Typical absences
2. Atypical absences
B. Myoclonic seizures
C. Clonic seizures
D. Tonic seizures
E. Tonic-clonic seizures
F. Atonic seizures (astatic seizures)
III. Unclassified epileptic seizures

(Commission on Classification and Terminology of the International League Against Epilepsy 1981)

Partial seizures involve focal neuronal activation, restricted to a part or one brain hemisphere. In generalized seizures both hemispheres are involved in seizure propagation. Tonic-clonic seizures are a type of generalized seizure characterized by sustained muscular contraction (tonic phase) followed by relaxation (clonic phase).

Seizures are usually spontaneous short-lived events, and as such do not regularly cause brain damage. However if a seizure progresses in duration to more than 30 min, or to multiple seizures without regained consciousness, it is defined as *status epilepticus* (SE) (DeLorenzo, et al. 2005). The ILAE describes SE as a seizure that "persists for a sufficient length of time or is repeated frequently enough that recovery between attacks does not occur" (Engel, et al. 2008).

1.2.1 Temporal Lobe Epilepsy

Temporal lobe epilepsy (TLE) is the most common form of human partial epilepsy. The hallmark pathological lesion of TLE is sclerosis, which is found in 60% to 70% of patients with intractable TLE (Babb and Pretorius 1993, Engel 1996). A typical hippocampal sclerosis, of one or both mesial temporal lobes, consists of hippocampal atrophy involving an extensive loss of dentate hilar neurons and CA1 and CA3 pyramidal cells. Neuronal death has been also found in extrahippocampal regions, particularly in the amygdala and enthorhinal cortex (Kälviäinen and Salmenperä 2002; Sharma, et al. 2007).

Deregulation of the excitation/inhibition balance critically affects hippocampal network activity, and loss of both excitatory glutamatergic (granule and pyramidal cells) and inhibitory GABAergic neurons has been reported in TLE (Pitkänen and Sutula 2002).

The glutamate, which is the main excitatory neurotransmitter in the hippocampus, acts upon the ionotrophic glutamate receptors: Kainate, AMPA and NMDA receptors. Kainate and AMPA receptors are responsible for fast depolarization of neurons by allowing influx of monovalent cations (Na^+ and K^+), whereas NMDAR causes a slower depolarization by allowing influx of divalent cations, primarily Ca^{2+} (reviewed in Platt 2007). One perspective on cellular mechanisms underlying TLE states that the glutamate-mediated hyperexcitability of dentate granule cells results from aberrant mossy fiber (MF) sprouting – recurrent excitation hypothesis. MF sprouting cause axons of dentate granule cells to reinnervate their own dendrites, forming abnormal hyperexcitable recurrent loops. Indeed, this pathophysiological feature has been reported in both human (Sutula, et al. 1989) and animal models (reviewed in White 2002).

The neuronal loss caused by repeated seizures involves hippocampal GABAergic interneurons as well, contributing to the reduced inhibition (Sayin, et al. 2003). This evidence is in accordance with the recurrent inhibition hypothesis (Sharma, et al. 2007).

Gamma amino butyric acid (GABA), the major inhibitory neurotransmitter in the brain, exerts its inhibitory actions through two types of receptors: $GABA_A$ receptors ($GABA_AR$), a Cl^- channel, and $GABA_B$ receptors ($GABA_BR$), a G-protein-coupled metabotropic receptor. $GABA_AR$ and $GABA_BR$ mediate fast and slow inhibition, respectively (Moss and Smart 2001).

Altered expression of $GABA_AR$ subunits has been reported in kainate-induced TLE model (Poulter, et al. 2000) and human patients (Loup, et al. 2000). Interestingly a long lasting upregulation of $GABA_AR$ in the DG was reported by Fritschy and colleagues (1999) which is thought to be a predominantly compensatory phenomenon (Fritschy, et al. 1999).

Although the seizures in TLE may respond to AEDs, it typically tends to become refractory to anticonvulsant therapy. Surgical resection, such as anterior temporal lobectomy is curative in specific cases (Stafstrom 2006).

1.2.2 Experimental models of epilepsy

Validated experimental models of epilepsy are crucial research tools to gain insight into the pathophysiology of epilepsy and epileptic seizures.

It is not always feasible to study human epilepsy research in human patients due to the evident ethical limitations and prohibitive costs. Hence, *in vivo* (animal) and *in vitro* models of epileptic disorders are (and will most likely remain) indispensable to epilepsy research (Engel and Schwartzkroin 2006).

Experimental models of epilepsy are generally employed to investigate the neural mechanisms; devising new diagnostic, therapeutic, and preventative approaches; and to study putative basic mechanisms of human epilepsy (Najam, et al. 2006).

When referring models of epileptic seizures and epilepsy it is essential to distinguish between (1) models of acute epileptic seizures and (2) models of epilepsy that are associated with permanent "epileptogenic" disturbances or chronic epilepsy models (Engel and Schwartzkroin 2006).

Nowadays more than 100 seizure models are available for epilepsy research, however only some develop epilepsy. Brain electrical stimulation (Swinyard 1972) and systemic injections of chemoconvulsants, namely kainate (Ben-Ari 1985) or pilocarpine (Turski, et al. 1983), lead to a state of chronic spontaneous recurrent seizures (i.e. epilepsy).

These animal models mimic several neuropathological features of clinical TLE, as so they can be considered, to some extent, mirrors of human TLE (reviewed in Engel and Schwartzkroin 2006).

Acute seizure models, on the other hand, are suitable for the study of the cellular and molecular bases of seizure activity, namely alterations in intrinsic properties of neurons, inhibition/excitation balance, and changes in the extracellular *milieu. In vitro* models of seizure are particularly appealing due to its simplicity, easy preparation and manipulation. By using this

type of experimental models it is possible to apply a variety of methods that would, otherwise, be difficult to employ under *in vivo* conditions (Heinemann, et al. 2006).

Acute *in vitro* models of epileptic seizures do not feature the behaviour or motor symptoms of clinical seizures, but rather depend on "equivalents" of seizures. These ought to fulfill criteria, concerning electrographic features and changes in ionic concentration, in order to be comparable to seizures reported in animal and human research.

1.2.2.1 *In vitro*: Free Mg^{2+}-induced epileptiform activity

The model of free Mg^{2+}-induced epileptiform activity relies on the removal of the Mg^{2+} block of excitatory NMDAR, which then can be readily activated by glutamate. Induction of this activity also depends on increased neuronal excitability resulting from reduced surface charge screening and facilitated transmitter release (Mody, et al. 1987). This model has been applied in both cell culture and brain slice studies.

DeLorenzo and colleagues developed a cell culture model of epilepsy through exploring the enhanced synchrony achieved by free magnesium exposure (Sombati and DeLorenzo 1995).

When hippocampal cultures, plated on 2-week-old astrocyte feeder layer, are maintained in the absence of Mg^{2+} for 3 hours neurons develop a continuous synchronous firing pattern reminiscent of a SE (Mangan and Kapur 2004; DeLorenzo, et al. 2005). Moreover, by returning the cultures to the original medium, the surviving neurons display spontaneous recurrent epileptiform discharges (SREDs), which persist throughout the culture's life. This was dubbed Acquired Epilepsy (AE) model (DeLorenzo, et al. 1998). While being conscious that neuronal cultures are an oversimplified model, since they lack anatomical connections and do not exhibit clinical seizures, this approach has been a valuable tool to investigate biochemical, electrophysiological and molecular mechanisms underlying SE and epilepsy (Deshpande, et al. 2007).

A more complex and physiological model is the brain slice, introduced by Henry McIlwain in the 1950's (reviewed in Collingridge 1995).

In particular, the expanded hippocampal slice that preserves the interconnectivity between the hippocampus and parahippocampal areas, such as the EC and temporal cortex area, the perirhinal cortex (Dreier and Heinemann 1991). Decreasing the extracellular concentration of Mg^{2+} in the combined Hippocampus-EC slice induces aspects of epileptogenesis observed *in vivo*, including tonic-clonic discharges, named seizure-like events (SLEs). These can be recorded from the medial EC and usually involve large elevations of extracellular K^+ and decreases in extracellular Ca^{2+}, Na^+ and Cl^- concentrations (Dreier and Heinemann 1991), as well as alterations extracellular space (Lux, et al.1986) and pH (initial alkaotic shift followed by acidosis) — reviewed in Heinemann, et al. 2006.

SLEs are eventually replaced by late recurrent discharges (LRDs), which occur in higher frequency and are of shorter duration and have electrographic characteristics of SE. LRDs are resistant to standard AEDs (Dreier and Heinemann 1990, Zhang, et al 1995), as so it can be especially useful for the study of pharmacoresistance and the development of new antiepileptic therapeutics.

In opposition, activity from CA1 and CA3 stays constant over time, in the form of short-duration discharges that share the properties of interictal discharges - recurrent short discharges (RSDs) (Mody, et al. 1987).

1.2.3 Antiepileptic drugs

Hypersynchrony of neuronal networks and hyperexcitability are conspicuous features of a seizure. The neurotransmitter-regulated channels that mediate synaptic transmission, allow synchronization and propagation of the abnormal discharges to local and distant sites. On the other hand, hyperexcitability relates to the level of excitation required for seizure generation. The balance between excitation and inhibition controls each phase in seizure generation, propagation, and termination, either by excessive excitation, reduced inhibition, or both (Stafstrom 2006) — see section 1.2.1.

Hence, antiepileptic drugs (AEDs) attempt to restore the inhibition/excitation balance underlying the epileptic hyperexcitable state, and therefore suppress bursting, synchronization and seizure spread (Czapiński,et al. 2005).

There are approximately two-dozen distinct molecules commercialized worldwide for epilepsy treatment, namely for seizure prevention (Rogawski and Löscher 2004).

AEDs interact primarily with voltage-gated ion channels, such as Na^+ and Ca^{2+} channels, metabolic enzymes and neurotransmitter receptors and transporters in the brain.

One key mechanism of AEDs action is the potentiation of inhibitory neurotransmission. The GABAergic system has long been implicated in epilepsy, evidenced by a change in GABAergic function in epileptic patients as well as in animal models of epilepsy, and by the observation that some antiepileptic drugs increase GABA levels in the central nervous system (CNS) (Böhme and Lüddens, 2001).

Benzodiazepines and barbiturates potentiate the inhibitory effect of GABA by acting upon postsynaptic $GABA_AR$. Likewise GABA uptake blockers (GABA transporters inhibitors, e.g. Tiagabine) and GABA degradation blockers (GABA-transaminase inhibitors, e.g. vigabatrin) increase the GABA levels in the synaptic cleft, enhancing GABA mediated transmission (Engel, et al. 2000, Simeone 2010) — see **Figure 2**.

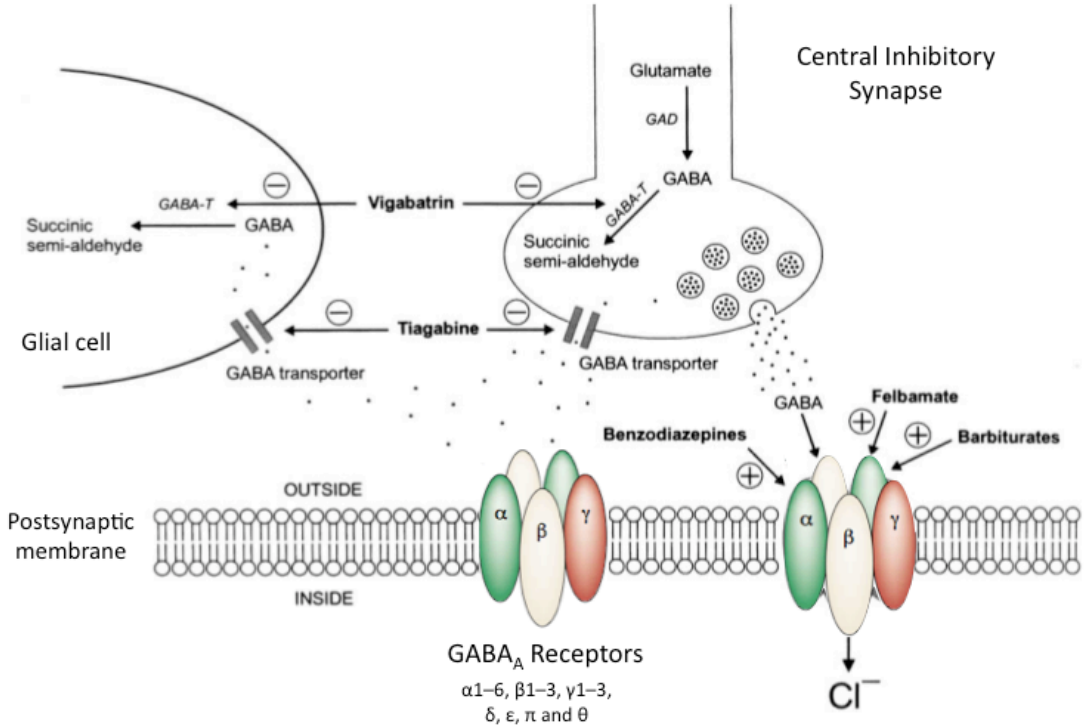

Figure 2 Schematic diagram of an inhibitory synapse in the central nervous system, and the putative major sites of actions of various antiepileptic drugs. Plus and minus signs represent activation/potentiation or inhibition, respectively. Typically $GABA_A$ receptors are composed of α, β and γ subunits in the ratio of 2:2:1. The δ, ε and θ subunits replace the γ subunit in some receptor subtypes. GABA, γ-aminobutyric acid; GABA-T, GABA transaminase; GAD, glutamic acid decarboxylase (Adapted from Rho and Sankar 1999, Moss and Smart 2001, Simeone 2010).

Although drugs that act through these mechanisms typically have a broad spectrum of antiepileptic activity in human seizure disorders, they also exert adverse effects, such as somnolence, dizziness, drowsiness, and mental slowing. Furthermore, chronic use causes, in some cases (*e.g.* benzodiazepines), tolerance and dependence. Adding to these facts, 20-25% of patients are still refractory to the existent therapy and thus the research of novel pharmacological approaches targeting inhibitory transmission towards less toxic substances is critical (Czapiński, et al. 2004).

1.3 Glycine as a neurotransmitter

Glycine is a non-essential aminoacid synthesized by animals, microorganisms and plants. It is the smallest of the 20 amino acids and the only one that is not optically active. Glycine serves as a common precursor to proteins and a biosynthetic intermediate that fulfills important physiological functions in the body.

Glycine's role as a neurotransmitter was first described when Aprison and Werman (1965), a decade after GABA's discovery, noted that glycine concentration in the spinal cord was far higher

than in the brain. Glycine levels were found to be particularly elevated in ventral horn, the location for spinal interneurons terminals, indicating that these may be the repository of stored glycine. Electrophysiological data demonstrating that glycine decreased action potential firing in spinal neurons (Curtis and Watkins 1960) and was released upon stimulation (Hopkin and Neal 1970) along with the discovery of glycine's uptake system and strychnine's antagonism of glycine receptor (Graham, et al. 1983) constituted the seminal criteria for glycine to be considered a neurotransmitter (Werman 1966).

1.3.1 Synthesis and metabolism

Glycine is the simplest aminoacid and its molecular structure is characterized by a side-chain consisting of a single hydrogen atom. It exists in equilibrium with serine, which functions as a precursor for glycine by transferring the β-carbon in its side-chain to tetrahydrofalate. This reaction is reversible and catalysed by the enzyme serine hydroxymethyl transferase (**Figure 3**).

As a classical neurotransmitter, glycine is packaged into vesicles in the presynaptic terminals by the vesicular inhibitory amino acid transporter (VIAAT). While being present at glycinergic buttons, VIAAT is also responsible, for vesicular loading of GABA, as so it can be found in all inhibitory synapses (Dumoulin, et al. 1999).

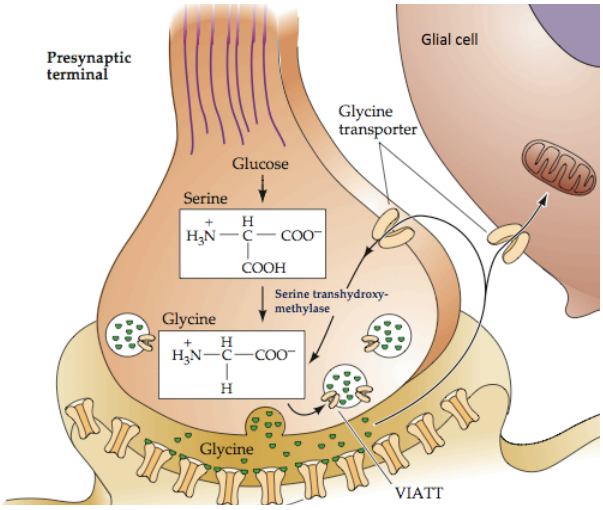

Figure 3 Synthesis, release, and reuptake of the inhibitory neurotransmitter, glycine in the presynaptic terminal. Glycine can be synthesized by a number of metabolic pathways; in the brain, the major precursor is serine which is converted into glycine in through a serine hydroxymethyl transferase (also known as serine transhydroxy-methylase) - mediated reaction. The vesicular inhibitory amino acid transporter (VIATT) loads glycine into synaptic vesicle that is released into the synaptic cleft in a calcium-dependent manner.(Purves 2004).

Upon depolarization, glycine is released from nerve terminals by calcium-dependent exocytosis, in a fusing process mediated by the synaptophysin-synaptobrevin complex.

Once released, glycine freely diffuses across the synaptic cleft to interact with its appropriate receptors on the postsynaptic membrane (reviewed in Legendre 2001). Presynaptic pools of glycine in synaptic vesicles are derived from both metabolic precursors and reuptake.

1.3.2 Glycine uptake

The removal of glycine from the synaptic cleft is ensured by two Na^+/Cl^--dependent transporters, the glycine transporters GlyT1 and GlyT2. These belong to a large protein family, which include monoamine and GABA transporters. GlyT and are composed of twelve α-helical transmembranar domains connected by six extracellular and five intracellular loops. GlyT1 and GlyT2 distinct transport stoichiometries, but both are energetically dependent to the Na^+ gradient maintained by the Na^+/K^+ ATPase (Eulenburg, et al. 2005). GlyT1 has a stoichiometry of $2Na^+/Cl^-$ per substrate molecule (i.e. glycine), whereas GlyT2 stoichiometry has been determined to be 3Na+/Cl- per glycine molecule (Roux and Supplisson 2000).

Concerning GlyT localization, GlyT1 is highly expressed in glial astrocytic cells, in the spinal cord, brain stem and cerebellum, as well as in the brain, namely in the hippocampus.

The described broad expression pattern is indicative its primary function, which is believed to be the modulation excitatory NMDAR-dependent neurotransmission, by regulation ambient levels of glycine. Accordingly, GlyT1 expression has also been reported in glutamatergic synapses (Cubelos, et al. 2005).

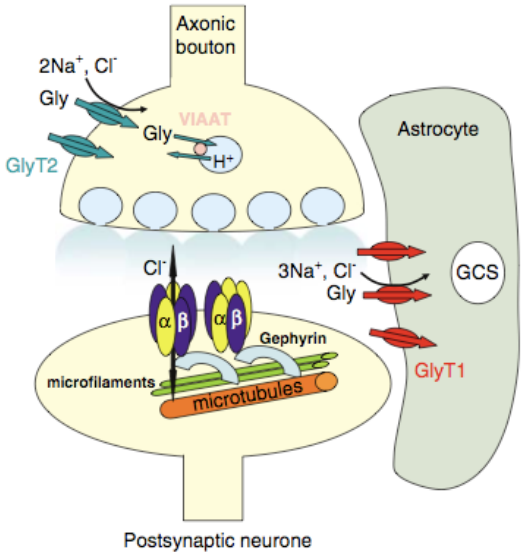

Figure 4 Schematic representation of the glycinergic synapse. Glial and neuronal glycine transporters, GlyT1 and GlyT2, sequester glycine, which can then be re-packaged into synaptic vesicles by VIAAT or hydrolyzed via the glycine cleavage system (GCS), respectively. Glycine receptors, GlyR, are shown as pentamers which interact with cytoskeleton through gephyrin (Adapted from Bowery and Smart 2006).

On the other hand, GlyT2 is present in glycinergic presynatic terminals in the brain stem and spinal cord. It is considered the main uptake mechanisms at glycinergic synapses, by sequestering glycine, which can then be repackaged and recycled into synaptic vesicles via VIAAT – see section 1.3.1 (Zafra, et al. 1995, Gomeza, et al. 2003).

GlyT2 have also been identified in hippocampal GABAergic interneurons, suggesting the co-localization of glycine and GABA. This data raises the interesting possibility that these neurons use both neurotransmitters, similar to interneurons in spinal cord, brain stem, and thalamus and golgi cells in cerebellum (Danglot, et al. 2004, Song et al., 2006).

1.3.3 Glycine receptor

Glycine inhibitory postsynaptic actions are mediated by the glycine receptor. GlyR consist of a strychnine-sensitive pentameric chloride channel, which belongs to the acetylcholine receptor superfamily.

GlyR were the first neurotransmitter receptor to be isolated from the mammalian CNS (Betz and Laube 2006) and are composed of α (α1-α 4) and β subunits (**Figure 5**b). These form heteromeric channels with a stoichiometry of 3α:2β or 2α: 3β or may exist as α-homomers (Kirsch 2006).

The β subunit binds to the postsynaptic scaffolding protein gephyrin, which is essential in synaptic anchoring of GlyRs (Moss and Smart 2001). This GlyR-gephyrin interaction is reversible and highly dynamic, therefore controlling the subcellular distribution of GlyR (Meier, et al. 2001).

GlyR's subunits share a common proposed structure (**Figure 5**a) that encompasses a large extracellular amino terminus, four transmembrane domains (TM) and a large intracellular domain between TM3 and TM4. TM2 is believed to form the lining of the ion channel (Moss and Smart 2001).

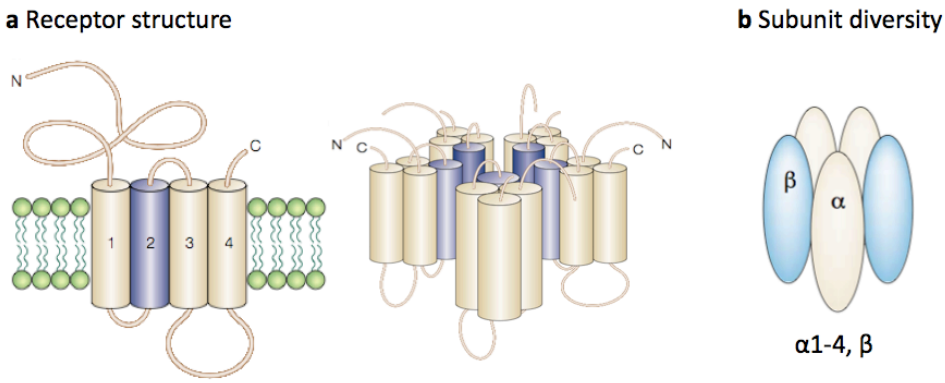

Figure 5 Structure and diversity of inhibitory GlyR. (a) Proposed structure of a ligand-gated ion channel. Receptor subunits contain four hydrophobic transmembrane (TM) domains. The large amino-terminal domain is located extracellularly and is believed to incorporate neurotransmitter and some modulator binding sites. The intracellular domain between TM3 and TM4 comprises ~10% of the mass of each subunit. (b) Proposed pentameric structure of

glycine receptor. Glycine receptors are pentamers constructed from α and β subunits in a ratio of 3α:2β (Adapted from Moss and Smart 2001).

Endogenous ligands of GlyR include glycine, β-alanine and taurine, from higher to lower affinity (Lewis, et al. 2003).

Activation of GlyR, through the recognition site at α-subunits, leads to conformational change, which causes the influx of chloride ions, producing inhibitory postsynaptic currents (IPSC). The hyperpolarization of the membrane reduces the likely wood of neuronal firing (Legendre 2001).

Interestingly, GlyR are the only members of the group I ligand-gated ion channel family that do not have a counterpart in the metabotropic receptor families (Betz and Laube 2006).

The GlyR are expressed in the entire mammalian CNS, including in forebrain regions (Hernandes and Tronco 2009), auditory system (Friauf, et al. 1997), retina (Wässle, et al. 2009) and in the hippocampus (Aroeira, et al. 2011).

1.3.4 Glycine receptor function in the hippocampus

GlyR role in brain areas, such as the hippocampus, have been given little consideration due to the fact that IPSCs are completely abolished by $GABA_AR$ antagonists (Mody, et al. 1994; Song, et al. 2006).

However, "despite previous misconceptions" (Song et al., 2006), functional GlyR were described in the hippocampus (Chattipakorn and McMahon 2002, Chattipakorn and McMahon 2003, Kirchner, et al. 2003, Song, et al. 2006).

Evidence suggests the presence of both α homomeric and αβ heteromeric GlyRs in the hippocampus (Chattipakorn and McMahon, 2003) and predominance of α2 and α3 over α1 and β subunits has been observed (Aroeira, et al. 2011). Despite glycinergic synapses have been morphologically identified in the hippocampus, no GlyR-mediated fast synaptic transmission has been recorded (Danglot, et al. 2004).

These data corroborates the extrasynaptical location of hippocampal GlyR (Mori, et al. 2002, Aroeira, et al. 2011) and reinforces the assumption that GlyR exert tonic inhibition. In fact, tonic currents mediated by GlyRs in hippocampal CA1 neurons have been recorded (Zhang, et al. 2008).

1.3.4.1 The dual role of glycine

Besides its inhibitory actions, glycine can act as a co-agonist of NMDA receptors thus increasing its affinity for glutamate. As so, glycine has an excitatory effect by binding to strychnine-insensitive glycine site at NR1 subunit of NMDAR. Although several studies point to D-serine as the endogenous co-agonist of NMDAR (Mothet, et al. 2000), extracellular glycine has been

demonstrated to enhance NMDAR function. Namely, GlyT1 blockage was proven to potentiate NMDA-dependent plasticity (Zhang, et al. 2008).

Besides glycine's role in NMDA-mediated excitation, it has also been shown that GlyR-mediated effects shape both excitatory and inhibitory synaptic transmission. Intriguingly, GlyR activation can depress not only excitation but also inhibition, through the "shunting effect" (Legendre, et al. 2009). Shunt inhibition functions as a "mechanism for gain control" (i.e. by changes in cells' input resistance) in cells with variable inputs (Mitchell and Silver 2003). Further studies also revealed a state-dependent cross-inhibition between GlyR and $GABA_AR$ in the hippocampus (Li and Xu 2002). Altogether, these raise the possibility that GlyR activation might be required for homeostatic regulation of inhibition. In the way that when there is less GABAergic inhibition, tonic GyR-mediated inhibition prevails, whereas if there too much inhibition, GlyR suppress the GABAergic transmission, thereby indirectly modulating excitation - **Figure 6** (Xu and Gong 2010).

On the other hand, GlyR tonic inhibition may control neuronal hyperexcitability not only via membrane hyperpolarization (direct effect), but through shunting and/or glycine-mediated regulation of AMPARs or NMDARs, such as receptor internalization - **Figure 6** (Nong, et al. 2003).

Therefore, hippocampal glycine and its receptors may operate as fine-tuner mechanism, acting as an effective system in homeostatic regulation of hippocampal synaptic and network plasticity in both normal and pathological conditions (Xu and Gong 2010).

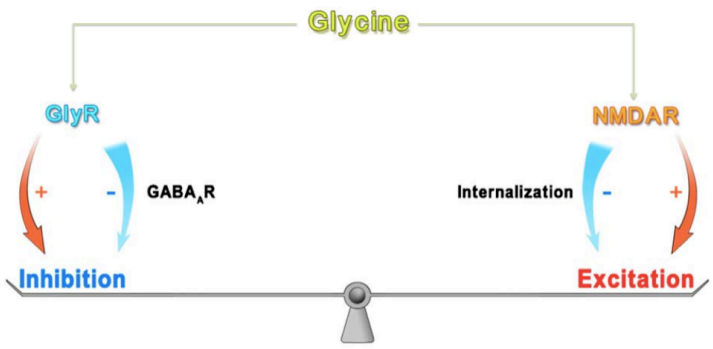

Figure 6 A proposed model for hippocampal glycine-mediated regulation. Glycine and its receptors in the hippocampus may constitute an effective regulatory system of hippocampal network activity under physiological and pathological conditions, by regulating the balance between excitation and inhibition – see text for further details. Plus and minus signs denote activation/potentiation or inhibition, respectively (Adapted from Xu and Gong 2010)

1.3.5 Glycinergic transmission in Epilepsy

For the last decades a body of evidence has grown regarding glycine's and other GlyR agonits' anticonvulsant effect. The first records date to late 1970s.

One of earliest reports demonstrates that taurine is able to decrease the occurrence of seizures in cobalt-induced model of epileptic seizures in mice (Carruthers-Jones and Gelder 1978).

Later on, Cherubini and colleagues in 1981 described that exogenous application of glycine decreases seizure activity in a rat epileptic foci induced by strychnine or penicillin. Further studies in 1984, in DBA/2 audigenic seizure mice and in MPA-induced seizures in mice, revealed that glycine potentiates the action of some anticonvulsants, such as phenobarbital, dilantin, and GlyT inhibitors (Toth and Lajtha 1984; Seiler and Sarhan 1984).

More recently, emerging evidence suggests that GlyRs mediate the antiepileptic effect of glycine. In rat dentate gyrus and area CA1 exogenous application of glycine decreases hyperexcitability via GlyR activation (Chattipakorn and McMahon, 2003) and strychnine-sensitive GlyR activation depresses synaptically generated action potentials in pyramidal cells and interneurons (Song, et al. 2006). Taurine, a GlyR agonist, has been shown to significantly depress epileptiform activity induced by Mg^{2+} removal in hippocampal CA1 neurons (Kirchner, et al. 2003). Additionally, it has been reported that α2/α3-GlyRs expression is increased in temporal lobe epilepsy patients (Eichler, et al. 2008), and that GlyR α3 subunit knockout mice have higher susceptibility to pharmacologically induced seizures (Xu and Gong 2010). These results strongly support the possibility that acting upon glycinergic transmission might exert a beneficial effect on the control of abnormal hyperexcitability associated with epileptiform activity.

2 AIM

The experimental work described in this thesis was designed to address a putative role of inhibitory glycinergic transmission in hyperexcitability conditions, as in the case of epilepsy.
In order to accomplish this general aim, three specific objectives were pursued:

I. To establish and characterize an *in vitro* model of epileptiform activity induced by lowering extracellular [Mg^{2+}];

II. To assess mRNA transcript expression of glycinergic transmission markers associated with epileptiform activity occurrence;

III. To evaluate protein expression pattern of both excitatory and inhibitory transmission mediators in control and “epileptic” conditions.

3 TECHNIQUES

3.1 Electrophysiological recordings - Field potentials

Electrophysiology is the branch of neuroscience that explores the electrical activity of single neurons and neuronal circuits, providing a window into the cellular and molecular processes that mediate electrical signaling in living cells.

The beginnings of brain electrophysiology were laid in the 1660s with development of the neuromuscular preparation of the frog leg by the Dutch microscopist and natural scientist, Jan Swammerdam. In his experiments Swammerdam induced muscle contraction upon stimulation of the nerve - "irritation" (Swammerdam 1758). Swammerdam came close to understanding the nature of signal propagation between nerves and muscles, when he used a silver wire to deliver "irritation", a setting that generates true electrical stimulation (**Figure 7**a).

However it was Isaac Newton who first grasped the electrical nature of nerve signals by proposing that "electric bodies operate to greater distances...and the members of animal bodies move at the command of the will, namely, by the vibrations of this spirit, mutually propagated along the solid filaments of the nerves, from the outward organs of sense to the brain and from the brain into the muscles" (reviewed in Verkhratsky, et al. 2006).

It was not until 80 years later, in 1791, that experimental support for this concept arose from the publication of Luigi Galvani's fundamental work *De Viribus Electricitatis in Motu Musculari Commentarius* on animal electricity. Galvani revealed the electrical excitation of the nerve-muscle preparation and the relationship between stimulus intensity and muscle contraction by introducing a metal wire into frog spinal cord connected by the crural nerves to the inferior limbs (**Figure 7**b-I).

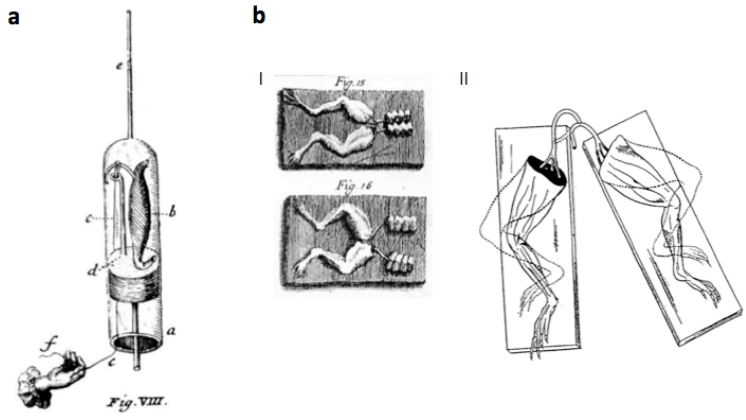

Figure 7 First neuromuscular preparations. (a) Neuromuscular preparations of Jan Swammerdam, with his original descriptions – "The stimulation of neuromuscular preparation by silver wire." (b) Galvani experiments of the contraction. (I) Original drawings of neuromuscular preparation of Luigi Galvani – Section of Plate III of the

Commentarius (1791). (II) The 1797 experiment- contraction without metals: when the surface of section of the right sciatic nerve touches the intact surface of the left sciatic nerve, both legs contract. (Adapted from (a) Swammerdam 1758, (b) Galvani 1971 and Sirol 1939).

Further studies led him to the first demonstration of an action potential (**Figure 7**b-II) and the formulation of his theory on animal electricity, in which Galvani states that biological tissues exist in a "disequilibrium" (at rest) state that allows the tissue to respond to external stimuli. More remarkable was Galvani's interpretation of "animal electricity", proposing that it results from the accumulation of positive and negative charges on the external and internal surfaces of the muscle or nerve fibre (Galvani 1841, reviewed in Piccolino 1998).

Galvani's pioneering findings set the ground to the instrumental period, during which major technical breakthroughs led the way to modern electrophysiology.

The introduction of galvanometers allowed Hermann von Helmoltz to calculate the speed of propagation of the nervous signal (Helmholtz 1850) and Emile du Bois-Reymond to measure the decrease in potential difference that accompanies excitation of nerve and muscle (du Bois-Reymond 1884). This "negative Schwankung" or negative fluctuation represents what were to be later called action potential.

Another fundamental event was the development of the differential rheotome by Julius Bernstein, which enabled precise recordings of very fast electrical events and the first true recording of resting (–60mV) and action potentials (Bernstein, Ueber den zeitlichen Verlauf der negativen Schwankung des Nervenstroms. 1868). Bernstein determined that the action potential lasted ~0.8–0.9 ms and that this potential deflection caused "sign reversal" - action potential overshoot. By applying Nernst's electrolytic theory to biology Bernstein hypothesized that the membrane's resting potential resulted from selectivity to K^+ (Bernstein 1902).

Charles Overton further developed this view by arguing that both K^+ and Na^+ are responsible for membrane excitability, and consequently for the "negative fluctuation" (Overton 1902). Interestingly he was also the one who postulated the "*lipoidal membrane*" model of the cell plasmatic membrane.

However it was not until the famous experiments of Hodgkin and Huxley in the giant squid axon that the ionic principles of the action potential were finally laid. By inserting intracellular electrodes into the axon they measured the axon's potential at rest (~ -45 mV) and at the peak of an action potential (~ +40 mV) (Hodgkin and Huxley 1939).

Hodgkin and Huxley's continuing studies along with development of voltage-clamp technique (Cole 1949), culminated in the ionic theory of membrane excitation. According to which passive

ion fluxes driven by electro-chemical gradients through transmembrane aqueous pathways (later identified as ion channels) are responsible for membrane excitability.

Concomitantly, Lorento de Nó studied evoked responses from excised bullfrog sciatic nerve, recording triphasic potential (Lorento de Nó 1947a). Even more impressive, de Nó identified the three neuronal assemble geometries (open field, closed field and mixed field) this classification is still employed nowadays (Lorento de Nó 1947b).

Brain extracellular recording arose with the advent of microelectrodes, making it possible to record from the hippocampal formation, which due to its laminar organization it is especially suited for field potentials studies.

Cragg and Hamlyn were the first to record what we today know as population spike, large compound action potential that followed close range stimulation (Cragg and Hamlyn 1955). Although they placed the stimulation electrode too close to the recording site, they were still able to report evidence of conductance along apical dendrites. Cragg and Hamlyn also found that shape and conduction of the responses when applying commissural stimulation were similar to close-range stimulation (Cragg and Hamlyn 1957). In the 1960's Adersen, by recording from different dendritic positions, observed that commissural stimulation resulted in local negative field potential in CA1 and CA3 dendridic strata. These were identified has field excitatory postsynaptic potentials (fEPSP) and above a given intensity give rise to a compound action potential – population spike – that results from the synchronous discharge of a group of pyramidal cells (Andersen, et al. 1971a). Andersen and his colleagues' continuing studies on the hippocampus cellular neurophysiology contributed to great extent of today's knowledge of hippocampal circuit network function (Andersen, et al. 1971b).

Nowadays, three main electrophysiology techniques can be categorized, defined by the position of the recording device, the electrode, in the preparation (**Figure 8**). In an intracellular recording experiment the recording electrode is inserted inside the targeted neuron. In the patch clamp technique the recording electrode is placed in close opposition to the plasmatic membrane, forming a thigh seal with a patch of membrane. Finally, in extracellular recordings also known as field potential recordings electrical signals are measured in the extracellular space (Carter and Shieh 2010).

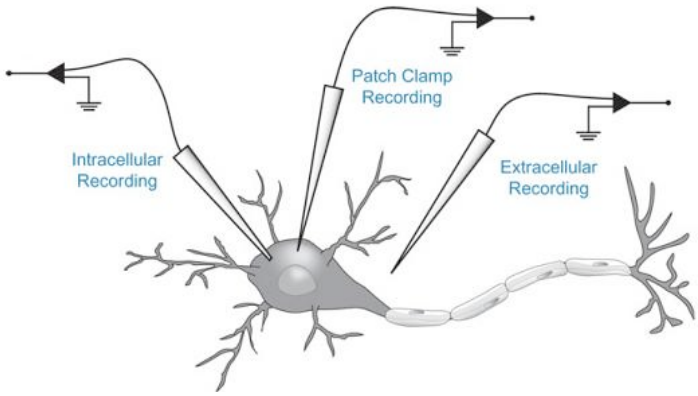

Figure 8 Types of electrophysiological recordings. The type of recording is identified according to the position of the recording electrode: inside the neuron – intracellular recording; attached to the plasmatic membrane – patch clamp recording; and outside the neuron – extracellular recording (Carter and Shieh 2010).

These different recording settings are applied both *in vitro* (e.g. cell culture and brain slices) to investigate electrical properties of the signal-mediating molecules and *in vivo* allowing the study of electrical activity mediating animal behaviour.

Field potentials recordings, as the term implies, are not restricted to the spatial domain of a neuron. As a result of the volume-conducting properties of the brain, field potentials reflect the activity of a population of neurons (Leung 1991). Hence, these are often employed in sleep, behavioural and epilepsy research.

Field potentials yield important physiological information that is not otherwise available. Postsynaptic potentials in a population of neurons manifest themselves in the field, and such potentials may be difficult to record intracellularly, especially in a behaving animal. Field potentials also yield spatiotemporal data that can be used for the study of neuronal interactions in a neuronal population.

Extracellular field potentials are electrical signals that result from electrical fields generated by single neurons, such as action potential recorded from the nerve fibre, or by the synchronous activity of a group of neurons within a particular brain region.

The extracellular fluid surrounding neurons is a conductive medium, as so when neuronal membrane is uniformly polarized (at rest potential) there is no net current flow. But as different parts of neuron's membrane become depolarized, a difference of potential between the soma, the dendrites and the axon is generated. Such spatial potential fluctuations lead to a flow of current from one part of the neuron to another through the extracellular *milieu*(Johnston e Miao-Sin Wu 1995).

The extracellular space is therefore considered volume conductor, which produces a time-varying potential gradient in the extracellular volume and a potential difference that can be measured between a point near the cell and a distant reference location – ground electrode.

At any location, the field potential depends on the linear sum of potentials from each of the current sources (outwards positive currents) and sinks (inwards negative currents), weighted according to distance and the extracellular conductivity(Leung 1991). Thus providing a measure of the sum of all postsynaptic activity within a volume of neural tissue (Carter e Shieh 2010).

Extracellular recordings can be performed with either fine metal electrodes or glass micropipettes filled with electrolyte (e.g. 2– 4 M NaCl), and have best resolution in laminar, densely-packed, structures such as the hippocampus (Suter, et al. 1999).

As previously referred there are three main field potential configurations determined by different neuronal geometrical arrangements: the open field, the closed field, and the open-closed field. The open field, as illustrate on **Figure 9**a, is characteristic of laminated structures where palisades of neurons are aligned in parallel, with the dendrites and somata are facing opposite directions. It is usually found in the cerebellum, neocortex, and hippocampus.

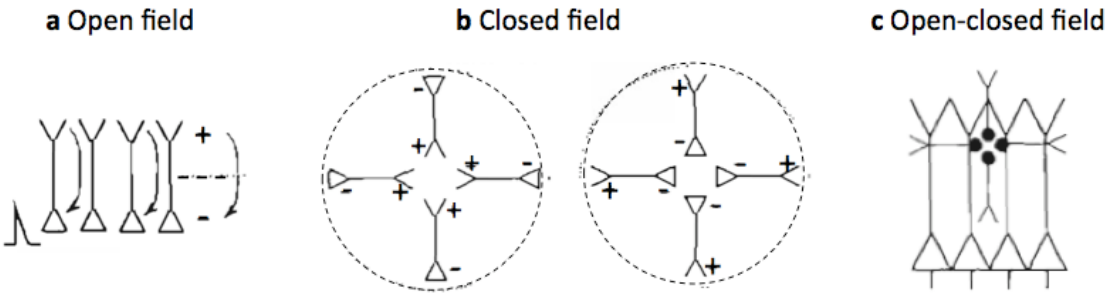

Figure 9 Diagram of open, closed and open-closed fields. The effect of geometry on field potential recording. Current flow and potential field are produced by (a) synchronous depolarization of cell bodies of parallel oriented neurons – open field; (b) with cell bodies clustered and dendrites spreading radially (or vice versa) – closed field; and with a combination of parallel and radial elements – open-closed field. Dotted lines represent zero potential lines for each type of field. (Adapted from Johnston and Miao-Sin Wu 1995).

If this array of neurons is activated by a synchronous synaptic input (e.g., by stimulation of an afferent pathway), a dipole will be established between the dendrites and the somata. In the hippocampus the field potential recorded in the dendrites is a population or field EPSP (fEPSP), while the potential corresponding to the action potential is called the population spike (pSpike) (Johnston e Miao-Sin Wu 1995). Unlike the all-or-none action potential generated by a single neuron, the pSpike is a graded response; as stimulus intensity increases, the number of responding neurons increases and the pSpike becomes correspondingly larger.

As with all extracellular techniques, membrane potential is not measurable with field recordings. Despite some limitations, extracellular recordings have been proven useful when examining firing behaviours, determining slice viability, synchronous activity (e.g epileptiform activity) as well as hippocampal rhythms (Suter, et al. 1999).

3.2 Western blot

Western blot technique arose from the need to create a sensitive assay to visualize specific antigens.

The key principle of electrophoresis and western blot is based on the law of electrolysis conceived and presented by Faraday in 1791. Faraday's law of electrolysis states that the mass of a substance liberated at an electrode during electrolysis is directly proportional to the quantity of charge passing through the electrolyte (Faraday 1834).

In 1930, a new technique emerged when Arne Tiselius developed the moving boundary electrophoresis in the Tiselius apparatus (Tiselius 1930). This U-shaped glass tube filled with an aqueous buffer and connected to an electrode at each end, allowed the electrophoretic separation of ionized molecules upon application of voltage (Tiselius 1937). Tiselius was able to describe the *moving boundaries*, formed by the protein fronts, of albumin, α-, β- and γ-globulin in serum, which earned him the Nobel Prize (1948). Despite Tilselius' vital contribution, this method was prone to impaired resolution and unable to accurately discriminate between similar molecules (Tiselius 1930).

Later on, Smithies demonstrated that a starch gel could serve as a molecular sieve through which electrophoretic separation of proteins could be carried out. Several other supports were developed such as, gelatine and agarose gels, cellulose acetate strips and more recently and widely used the polyacrilamide gel (PAG) (Raymond and Weintraub 1959, reviewed in Vesterberg 1993). PAG is ideal for electrophoretic applications, since it is a thermostable medium, is transparent, strong and relatively chemically inert and can be prepared with a wide range of pore sizes. However, identification of proteins separated by electrophoresis in the gel matrix itself is difficult due to the small sized pores that limit the penetration of molecular probes (Gershoni and Palade 1983).

Overcoming this limitation was made possible by electroeluting proteins from gels onto a membrane (Towbin 1979; Burnette 1981). The process of transferring macromolecules from gels to an immobilizing matrix, termed blot, was originally used by Arnheim and Southern in 1977 with DNA samples ("Southern blot"). The nitrocellulose membrane constitutes a replica of the gel's protein band pattern, allowing easy detection by immunological procedures.

The principles of western blot were established as the modern technique used nowadays. The simplicity and relevance of the method has let to its expansive and ubiquitous application in the clinical sector as well as in basic research.

The protein immunoblot, as it is also called, involves several steps, grouped in three major procedures: separation of a complex protein mixture by gel electrophoresis; protein transfer onto a membrane; and detection of target proteins by means of antibody-antigen specificity.

Prior to these procedures is sample preparation, which includes protein extraction from the tissue. This can be attained using a variety of strategies, such as detergent-mediated lysis, ultrasonication or mechanical homogenization. During extraction endogenous proteases may be released upon cell disruption. To reduce protein degradation a cocktail of protease inhibitors is commonly added, as well as a suitable buffer to maintain pH, ionic strength and stability. In addition, the procedure is performed at low temperatures (0°C to 4°C) and the samples are kept on ice at all times.

Preceding the protein separation by means of gel electrophoresis, protein samples are routinely quantified in order to ensure equal loading in all lanes.

Several spectrophotometric methods are available to calculate protein concentration, namely methods based on protein-dependent colour change. These include the copper-based Lowry assay (Lowry, et al. 1951), the Smith copper/bicinchoninic assay (BCA) (Smith, et al. 1985) and the Bradford dye assay (Bradford 1976).

The Lowry procedure as well as more efficient modified versions of the original protocol are widely used. This protein assay is based on a two-step reaction, where firstly the protein reacts with an alkaline copper tartrate solution, followed by the reduction of Folin reagent by the copper-treated protein. Colour development is primarily due to the amino acids tyrosine and tryptophan. The final blue colour is optimally measured at 750 nm, but it can be measured at any wavelength between 650 nm and 750 nm (Lowry, et al. 1951).

The most widespread technique to separate protein mixtures is the sodium dodecyl sulphate-polyacrylamide gel electrophoresis (SDS-PAGE), which allows proteins discrimination according to their molecular weight.

In order to ensure that proteins are separated solely on the basis of size and not on charge or three-dimensional structure, samples are previously denaturated with Laemmli (Tris-glycine) buffer, which contains SDS, and subjected to 95ºC for 5 min (Laemmli 1970). SDS is an anionic detergent that binds to hydrophobic regions, and causes the protein to acquire a net negative charge. Along with the other components of the Laemmli buffer, such as β-mercaptoethanol, a reducing agent, proteins assume a linearized form (Luttman, et al. 2006).

A typical gel (discontinuous SDS-PAGE) consists of two sections of different densities, cast between two glass plates (**Figure 10**a). Hence, protein samples initially run through a lower density or stacking gel, which concentrates the proteins into a thin and sharp starting zone before

they migrate to the resolving or higher density gel. This results in high sharpness of protein bands and better resolution in the separation (Luttman, et al. 2006; GE Healthcare 2011).

Both gels have polyacrylamide as the main component. Polyacrylamide is a polymer composed of acrylamide monomers that by virtue of N,N-methylenebisacrylamide, a cross-linking reagent, creates a three-dimentional network (**Figure 10**b). The crosslinking chain reaction is propagated by adding a chemical initiator and catalyst (e.g. ammonium persulphate (APS) and TEMED).

As negative charged linearized proteins are forced through the gel by an electric field, towards the anode, larger molecules are retarded by the gel more than smaller molecules (**Figure 10**b).

Gel density (pore size) affects the separation profile of proteins. Therefore according to the size of the protein of interest the density of the resolving gel should be determined for optimal separation, with lower density matrices providing better resolution of larger proteins.

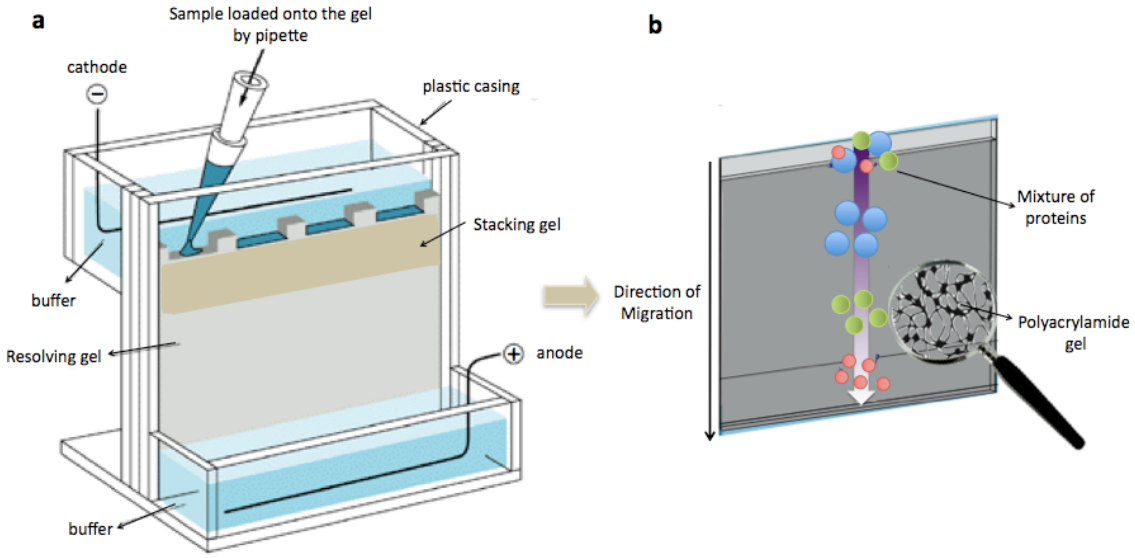

Figure 10 Discontinuous SDS-PAGE electrophoresis apparatus. (a) Samples are loaded into the wells of the gel, routinely one lane is used for a molecular weight maker (commercially available mixture of proteins of defined molecular weights, stained to form visible, coloured bands). (b) Upon current application proteins migrate towards the positive pole, with the smaller molecules progressing further than larger molecules. Through the magnifying glass it is visible the covalent crosslinks formed by bisacrylamide (•) between strands of acrylamide polymers in a polyacrylamide gel (Adapted from GE Healthcare 2011).

Protein separation by gel electrophoresis is followed by protein transfer onto an adsorbent porous membrane. Membranes are typically made of chemically inert substances such as nitrocellulose or polyvinylidene difluoride (PVDF). Electrotransfer, the most widely used transfer method, relies on the same electromobility principles that drive the migration of proteins during separation in PAGE. The gel, membrane, and electrodes are assembled in a sandwich so that proteins move from gel to membrane (blot), where they are captured, in a pattern that perfectly

mirrors their migration positions in the gel (**Figure 11**a). In the case of wet transfer method the gel and membrane are both fully immersed in transfer buffer. This transfer procedure usually leads to heat generation, and requires cooling of the unit.

A broadly used transfer buffer is the classical Towbin buffer: Tris base, glycine, methanol and SDS. This low ionic strength buffer (pH 8,3) provides an electrically conducting medium in which proteins are soluble. Methanol allows an efficient binding to the membrane by removing SDS bounding proteins.

Current application and transfer time should be balanced to enable optimal transfer. The use of large currents should be avoided since it causes proteins to migrate at high speeds, thus they may not adsorb to the membrane (GE Healthcare 2011).

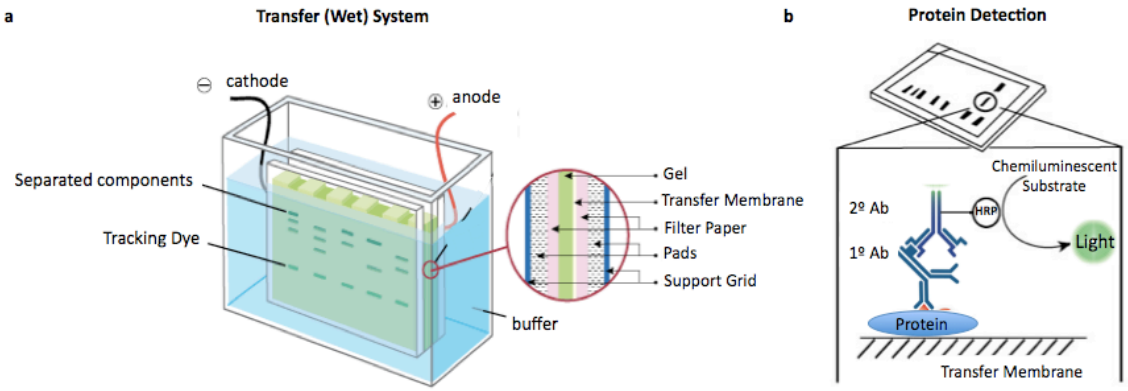

Figure 11 Protein (Western) blot apparatus and Immunobloting. (a) Wet transfer system with a sandwich-like configuration submerged in a tank filled with transfer buffer. Proteins migrate from the cathode (gel) to the anode (membrane) (b) Protein detection by immunobloting. After the specific primary antibody is bound to the target, it forms a complex with a HRP-linked secondary antibody. The addition of HRP substrate causes light emission, by means of an enzyme catalyzed decomposition reaction (Adapted from Leinco 2011; Cell Signaling Technology 2011).

Once transferred to the membrane, the separated proteins can be further examined. Identification of target proteins involves probing the blot with specific antibodies. Although there are several protein detection procedures, all encompass the following work steps: saturation of the membrane (block), immunodetection and visualization (Luttman, et al. 2006).

Blocking minimizes background of non-specific binding, thus increasing detection sensitivity. This is achieved by incubating the membrane with blocking agents, such as protein-enriched solutions (e.g. nonfat power milk or albumin) and anionic detergents (e.g. Tween 20).

Following the blocking step, the protein of interest can be targeted using antibodies. The primary antibody, which is specific for the target protein, can be labeled or unlabeled. To maximize sensitivity and signal-to-noise ratio, most western blotting procedures use an unlabeled primary antibody that is specifically recognized by a labeled secondary antibody – indirect staining. The

secondary antibody is directed against the IgG of the species that provided the primary antibody. Anti-species IgG are commercially available, with choice of different labels attached (Wilson and Walker 2010).

A variety of visualization systems, based on chemiluminescence, chemifluorescence, fluorescence, chromogenic or radioisotopic detection are available.

The most commonly used enzymatic detection system is chemiluminescence, based on antibodies conjugated to horseradish peroxidase (HRP) that catalyze the oxidation of luminol in presence of peroxide, and results in light emission (**Figure 11**b). The reaction is accompanied by the emission of low intensity light at 428 nm, which when in contact with an X-ray film, impresses a band pattern.

The signal intensity is proportional to the protein quantity on the blot, which thus allows relative precise quantification. All protein bands are normalized to housekeeping protein (e.g. α-tubulin or β-actin). Densitometric analysis of protein bands is carried out by using an imaging software (Carter and Shieh 2010).

3.3 Quantitative real-time PCR (RT-qPCR)

The polymerase chain reaction (PCR) has become a fundamental tool in molecular biology and clinical diagnosis. It is arguably the greatest technical breakthrough of the last century in molecular biomedicine.

Before the PCR, nucleic acid amplification and quantification was laborious and time consuming, involving either radioactive incorporation or later on Southern (for DNA) and Northern (for RNA) blot analysis (Dorak 2006). These early techniques required large amounts of nucleic acids and strong technical expertise, since they implicated multistepped protocols, in order to obtain reproducible results. Unfortunately, despite the efforts to extract quantitative information, neither of these techniques was considered a quantitative assay (Wittwer and Farrar 2011).

The theoretical concepts supporting the PCR procedure were first reported by Kleppe and colleagues (1971). It is the earliest description of the application of a cycling process using a DNA polymerase and oligonucleotide primers to produce copies of a specific DNA sequence. However, due to the cost and difficulty in producing oligonucleotides, the non-availability of thermostable DNA polymerases and the absence of automated instrumentation the practical application of this process was no more than a remote thought for many years (Logan, et al. 2009).

The first demonstration of experimentally defined basic steps of PCR was performed by Mullis and Falloona in 1987, using a modified version of DNA polymerase I from *E. coli*, known as the Klenow fragment (Saiki, et al. 1985; Mullis and Faloona 1987). By using a non-thermostable polymerase, fresh enzyme had to be added to the reaction mixture after each denaturation step.

The solution to this limitation came across more than a decade before the advent of PCR in the Yellowstone National Park hot springs, where a hyperthermophilic bacterium named *Thermus aquaticus* was discovered (Brock and Freeze 1969). The isolation and purification of the *Thermus aquaticus* (*Taq*) DNA polymerase, and its optimum enzymatic temperature of 80°C, were reported by Chien and colleagues in 1976.

The introduction of a thermostable polymerase in PCR (Saiki, et al. 1988), 12 years later, allowed the reduction of both hands-on technical time required to perform an assay and the likelihood of cross-contamination, since DNA polymerases were no longer inactivated after every cycle and therefore did not needed to be added repeatedly.

The use of *Taq* polymerase along with the development of automated thermocyclers, which eliminated the need for separate water baths at different temperatures, turned PCR into a technique performed routinely in every molecular biology laboratory (Pelt-Verkuil, et al. 2008).

A typical PCR reaction requires target DNA, specifically designed oligonucleotide primers complementary both to sense and antisense strand, a thermostable DNA polymerase, the four deoxyribonucleotide thriphosphate (dNTPs) DNA building blocks, magnesium ions, a co-factor of DNA polymerase and a Tris-buffer (pH 8,3). The composition of the reaction mix should ideally be optimised for every new PCR protocol developed, as any change in PCR methodology can affect the specificity and efficiency of the amplification.

PCR amplification, as shown in **Figure 12**, is a cyclical process in which the reaction mix is initially heated at a temperature of 90-95°C (30 s to 5 min), denaturing the DNA sample into single stranded DNA. Hybridisation of the specific oligonucleotide primers to each strand is achieved by setting the reaction mix at the annealing temperature, usually between 40°C and 70°C (30-60 s), dependent on the composition of the primers in terms of adenine (A), thymine (T), cytosine (C) and guanine (G) content. The annealing step is followed by the elongation or extension step, in which the temperature is set at approximately 72°C (60-120 s), the optimal temperature for *Taq* polymerase mediated replication. The entire cycle is then repeated a pre-determined number of times. After each cycle, newly synthesised double stranded DNA (dsDNA) molecules, known as amplicons, contain terminal sequences complementary to the primers used. This allows each amplicon to serve as a template for replication in the subsequent PCR cycles, resulting in an exponential amplification of the number of target molecules during each cycle (reviewed in Pelt-Verkuil, et al. 2008).

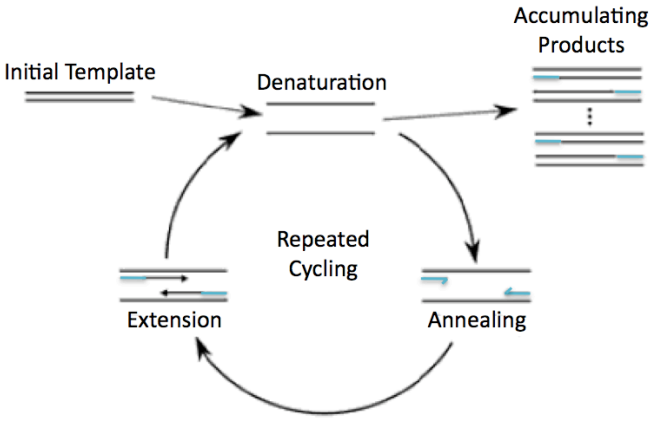

Figure 12 Schematic representation of the PCR cycle. Initial template dsDNA is denaturated at high temperature (95°C). The duplication of the DNA target molecule is facilitated by the specific hybridization of two oligonucleotide primers (blue dash). Each primer anneals to opposite strands with their 3'-ends pointed inwards. A thermostable DNA-dependent DNA polymerase recognises the primers and extends the DNA strand in the 5' to 3' direction. The cycle is repeated 20 to 50 times through successive steps of strand denaturation (melting), primer annealing and new DNA synthesis (extension/elongation), which results in exponential amplification of a specific DNA sequence. (Adapted from Wittwer and Farrar 2011).

It did not take long for biologists to realize the potential of the PCR amplification automated methodology, creating the impetus to adapt and develop techniques based on nucleic acid amplification and detection.

The discovery of an RNA-dependent DNA polymerase or reverse transcriptase was first reported in 1970 (Baltimore 1970, Temin and Mitzutani 1970). This finding defied the widely accepted "central dogma of molecular biology" propounded by Watson and Crick, which described the flow of genetic information *in vivo*, from DNA to RNA (via transcription) and subsequently to protein (via translation). The process of reversed flow of genetic information, from RNA to DNA (via reverse transcription) was found to occur in some virus families (*Retroviridae, Hepadnaviridae* and *Caulimoviridae*) during the replication cycle. Shortly after the invention of PCR, the knowledge of this process was applied to study transcription levels in different tissues. This adapted version of PCR, known as reverse transcriptase PCR (RT-PCR) requires much less RNA, when compared to other assays (e.g. northern blot, *in situ* hybridization), making it ideal for detecting low copy mRNA or mRNA from small amount of tissue/cells samples. RNA molecules are transcribed into complementary DNA (cDNA) by the action of reverse transcriptase enzyme, which can then be amplified by PCR (reviewed in Wittwer and Farrar 2011, Pelt-Verkuil, et al. 2008). RT-PCR can take place in one-step or two-step reaction. In a one-step RT-PCR or one tube RT-PCR, both reverse transcription and amplification occur in the same tube and reverse gene-specific primers must be used. With two-step RT-PCR the RNA is first transcribed into cDNA using

oligo-dT primers or random oligomers and subsequently amplified the PCR step using gene-specific primers, leading to specific cDNA amplification.
The RT step is typically performed at 40-50°C, though if random primers or oligo-d(T) are used – two-step RT-PCR – an initial 10 min-step at 25 °C is needed in order to maximize the annealing efficiency, as the short oligo d(T) have a lower Tm (Qiagen 2004).

The validity and accuracy of gene expression evaluation is also known to be profoundly affected by the quality of the starting RNA. Thus, preparation of intact cellular total RNA or mRNA is critical to all gene expression analysis techniques. RNA quality encompasses both its purity (absence of protein and DNA contamination, absence of inhibitors) and its integrity. The purity of extracted RNA can be assessed by several methods including spectrophotometry, in which the A_{260}/A_{280} ratio may be used to monitor protein contamination. High purity RNA has an A_{260}/A_{280} of 1.9 to 2.1. Since both DNA and RNA absorb at 260 nm, the absence of genomic DNA is commonly assessed by an agarose gel electrophoresis and/or by the use of a negative control (RT-PCR from samples with no added RT) in each experimental setup. Genomic DNA is typically removed during the RNA isolation procedure by RNase-free DNase treatment or extraction with acid phenol/chloroform. Furthermore, the design of the PCR product should incorporate at least one exon-exon splice junction to allow a product obtained from the cDNA to be distinguished on electrophoresis from genomic DNA contamination (reviewed in Reiter and Pfaffl 2011).
Although traditional RT-PCR is a quantitative assay it is rather challenging to accurately quantify the initial amount of cDNA. As a PCR of only 20 cycles amplifies the initial cDNA over a million-fold (assuming 100% efficiency), there is also the potential for enormous errors. Thus accurately RT-PCR quantitation requires that all samples have equal amplification efficiency, which is extremely difficult to control (VanGuilder, et al. 2008).

Currently real-time, reverse transcriptase, quantitative PCR (RT-qPCR) is the most commonly used protocol for transcript quantification. Real-time PCR not only automates both amplification and detection, but integrates them so that they can occur concurrently. Time, temperature and fluorescence are monitored during PCR in real-time instruments (Wittwer and Farrar 2011). Early work by Huguichi and collegues (Higuchi, et al. 1992, 1993) first described real-time monitoring during a PCR by using a dsDNA specific dye - ethidium bromide (EtBr). By acquiring the fluorescence at each cycle it allowed simultaneous quantification and detection of specific DNA sequences in a “close-tube” homogenous format, reducing post-processing steps and minimizing experimental error (reviewed in Logan, et al. 2009).
The first commercially available real-time qPCR platform was the Applied Biosystems ABI Prism

7700 Sequence Detection system. This instrumentation, along with more recent and sophisticated models, consists of a thermocycler with an integrated optical detection system, for both excitation and emission, and computer software for data acquisition and analysis. Real-time qPCR platforms utilize fluorogenic chemistry, which involves the employment of a fluorescent detector molecule that allows detection and quantification of newly synthesized DNA.

There are two main classes of real-time qPCR fluorescent indicators (**Table 2**): fluorescently labelled probes or strand specific detection and dsDNA dyes or non-specific detection.

Table 2 Real-time qPCR technologies (Adapted from VanGuilder, et al. 2008).

Technology	Supplier	Fluorescent Signal	Multiplexing	Melting curve analysis
TaqMan	Applied Biosystems	Probe hydrolysis	Yes	Not necessary
LightCycler	Roche	Probe hybridization	Yes	Not necessary
LUX	Invitrogen	Hairpin probe hybridization	Yes	Necessary
Molecular Beacons	Sigma - Aldrich, IDT	Hairpin-loop hybridization	Yes	Necessary
SYBR Green	Multiple	Intercalating dye	No	Necessary

Probe-based detection uses sequence specific DNA-based fluorescent reporter probes, and as a result they only detect the sequence of interest and not all dsDNA. These probes typically contain a fluorescent reporter and a quencher, which are positioned in close proximity so that the quencher molecule is preventing the reporter from emitting fluorescence. The process by which an acceptor molecule absorbs and dissipates the energy from a fluorescent component or donor can occur either by proximal quenching or fluorescence resonance energy transfer (FRET).

Once the probe hybridizes to the complementary target, the reporter and quencher are separated and a fluorescent signal is generated and measured to quantitate the amount of DNA. These include probes that fluoresce upon hydrolysis (e.g. Taqman), hibridization (e.g. LightCycler) and fluorescent hairpins (e.g. LUX and Molecular Beacons) - **Table 2**.

The main advantage to using probes is their specificity and sensitivity, however they are quite expensive.

Alternatively, intercalating or dsDNA dyes, as the term implies, bind reversibly, but tightly, to DNA's double strand structure by intercalation, minor groove binding, or a combination of both. Of these, SYBR® Green I is by far the most commonly reported non-specific dye in RT-qPCR. Prior to binding SYBR® Green I exhibits low fluorescence (497 nm). In contrast as the dsDNA product is generated, SYBR® Green I binds to the minor groove of the dsDNA resulting in an increase in the

fluorescence output (520 nm), which can be nearly 2000 times the initial unbound fluorescence signal (Dorak 2006).

Assays using SYBR Green I binding dye are less specific than sequence-specific probes, since the specificity of the reaction is determined entirely by the primers. Still, PCR specificity can be verified by melting curve analysis, which plots the first negative differential of the fluorescence signal with respect to temperature. This plot displays one or more peaks representing the point(s) at which the maximum rate(s) of change in fluorescence occurs corresponding to a specific dsDNA product − specific amplicons normally melt at higher temperature than artefacts (e.g. dimers and misprimed products) (reviewed in Logan, et al. 2009).

Overall, real-time PCR can be defined as the continuous collection of fluorescent signal from one or more PCRs over a range of cycles. Quantitative real-time PCR (qPCR) is the conversion of the fluorescent signals from each reaction into a numerical value for each sample (Dorak 2006).

RT-qPCR data analysis can be either absolute (i.e. number of copies of a specific RNA template per sample) or relative (treated sample changes by X fold of control sample). The majority of analysis use relative quantitation since it is easier to measure and it is particularly suited when evaluating variations associated with disease states (VanGuilder, et al. 2008).

Real-time qPCR relies on measuring the increase in fluorescent signal during amplification. The fluorescence values are recorded during each cycle at the end of the elongation step. Since the fluorescence signal is directly proportional to DNA concentration over a wide dynamic range, the correlation between PCR product and fluorescence intensity is used to calculate the amount of template present at the beginning of the reaction.

Individual reactions are characterized by the PCR cycle at which fluorescence first rises above a defined or threshold background fluorescence, a parameter known as the threshold cycle (Ct) or crossing point (CP) (Nolan, et al. 2006). The concept threshold fluorescence is the basis of an accurate and reproducible quantification using fluorescence-based RT-qPCR methods (Higuchi, et al. 1993).

Theoretically, an equal number of molecules are present in all of the reactions at any given fluorescence level. Therefore, at the threshold level, it is assumed that all reactions contain an equal number of specific amplicons. The higher the initial amount of sample DNA, the sooner the accumulated product is detected in the fluorescence plot and the lower the CP value.

In the mathematical model developed by Michael W. Pfaffl (Pfaffl 2001), the relative expression ratio (R_{Pfafll}) of a target gene is calculated based on RT-qPCR efficiency (E) and CP deviation of a treated sample versus a control, and expressed in comparison to a reference gene. This mathematical model of relative expression is represented by equation (1) in **Figure 13**, in which

E_{target} and E_{ref} are, respectively, the real-time RT-qPCR efficiencies of the target and reference genes, calculated according to [E= 10^(-1/slope)]. The slope value is calculated by plotting the CP values vs. log cDNA concentration (ng/ul) from a dilution series. This standard curve, will not only allow efficiency determination, but will also indicate the linearity, sensitivity and reproducibility of the assay.

CP deviation values (ΔCP) are also required in order to calculate R_{PfaffI}. These are determined by subtracting the CP values in control and sample conditions for both target (ΔCP_{target}) and reference (ΔCP_{ref}) genes.

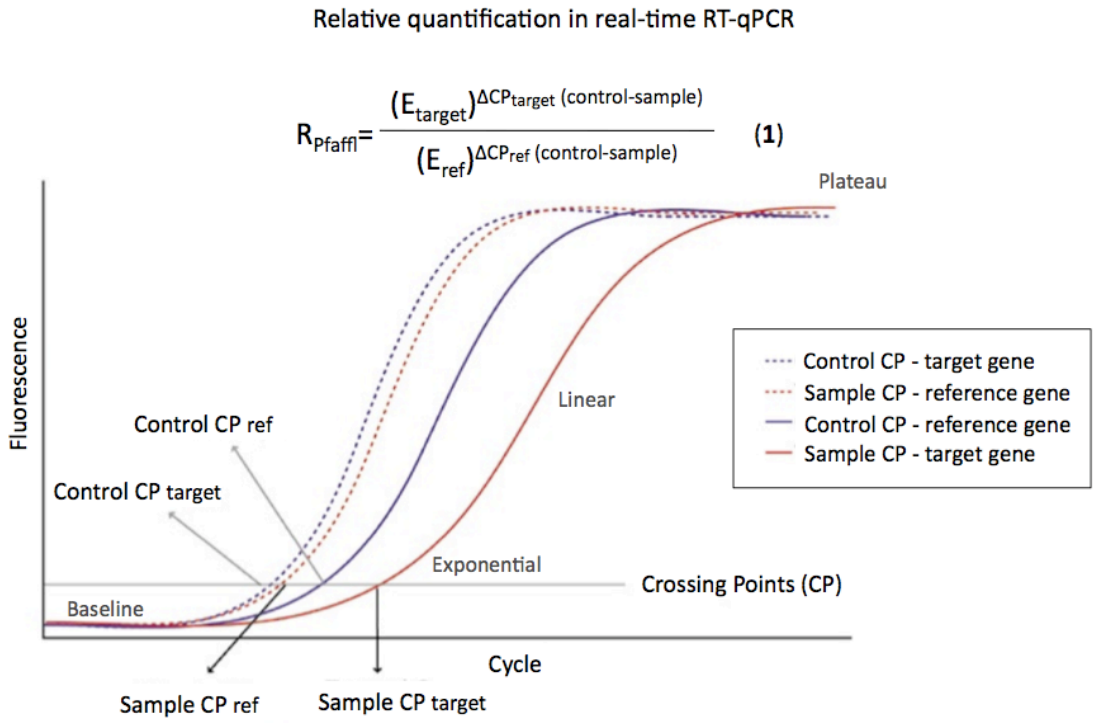

Figure 13 Mathematical model for relative quantification (R_{PfaffI}) in real-time PCR. The Pfaffl method enables relative quantification (treated sample is X fold of control sample) through measurements of crossing points (CP) and determination of the real-time qPCR efficiency [E= 10^(-1/slope)] – Equation (1). As described in the text, the comparative differences between the gene of interest (CP_{target}) and a reference gene (CP_{ref}) for each condition (sample and control) allow a quantitative comparison between the samples. Note that the CP endogenous control genes (dotted lines) does not vary significantly with the treatment. Each amplification curve illustrates the four phases of PCR (in grey): Baseline – signal generated but not detectable; Exponential – detectable signal with maximal PCR efficiency; Linear – post-exponential phase with declining in PCR efficiency; Plateau – no or very little new product is generated. (Adapted from Pfaffl 2001; VanGuilder, et al. 2008).

Since the fluorescence threshold is set above the amplification baseline and within the exponential increase phase - **Figure 13**, the quantification will not be influenced by reagent limitation in the plateau phase. Furthermore, in this model the relative expression ratio of a target gene is normalised with the expression of an endogenous reference gene, which ensures

compensation for inter-PCR variations between runs. Housekeeping genes are commonly used, since they are present in all nucleated cell types and their mRNA synthesis is considered to be stable even in different tissues and under various experimental conditions (Thellin, et al. 1999).
The Pfafll model of relative expression is a simple mathematical model that only takes into account efficiencies and CP deviation of a control and an unknown sample. Standard curve is not needed and normalisation with an endogenous standard is included in the model to standardise each reaction run in relation to RNA integrity, sample loading and inter-PCR variations (Pfaffl 2001).

In sum, real-time RT-qPCR protocol encompasses three fundamental steps: (i) the reverse transcriptase (RT)-dependent conversion of RNA into cDNA, (ii) the amplification of the cDNA using the PCR and (iii) the detection and quantification of amplification products in real time.
The detection and expression analysis of transcript(s) in real-time by RT-qPCR has revolutionized the 21st century biological science due to its tremendous applications in both basic and clinical fields.

4 METHODS

4.1 Animals

Animals were handled according to the Portuguese law on Animal Care and European Union guidelines (86/609/EEC).

Animals were group housed in a conventional rodent room under controlled environmental conditions, with a constant room temperature of 22°C and a 12-h light-dark cycle with light on at 7.00 am and light off at 7.00 pm. Rats were fed and watered *ad libitum*.

The home cages, which include the bedding material made of wood-cuttings, were changed once a week.

All animals used in the experiments, both Sprague-Dawley and Wistar rats, were acquired from Harlan Interfauna Iberia (Barcelona).

4.2 Anaesthesia

Animals were anesthetized with Halothane (2-Bromo-2-Chloro-1,1,1-Trifluoroethane, Sigma) in an anaesthesia chamber. This choice allows for a reliable anaesthesia with a reasonable therapeutic gap between deep and irreversible levels.

The first indications of anaesthesia include the lack of a righting reflex and reduction in respiratory rate. A noxious stimulus (i.e. toe pinch) was also applied to ensure deep plane of anaesthesia. If no response was noted, the animal was sacrificed by decapitation in a guillotine (Costa and Antunes 2010).

It should be noted that very deep anaesthesia leads to circulation arrest and hypoxia and causes cessation of protein synthesis. Gas anaesthesia works well in both sexes (Heinemann, et al. 2006).

4.3 Hippocampal neuronal culture model of acquired epilepsy (AE)

4.3.1 Primary hippocampal culture

Primary hippocampal cultures were prepared from E18 Sprague-Dawley embryos. Pregnant rats were anesthetized and decapitated as previously described. Uterus containing the embryos was removed from the rat abdomen by lifting while cutting the mesometrium (red line in **Figure 14** I) and placed in cold Ca^{2+} and Mg^{2+} free Hanks' balanced salt solution supplemented with 0,37% glucose (CMF-HBSS, Gibco). Under a laminar flow hood, embryos were removed from the uterus, and the brain was exposed and isolated by pushing the skull down and sidewise as shown in **Figure 14** III. Using a dissecting microscope, meninges and choroid plexus, which are highly vascularised, were gently removed (**Figure 14** b), and the hemispheres were separated via a

midline sagittal cut (**Figure 14** c). On the inner surface of the forebrain the hippocampus is observable (**Figure 14** d) and was kindly dissected out with Dumont no. 7s forceps (Fine Science Tools). All hippocampi were collected in fresh CMF-HBSS and transferred to a 15 mL Falcon tube in a final volume of 2,7 mL. The hippocampi were trypsinized (0.350 ml of 2.5% trypsin, Invitrogen) and incubated for 15 min in a water bath at 37°C. Trypsin solution was gently removed, leaving the hippocampi at the bottom of the tube. Afterward 5 mL of CMF-HBSS was added and let stand for 5 min at room temperature. This procedure was repeated twice allowing trypsin to diffuse from the tissue (Kaech and Banker 2006). The hippocampi were resuspended in Neurobasal medium (supplied by Gibco) supplemented with 0.5 mM glutamine, 2% B27 and 25 U/mL penicillin/streptomycin in a final volume of 2-3 mL. Hippocampi dissociation was achieved by repeatedly pipetting the suspension up and down. Cell suspension was expelled forcefully against the wall of the tube to minimize foaming. Cell density was determined by counting cells in a 0.4% trypan blue solution using a hemacytometer. Cell suspension was plated at low density ($4x10^4$ cells/mL), in a 12 mm poly-D-lysine (PDL, 50 µg/mL, Sigma) coated glass coverslips (Marienfeld, Germany) for whole cell recording experiments and in 6 well PDL-coated plates (TPP, Switzerland) for western blot analysis.

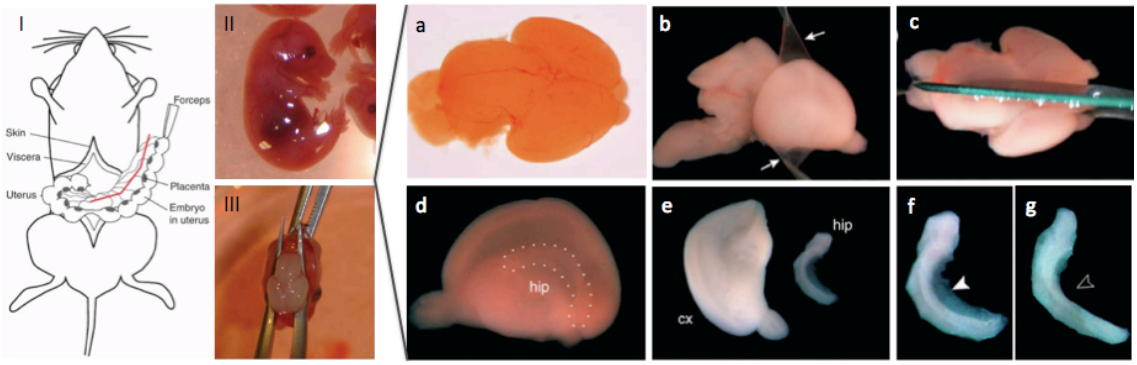

Figure 14 Collecting brains and dissection of hippocampus from embryos. (I) Sacrificed pregnant mouse on its back with expose abdomen. (II) E16.5 embryo removed from the uterus. (III) Brain isolation from the skull. (a) E16.5 mouse brain. (b) Meninges (arrows) being removed from the hemispheres by gently pulling. (c) Brain cut into halves via the midline sagital section. (d) The hippocampus (hip) is visible on the inner surface of the forebrain. (e) Cortex (cx) and hippocampus (hip) are separated. (f,g) The fimbriae (arrowhead) on the concave side of the hippocampus are removed (open arrowhead). This procedure is identical in rat embryos (Adapted from Fath, et al. 2008).

Hippocampal primary cultures were maintained in an incubator with a humidified 37°C and 5% CO_2 atmosphere, and the medium was changed twice a week, by replacing one-third of the volume with fresh supplemented Neurobasal medium (Kaech e Banker 2006). Hippocampal neurons were kept viable until 15 to 17 days in culture (DIC).

4.3.2 Induction of SREDs by free Mg^{2+} exposure of primary hippocampal cultures

At 10 DIC maintenance medium was replaced by a physiological recording solution (pBRS) either with or without $MgCl_2$, containing (in mM): 145 NaCl, 2.5 KCl, 10 HEPES, 2 $CaCl_2$, 10 glucose, and 0.002 glycine, pH 7.3, and osmolarity adjusted to 290 ± 10 mOsm with sucrose. Hence, free Mg^{2+} exposure was carried out with pBRS without added $MgCl_2$, while sham controls were exposed to pBRS containing 1 mM $MgCl_2$. Briefly, after removal of maintenance medium, cells were gently washed with pBRS and then incubated in this solution at 37ºC under 5% CO_2 atmosphere for either 30 or 60 minutes (Sombati and DeLorenzo 1995, Deshpande, et al. 2007, Blair, et al. 2009). Afterwards medium was again replaced by maintenance medium and incubated at 37 °C under 5% CO_2/95% air atmosphere. Neurons were examined 5 day after exposure.

4.3.3 Whole cell recordings

Glass coverslips, containing primary hippocampal neurons at 15 DIC, were mounted on the stage of a Carl Zeiss Axioskop 2FS upright microscope (Jena, Germany) equipped with infrared video microscopy and differential interference contrast optics. The recording chamber (5-6mL) was continuously superfused by a gravitational superfusion system at 2-3 mL/min with pre-warmed pBRS (containing $MgCl_2$ 1mM).

Patch pipettes were made from borosilicate glass capillaries (1.5mm outer diameter, 0.86 inner diameter, Harvard Apparatus) in two stages on a pipette puller (PC-10 Puller, Narishige Group). The resistance of the recording pipettes was 4-9MΩ when filled with an internal solution containing (in mM): K-gluconate 125; KCl 11; $CaCl_2$ 0.1; $MgCl_2$ 2; EGTA 1; HEPES 10; MgATP 2 ; NaGTP 0.3 and phosphocreatine 10, pH 7.3, adjusted with KOH (1M), 280-290 mOsm.

To optimize success of recording from pyramidal neurons, phase-bright cells were selected based on both size and pyramidal shaped soma (Blair, et al. 2009).

Whole-cell was recorded in a current clamp plus mode with an EPC-7 amplifier (List Biologic, Campbell, CA). Offset potentials were nulled directly before giga-seal formation. Immediately after establishing whole-cell access, the membrane potential (Vm) of the neurons was measured in current-clamp mode.

Data acquisition was carried out by WinLTP 0.96 (Anderson, 1991-2009) software program (Anderson and Collingridge 2007).

4.4 *In vitro* model of epileptiform activity in combined hippocampal-entorhinal cortex slices

4.4.1 Tissue preparation

Male Wistar rats (150–250g/5-7 weeks old) were anesthetized and decapitated as described in section 4.2. The skull was exposed and cut along the sagital suture from the foramen magnum to the forehead with a pair of surgical scissors. On each temporal side of the skull, one cut was made at the foramen magnum. The brain was exposed by carefully prying the skull open (Wang and Kass 1997).

Holding the skull upside down and using a spatula to sever the cranial nerves that hold the brain to the skull, the brain was removed and submerged in ice-cold (4°C) artificial cerebrospinal fluid (ACSF), containing (in mM): 124 NaCl, 3 KCl, 1.8 $MgSO_2$, 1.6 $CaCl_2$, 1.25 NaH_2PO_4, 26 $NaHCO_3$, and 10 glucose. The solution was equilibrated with carbogen gas (95% O_2/5% CO_2) to maintain a pH of 7.4 and the osmolarity of the solution was about 290 mOsm. This procedure was performed within less than a minute as recommended (Heinemann, et al. 2006).

After isolation, the brain was kept at 0–4°C, since low temperature slows down the cellular metabolic rate and reduces energy consumption. Therefore reducing metabolism-related ischemic damage and improving the texture for slicing.

The cerebellum was removed, and the brain was divided in two hemispheres (**Figure 15**a). Each hemisphere was placed on its medial surface and divided into rostral and caudal sections by a transverse cut in a plane approximately parallel to the main axis of the hippocampus (**Figure 15**b and c).

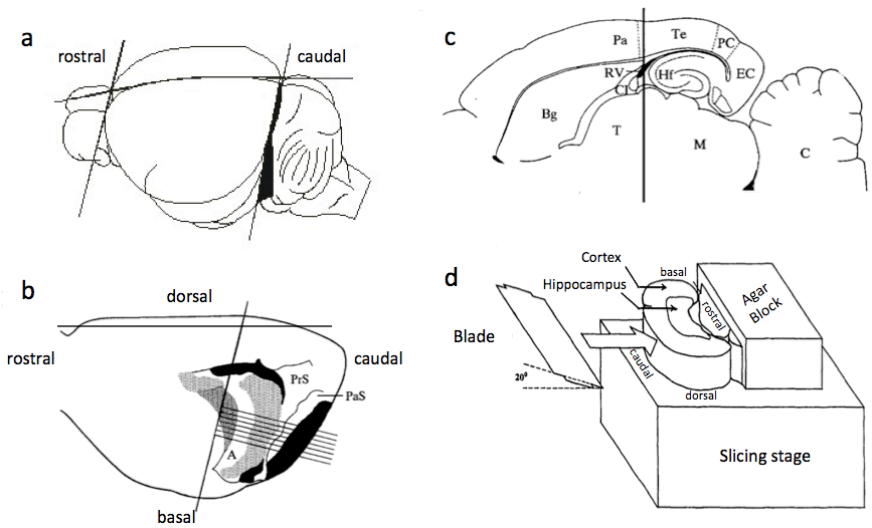

Figure 15 Preparation of horizontal combined hippocampal-entorhinal cortex slices. (a) Diagram of a rat brain in which the bold lines represent the cuts, which separate the olfactory bulbs and cerebellum from the cerebral hemispheres. (b) Medial view of the rat brain after removal of the mesencephalon and thalamus. A, cornu ammonis; PaS, parasubiculum;

PrS, presubiculum; light grey, dentate gyrus; medium grey, fimbria; dark grey, entorhinal cortex; black, subiculum. The bold lines indicate the cut which divides the two rostral thirds from the caudal third and the dorsal plane cut which allows the fixation onto the slicing stage. The slices are cut as indicated by the thin lines. (c) Anatomical relationships of the horizontal temporal lobe slice to neighboring structures in the intact brain. The bold line represents again the separation of the two rostral thirds from the caudal third. Bg, basal ganglia; C, cerebellum; CI, intern capsule; EC, entorhinal cortex; Hf, hippocampal formation; M, mesencephalon; Pa, parietal cortex; T, thalamus; Te, temporal cortex. (d) Arrangement of the agar and tissue blocks on the slicing stage (Adapted from Dreier and Heinemann 1991; Wang and Kass 1997).

A thin layer of cyanoacrylate glue (Continente, Portugal) was applied on the slicing stage of the vibratome (VT1000 S; Leica, Germany), to which an agar block was already mounted. Then the tissue was gently placed, with the help of a w-shaped piece of filter paper, with dorsal plane fixed onto the glue (**Figure 15**d). The slicing stage was transferred to the vibratome, and ice-cold ACSF was poured in and aerated with carbogen gas.

The vibratome section thickness was adjusted to 400 µm and the frequency of vibration to the maximum (9 Hz). Stainless steel razor blades (Gillette Platinum, UK) were cleaned with 75% ethanol and rinsed thoroughly with distilled water before use (Wang and Kass 1997).

Immediately after slicing, each slice was removed from the vibratome using a Pasteur pipette with the bulb placed over the narrow opening and stored in aerated ACSF (see **Figure 16**b). Eight to ten horizontal slices were cut, containing the temporal cortex area, the perirhinal cortex, the entorhinal cortex, the subiculum, the dentate gyrus, and the ventral hippocampus as illustrated in **Figure 16**a.

Slices were incubated in aerated ACSF at 35^{o}C for 30 minutes and then allowed to recover at room temperature (22-24^{o}C) for at least 60 to 90 minutes before starting the experiments. Thus, the recovery of swollen neurons and mitochondria, caused by ischemia and physical trauma during preparation was ensured (Heinemann, et al. 2006).

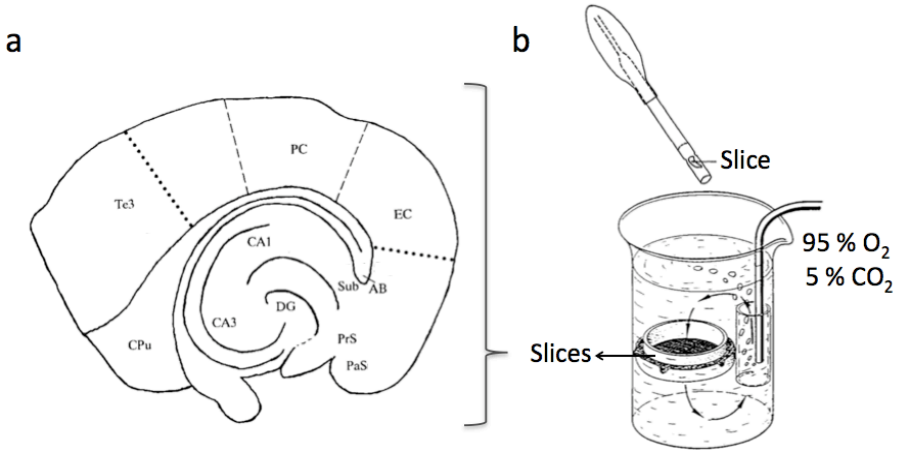

Figure 16 Horizontal hippocampal-entorhinal cortex combined slice and slices' storage. (a) Schematic representation of the horizontal temporal lobe slice preparation containing the hippocampal and parahippocampal areas and the

neocortical area Te3. The broken lines mark the borders of the different cortical areas. The dotted lines mark the laminar profiles. AB, angular bunble; CA1,3 Fields CA1,3 of Ammon's horn; CPu caudate putamen; DG, dentate gyrus; EC, entorhinal cortex; PC, perirhinal cortex; Sub, subiculum; Te3, temporal area 3. (b) Storage of hippocampal-entorhinal cortex combined slices in a 200 mL beaker containing ACSF bubbled with 95% O2 and 5% CO2. The bubbler is placed near the bottom of the tube the bubbles rise up the tube drawing solution with them and generating a current which flows down over the slices (adapted from Dreier and Heinemann 1991; Wang and Kass 1997; Gibb and Edwards 2006).

4.4.2 Extracellular recordings

After recovery slices were transferred to a Haas type interface chamber (Harvard Apparatus, Inc) and let to adapt for 20 minutes (Wang e Kass 1997). The floor of the chamber, which provides mechanical stability to the slices, was covered with lens cleaning paper (Kodak, USA).

The interface chamber was perfused continuously with aerated ACFS at 35^{o}C and at a rate of 2ml/min. A maximum of five slices were maintained in the interface chamber simultaneously. . Slices were perfused for approximately 3 hours, and then immediately deep frozen in liquid nitrogen for molecular analysis or incubated in paraformaldehyde (PFA) for immunohistochemistry assays (IHC).

Control slices (CTL) were perfused with regular ACSF. Regarding the experimental group, slices were perfused with free Mg^{2+} ACSF, containing (in mM): 124 NaCl, 5 KCl, 1.6 $CaCl_2$, 1.25 NaH_2PO_4, 26 $NaHCO_3$, and 10 glucose. The free Mg^{2+} ACSF, besides the absence of added Mg^{2+}, had slightly elevated K^+ concentration (5 mM vs 3 mM in regular ACSF). K^+ elevation increases excitability, making the induction of epileptiform activity easier and more reliable. After perfusion only slices that exhibit LRDs were kept for molecular analysis.

Recordings were performed with field potential recording electrodes positioned into the MEC; layer III/IV and stratum pyramidale of the hippocampal area CA1 (only one experiment).

Recording electrodes were made from borosilicate glass capillaries (1.5mm outer diameter, 0.86 mm inner diameter, Harvard Apparatus) in two stages on a pipette puller (P-87 Flaming/Brown Puller, Sutter Instruments Co., USA). The resistance of the recording pipettes was 2-6MΩ when filled with an internal solution of 4M NaCl.

Extracellular field potential recordings were amplified by Axoclamp 2B (Axon Instruments, NY, USA), digitized with a BNC-2110 (National Instruments, USA) and stored for subsequent analysis.

Data acquisition was carried out by WinLTP 0.96 (Anderson, 1991-2009) software program in continuous acquisition mode (Anderson and Collingridge 2007).

Viability of the slices was determined by external appearance of the slice or by the onset of epileptiform activity, in the case of free Mg^{2+} ACSF-perfused slices, since no adequate stimulation electrode (bipolar platinum wires) was available in the laboratory.

4.5 Molecular analysis

4.5.1 Whole tissue lysates

Frozen slices were placed in 300 µL of lysis buffer, containing 50 mM Tris base pH 8, 1 mM EDTA, 150 mM NaCl and 1% NP40; Fluka Biochemika, Switzerland), supplemented with protease inhibitors (Complete Mini-EDTA free, Roche, Germany)) and homogenized in a Potter-Elvehjem homogenizer with a Teflon piston. The suspension was left shaking for 15 min at 4°C. The insolubilized fraction was removed by centrifugation, 11000 g during 10 min at 4°C. The supernatant was collected and protein was quantified using the BioRad DC Protein assay Kit (Peterson 1979).

A similar procedure was applied to the primary hippocampal cultures, which were incubated with lysis buffer for 15 min on ice and then detached from the plates with a cell scraper. The cell suspension was incubated with slow agitation (15 min, 4°C), centrifuged (11000 g, 10 min, 4°C) and the solubilized protein was quantified.

4.5.2 Western blot

Samples (40µg total protein/lane), from both primary cultures and Hip-EC slices, and protein size marker (Precision Plus Protein Standards, Bio-Rad) were run on a standard 12% sodium dodecyl sulphate polyacrylamide gel electrophoresis (SDS-PAGE) and transferred to nitrocellulose membranes (Amersham). After blocking for 1 hr with 5% non-fat powder milk in TBS-T (20 mM Tris base, 137 mM NaCl and 0.1% Tween-20), membranes were probed with the primary antibodies listed on **Table 3**, and incubated overnight at 4°C.

Incubation with goat anti-mouse or goat anti-rabbit horseradish peroxidase (HRP)-conjugated secondary antibodies (1:10000, Santa Cruz Biotechnology) was performed at room temperature, for 1 hour.

Development of signal intensity was done using the ECL Plus Western Blotting Detection System (Amersham-ECL Western Blotting Detection Reagents, GE Healthcare, UK) and quantifications were attained by densitometric scanning of the films, performed with the Image J software 1.44b (http://rsbweb.nih.gov/ij/). α-Tubulin density was used as a loading control.

Table 3 Primary antibodies and related conditions used in the Western blot experiments. Primary antibodies were diluted in 3% Bovine Serum Albumin with 0.02% NaN_3.

Protein	Primary antibody, Cat. Nº	Host	Dilution
GlyR	Synaptic Systems (146011)	Mouse	1:250
GABAR β 2/3	Upstate (05-474)	Rabbit	1:1000
Gephyrin	Synaptic Systems (147003)	Mouse	1:5000

Protein	Primary antibody, Cat. Nº	Host	Dilution
GluR1	Millipore (AB1504)	Rabbit	1:1000
NR2B total	Cell Signaling (4212)	Rabbit	1:1000
NR1	Millipore	Mouse	1:500
Synaptophysin	Sigma (S5768)	Mouse	1:1000
α-Tubulin	Abcam (ab4074)	Rabbit	1:2000

Abbreviations: GlyR – Glycine Receptor; GABA β 2/3 – GABA receptor subunit β 2/3; GluR1 – Glutamate receptor 1; NR2B – NMDA receptor subunit 2B; NR1 – NMDA receptor subunit 1.

4.5.3 RNA isolation and quantification

RNA was isolated from combined Hip-EC slices according to the GE Healthcare RNAspin Mini RNA Isolation Kit. Slices, previously frozen, were homogenized with 300 µl Kit's lysis buffer (RA1) in a Potter-Elvehjem homogenizer with a Teflon piston.

RNA concentration was accurately determined using Nanodrop 1000 (ND-1000 Spectrophotometer, Thermo Scientific). The integrity of total RNA was confirmed in 3% agarose gel electrophoresis in TAE buffer (40 mM Tris-acetate, 1 mM EDTA).

4.5.4 Reverse transcription reaction

In vitro reverse transcription (RT) was performed from 3 µg of total RNA according to the SuperScript First Strand Synthesis Systems Kit (Invitrogen). Two reaction mixes were prepared: 1) RNA mix containing 4,2 ng/µL of random primers, 0,8 mM dNTPs and 3 µg of RNA extracted from CTL or free Mg^{2+} ACSF-perfused slices, in a total volume of 12 µL; 2) SuperScript mix containing 12,5 mM $MgCl_2$, 25 mM DTT and SuperScript II reverse transcriptase buffer in a total volume of 8 µL. RT-PCR was carried out in a thermoclycler (MyCycler – Bio-Rad). RNA mix was heated for 5 min at 65^{o}C and chilled for 2 min at 4^{o}C, followed by the addition of the SuperScript mix. When temperature reached 25^{o}C, 100 units of SuperScript II Reverse Transcriptase (EC 2.7.7.49, Invitrogen) was added followed by 60 min at 42^{o}C (optimal SuperScript II temperature). Reaction was terminated by inactivating the enzyme for 20 min at 72^{o}C.

For each RNA sample a reverse transcription reaction was carried out in the absence of reverse transcriptase, named -RT control, in order to ensure that product amplification did not arise from genomic DNA.

4.5.5 Quantitative real-time PCR (qPCR)

cDNA amplification was performed in a Rotor-Gene 6000 real-time rotary analyzer thermocycler (Corbett Life Science, Hilden, Germany) in the presence of SYBR Green Master Mix (Applied

Biosystems, Foster City, CA, USA) and 0.2 µM of each specific gene primer (**Table 4**). The PCR conditions included an initial denaturation for 2 min at 94ºC, 50 cycles with 30 s at 94ºC, 90 s at 60ºC and 60 s at 72ºC, followed by a melting curve to assess the specificity of the reactions. The threshold cycle (Ct) and the melting curves (**Figure 27**-**Figure 33**) were acquired with Rotor-Gene 6000 Software 1.7 (Corbett Life Science). In order to determine the PCR efficiency (E) for each gene, which is needed for the relative quantification by comparative Pfaffl method (see Section 3.3), a qPCR with cDNA samples from 5-fold sequential dilutions of a CTL cDNA was performed for each set of primers. Ultimately, the relative qPCR establishes the cDNA expression level by normalization with an internal control gene. Normalization of target gene expression is useful in order to compensate sample-to-sample and run-to-run variations and to ensure the experimental reliability. In all experiments β-actin was used as a reference internal gene. For each gene, replica reactions were performed and the mean of the two reactions was used to calculate the corresponding expression level. Two types of negative controls, "no reverse transcription" and "no template", were run with samples.

Table 4 Primers used in qPCR. All primers were purchased from Invitrogen.

Gene	Primer Sequence	Melting Temperature Tm (ºC)	Size (pb)
β-Actin	Forward: AGCCATGTACGTAGCCATCC	62	228
	Reverse: CTCTCAGCTGTGGTGGTGAA	62	
GlyR α1	Forward: ACTCTGCGATTCTACCTTTGG	64	300
	Reverse: ATATTCATTGTAGGCGAGACGG	68	
GlyR α2	Forward: CAGAGTTCAGGTTCCAGGG	54	330
	Reverse: TCCACAAACTTCTTCTTGATAG	49	
GlyR α3	Forward: GTGAGACACTTTCGGACACTAC	55	353
	Reverse: GATGGGTCGAGGTCTAATGAATC	55	
GlyR β	Forward: CTGTTCATATCAAGCACTTTGC	51	223
	Reverse: GGGATGACAGGCTTGGCAG	55	
GlyT1	Forward: CTGGAGGCTGTATGTGCTGA	54	439
	Reverse: GATGACGAAGCCAGCATAGA	52	
GlyT2	Forward: TCCGTCCTCATAGCCATCTA	51	278
	Reverse: T CACTCCCGCTGACAAATG	52	

Abbreviations: Tm = (°C) = 2x(C+G)+4x(A+T); GlyR – Glycine receptor; GlyT – Glycine transporter.

4.6 Statistics

The values presented are mean ± SEM of *n* experiments. To test the significance of the differences between CTR and LRD groups, a paired Student's *t* test was used; Unpaired Student's *t* test was applied when comparing between 30 min and 1-hour treated cultures; One-way ANOVA followed by Bonferroni's post hoc test was used for comparison between multiple experimental conditions in the enriched neuronal model of acquired epilepsy. Values of $p<0.05$ were considered to be statistically significant. Analyses were conducted with the GraphPad Software.

5 RESULTS

5.1 Characterization of Hippocampal neuronal culture model of acquired epilepsy (AE)

Rationale: Hippocampal low-density neuronal cultures are far less complex than neural tissue, while maintaining key phenotypic features of pyramidal neurons. This trait, along with the fact that living neurons are accessible to observation and manipulation, make it ideally suited to characterize biochemical, electrophysiological and molecular mechanisms underlying the development and maintenance of the "epileptic" condition. Exposure to Mg^{2+} free media leads to the development of spontaneous recurrent epileptiform discharges (SREDs) in mixed neuronal/astrocytic cultures (Sombati and DeLorenzo 1995). A 3-hour exposure to Mg^{2+} free environment is reported to result in permanent alteration of neuronal culture physiology, and even upon reintroduction to regular Mg^{2+} containing media cultures continue to express SREDs (Blair, et al. 2006). This *in vitro* model of acquired epilepsy (AE) can be a powerful tool when unravelling the potential role of glycinergic transmission markers, as inhibition mediators, in a hyperexcitability condition such as epilepsy.

The work described below was designed to establish an *in vitro* model of acquired epilepsy in neuronal enriched cultures and address the alteration in the protein expression pattern associated with the "epileptic" condition.

5.1.1 Epileptiform discharges in hippocampal neuronal cultures

Ten-day-old primary hippocampal cultures, kept in NB-B27, were subjected to different times of exposure to Mg^{2+} free solution (pBRS), in order to assess the efficiency of induction of an "epileptic" condition. After exposure, cultures were returned to NB-B27 at 37ºC and 5% CO_2/95% O_2 atmosphere.

Whole cell current clamp recordings performed at day 15 in culture showed that exposure to Mg^{2+} free solution for 30 min was unable to consistently induce epileptiform discharges, since only a subset (12.5%) of the neurons recorded displayed an epileptic phenotype, characterized by epileptic discharges with a mean frequency of 0.1818 ± 0.054 Hz or 11 ± 3 events per min, an amplitude of 59.240 ± 17.910 mV and a duration of 3.333 ± 0.335 ms (n=3).

The resting membrane potential from the "epileptic" neurons (-39.00 ± 1.000 mV, n=3) was significantly higher (13.15 ± 3.865, p<0.005) than the one observed from the neurons that did not develop an "epileptic" condition (-25.85 ± 1.462 mV, n=21) – see **Figure 17**.

The mean value of resting membrane potentials in all neurons recorded from 30 min Mg^{2+} free treated cultures was -27.57 ± 1.584 mV (n=24).

In contrast, 1-hour exposure to Mg^{2+} free solution was able to more reliably (20% of the recorded neurons) induce high-frequency burst discharges, characterized by a frequency of 0.3591 ± 0.1275 Hz or 22 ± 8 events per min, an amplitude of 70.119 ± 15.370 mV and a duration of 2.105 ± 0.335 ms (n=3).

Figure 18 illustrates a 1 min recording from a neuron after 1-hour of exposure to free Mg^{2+}. This hyperexcitable state consisted of repetitive individual burst discharges of which each burst comprises multiple spikes that overlay a depolarization shift. The mean value of membrane potentials in all neurons recorded from 1-hour Mg^{2+} free treated cultures was -31.14 ± 2.656 mV (n=15). There was no significant difference in membrane potential between neurons that developed an "epileptic" condition (-36.00 ± 1.000 mV, n=3) and the ones that did not (-30.33 ± 3.048 mV, n=12).

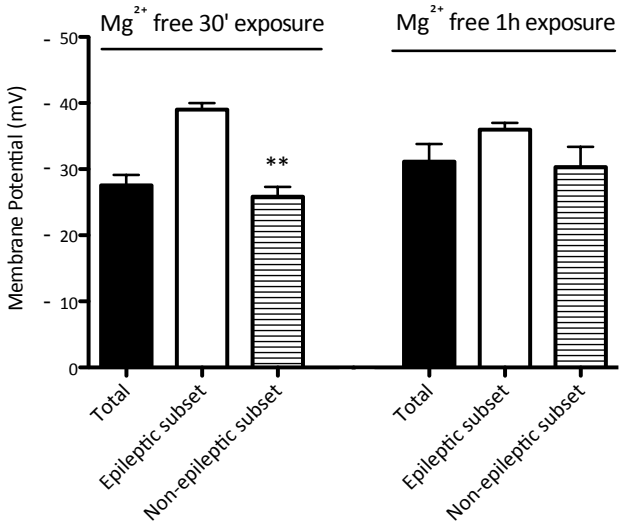

Figure 17 Resting membrane potential of recorded neurons exposed to 30 min and 1 hour of free Mg^{2+} solution. Of all the neurons recorded, which were exposed to free Mg^{2+} solution only a subset of neurons developed epileptiform activity (white bar), either in 30 min (n=3 in a total of 24) or 1 hour (n=3 in a total of 15) treatments. All values are mean ± SEM. **p<0.005 non-paired t-student

When comparing resting membrane potentials from 30 min and 1-hour Mg^{2+} free treated cultures no statistically significant difference was found (3.578 ± 2.895, p>0.05).

Whole cell current clamp recordings from age-matched (15 DIC) sham control neurons, for both 30 min and 1-hour exposures with Mg^{2+}-containing pBRS, showed baseline activity with occasional spontaneous miniature activity (**Figure 18**a).

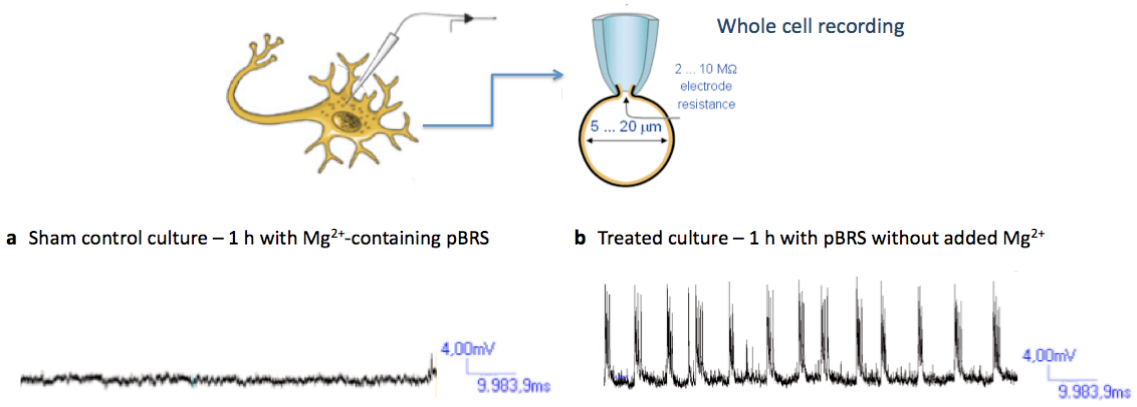

Figure 18 Induction of epileptiform activity following 1-h exposure of hippocampal neuronal cultures to free Mg^{2+} media. Whole cell recordings in current clamp mode were obtained from pyramidal neurons 5 days following the exposure to either Mg^{2+}-containing pBRS (sham control) or free Mg^{2+} pBRS (treated culture). (a) Recording from a representative control neuron displaying miniature spontaneous activity. (b) Recording from a representative "epileptic" neuron, characterised by tonic high-frequency epileptiform burst activity.

Although a subset of neurons displayed epileptiform burst activity, the number of neurons per culture that developed an "epileptic" condition after 1-hour exposure to Mg^{2+} free solution was still low and difficult to reproduce in different cultures. It was also detected substantial variability in terms of discharge frequency in the neurons that depicted the epileptic phenotype.

2- and 3-hour exposure periods, as described in the literature (Sombati and DeLorenzo 1995), were also attempted. However electrophysiological or molecular characterization studies were not possible to perform, due to the considerable neuronal death induced in both sham control and treated cultures (data not shown). These results might have been potentiated by general health-related culture issues.

This model proofed to be extremely difficult to establish, since it was variable and not reproducible both in terms of electrophysiological recordings and cellular death.

5.1.2 Protein expression pattern in control and free Mg^{2+}-treated hippocampal neuronal cultures

To evaluate temporal changes in the protein expression profile, western blot analysis at different time points during the life of the culture were performed. Cultures were kept in NB-B27 media

until day 10 in culture. At this time point cultures were exposed to both free Mg^{2+} and Mg^{2+}-containing (sham control) media during 30 min and 1 h and returned to NB-B27. Whole cell lysates were prepared at 15 DIC after electrophysiological experiments. For comparison and positive control, spinal cord homogenates were also analysed (data not shown).

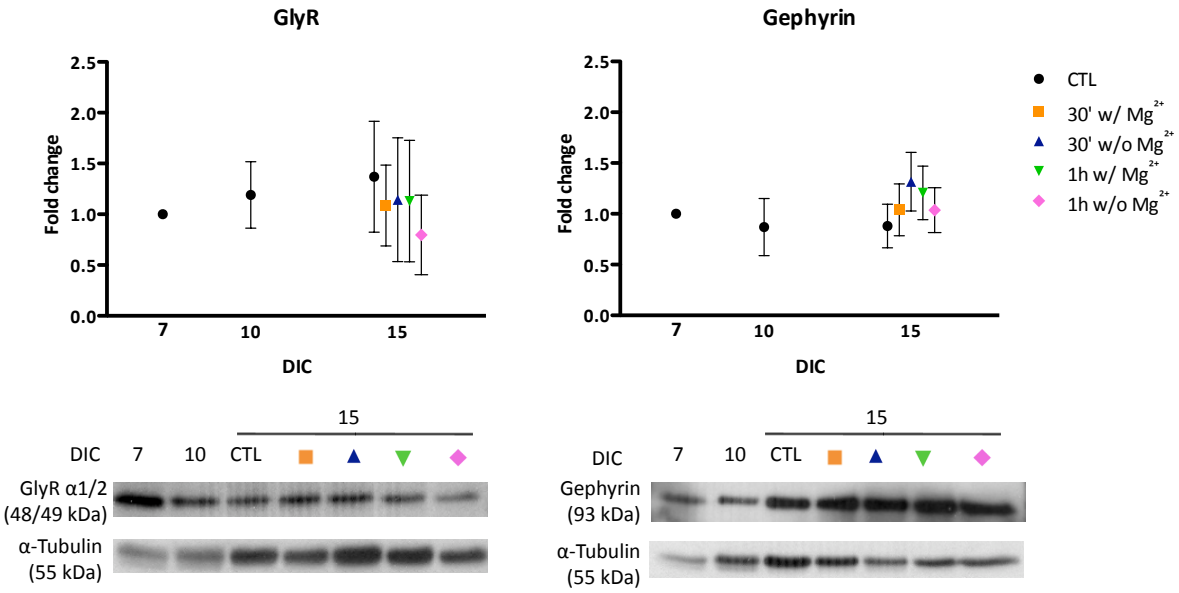

Figure 19 Time course of protein expression of glycine receptor and gephyrin during the period of maintenance of the hippocampal neuronal cultures. Levels of protein expression were assessed at day 7, 10 and 15 in culture from neurons exposed to 30 minutes or 1 hour to either Mg^{2+}-containing pBRS or free Mg^{2+} pBRS. The upper left panel shows glycine receptor expression levels (n=3) at three different time points in culture in NB-B27 medium (CTL) and at day 15 after different exposure periods to pBRS. The upper right panel displays gephyrin expression levels (n=3) at three different time points in cultures in NB-B27 medium (CTL) and at day 15 after different exposure periods to pBRS. Graphs' legend: black circle – CTL: NB-B27 medium; yellow square – 30 minutes with pBRS with Mg^{2+} (sham control); blue triangle – 30 minutes with pBRS without added Mg^{2+}; green triangle – 1 hour with pBRS with Mg^{2+} (sham control); pink diamond – 1 hour with pBRS without added Mg^{2+}; Lower panels show representative Western Blots. α-Tubulin was used as a loading control (bottom lanes). Values are average GlyR and Gephyrin immunoreactivity, normalized to α-tubulin. All values are mean ± SEM.

As shown in **Figure 19**, glycine receptor immunoreactivity remained unchanged throughout the cultures' life, even when neurons were exposed to Mg^{2+} free media.

Regarding gephyrin protein levels, no significant change was observed, since immunoreactivity values remained constant at each time point in all conditions tested - **Figure 19**, right panel.

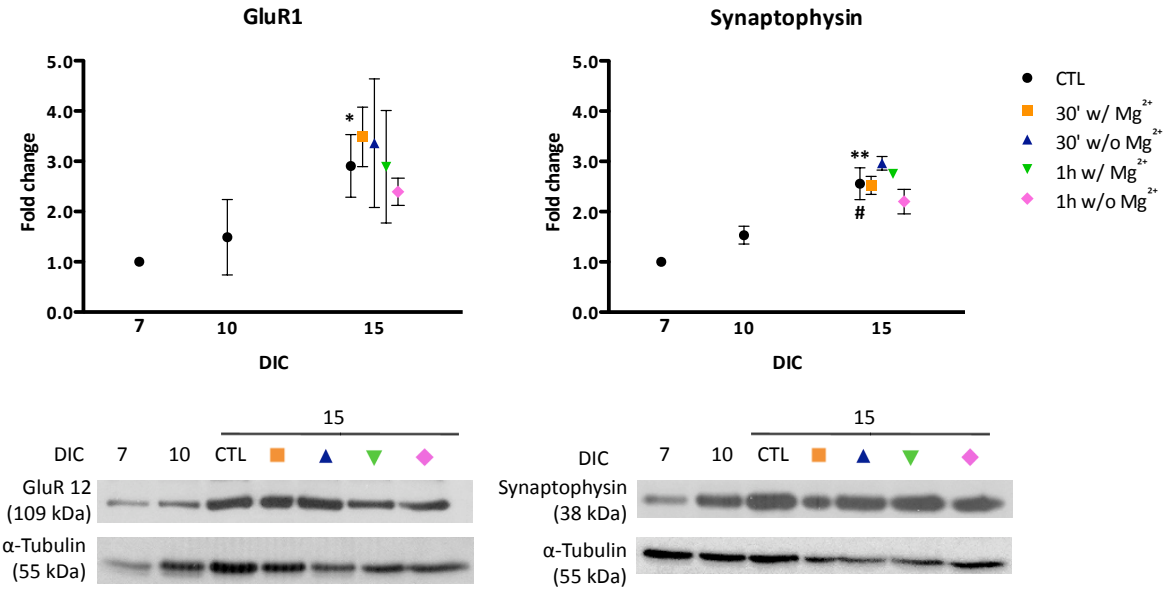

Figure 20 Time course of protein expression of AMPA receptor GluR1 subunit and synaptophysin during the period of maintenance of the hippocampal neuronal cultures. Levels of protein expression were assessed at day 7, 10 and 15 in culture from neurons exposed to 30 minutes or 1 hour to either Mg^{2+}-containing pBRS or free Mg^{2+} pBRS. The upper left panel shows AMPA receptor subunit expression levels (n=3) at three different time points in cultures in NB-B27 medium (CTL) and at day 15 after different exposure periods to pBRS. The upper right panel displays synaptophysin expression levels (n=3) at three different time points in cultures in NB-B27 medium (CTL) and at day 15 after different exposure periods to pBRS. Graphs' legend: black circle – CTL: NB-B27 medium; yellow square – 30 minutes with pBRS with Mg^{2+} (sham control); blue triangle – 30 minutes with pBRS without added Mg^{2+}; green triangle – 1 hour with pBRS with Mg^{2+} (sham control); pink diamond – 1 hour with pBRS without added Mg^{2+};
Lower panels show representative Western Blots. α-Tubulin was used as a loading control (bottom lanes). Values are average GluR1 and Synaptophysin immunoreactivity, normalized to α-tubulin. All values are mean ± SEM. *p<0.05; **p<0.005; one-way ANOVA followed by Bonferroni´s multiple comparison test, in comparison to 7 DIC. #p<0.05; one-way ANOVA followed by Bonferroni´s multiple comparison test, in comparison to 10 DIC.

On the other hand, AMPA receptor subunit, GluR1, protein levels, displayed at day 15 a significant increase in control conditions by 1.907 ± 0.3595 fold (n=3, p<0.05) when compared to 7 DIC. However none of the experimental conditions showed significant difference with respect to control culture conditions at the same time point (15 DIC).

When evaluating synaptophysin expression, a significant increase was observed at day 15 in culture in CTL conditions with respect to day 7 and 10 in culture, respectively. But once more, synaptophysin immunoreactivity at 15 DIC in experimental conditions did not change when compared to control conditions at 15 DIC (**Figure 20**, right panel).

Western blot experiments were performed only in three cultures (n=3) since, as referred previously, setting up the AE model was problematical, and healthy and functional cultures were not obtained in the laboratory for some time.

The lack of reliability and reproducibility when assessing both electrophysiological (see section 5.1.1) and molecular parameters led to the discard of the AE model in primary hippocampal cultures.

5.2 *In vitro* model of epileptiform activity in combined hippocampal-entorhinal cortex slices

Rationale: Complex slice preparations, which partly preserve inter-area connectivity, have been extensively used for experimental epilepsy studies. Namely, combined hippocampal-entorhinal cortex (Hip-EC) slices, since the EC is the main source of afferents to the hippocampus. Spontaneous epileptiform activity in the Hip-EC slice can be induced by lowering the extracellular Mg^{2+} concentration (Mody, et al. 1987, Dreier and Heinemann 1991). Reducing Mg^{2+} levels exerts convulsant effects by decreasing surface charge screening, increasing transmitter release, and unblocking NMDA receptors without any pharmacologic effect at GlyR. This model is particularly relevant given that low levels of Mg^{2+} have been associated with human epilepsy (Durlach 1967).

Since the development of epilepsy is thought to be associated with impaired neuronal inhibition, several AEDs have been developed targeting the major inhibitory system in the brain, GABAergic inhibition.

Recent findings, have demonstrated that GlyR, which were thought to operate only in the spinal cord and brainstem, are also functionally expressed in the cortex and the hippocampus (Danglot, et al. 2004, Zhang, et al. 2008, Aroeira, et al. 2011). Further evidence emerged that glycine and other GlyR agonists exert a GlyR-mediated antiepileptic effect (Chattipakorn and McMahon 2003, Kirchner, et al. 2003). This is of great appeal, giving the high number of epilepsy patients who are resilient to GABAergic transmission targeting drugs.

Therefore glycinergic transmission may serve as an alternative pharmacological target for controlling abnormal hyperexcitability associated with epileptiform activity.

As a first step towards elucidating the molecular mechanisms underlying the role of the glycinergic inhibitory system in hyperexcitability disorders, such as epilepsy, mRNA and protein expression studies were conducted using the free Mg^{2+} model of pharmacoresistant epileptiform activity.

5.2.1 Types of in epileptiform activity elicited by free Mg^{2+} ACSF in combined hippocampal-entorhinal cortex slices.

Three typical patterns of free Mg^{2+}-induced epileptiform discharges were observed in combined hippocampal-entorhinal cortex slices, as already described (Dreier and Heinemann 1991).

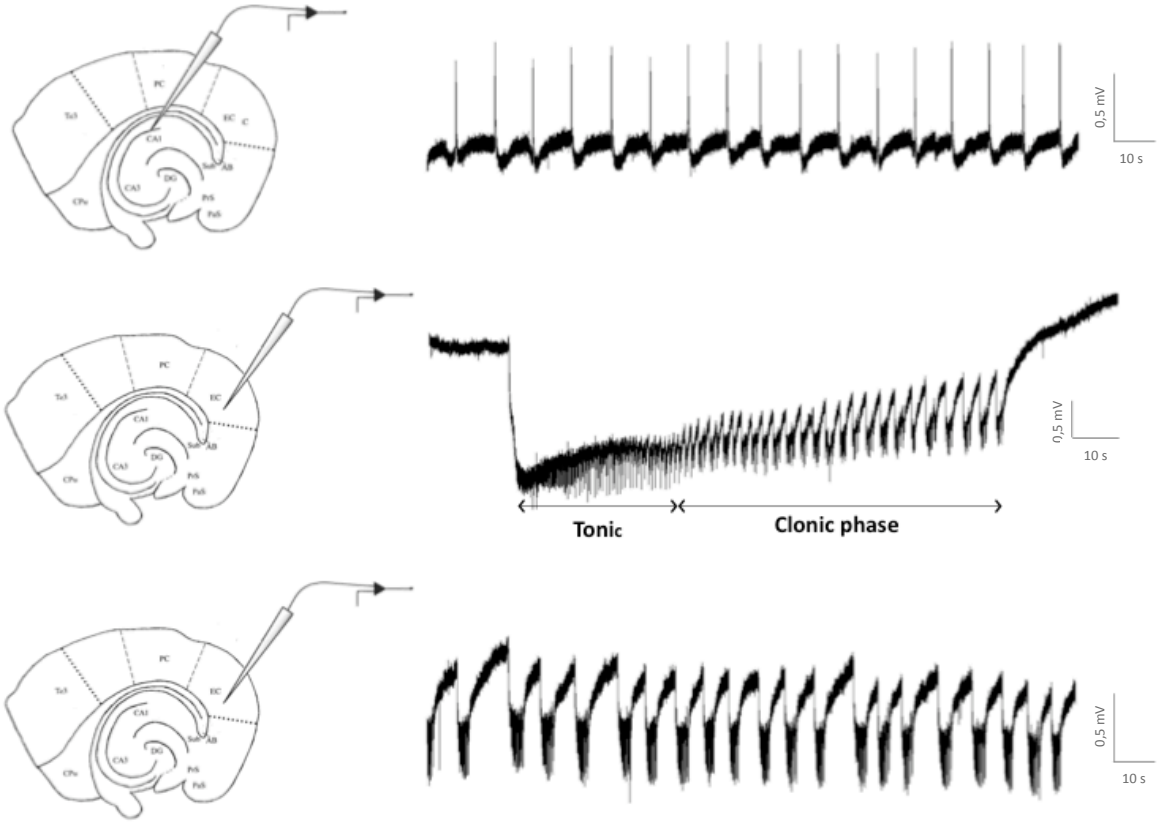

Figure 21 Spontaneous epileptiform activity induced by continuous bath application of free Mg^{2+} ACSF in combined hippocampal-entorhinal slices. Non-simultaneous field potential recordings were made in area CA1 of the hippocampus and the MEC. Field potentials in the hippocampus (upper trace) show positive going recurrent short discharges (RSDs) at high frequency, whereas the recordings in the MEC (midle trace) display a negative-going seizure-like event (SLE), lasting more than 30 s, with a tonic initial phase, and a clonic later phase. The lower trace illustrates a representative recording of late recurrent discharges (LRDs), which typically develop after SLEs.

Removing the Mg^{2+} from the ACSF allows NMDA receptors to respond directly to glutamate stimulus, which results in increased neuronal excitability. Initially the events are sensitive to application of NMDA antagonists, however these may lose their efficacy with increasing time after application of free-Mg^{2+} ACSF (Heinemann, et al. 2006).

In the hippocampus, particularly CA1, recurrent short discharges (RSDs) with a frequency of 14 ± 3 per min (0.215 ± 0.04245 Hz, n=1) were observed (**Figure 21**, upper trace). RSDs exhibited duration of 45.46 ± 0.3269 ms and an amplitude of 0.8331 ± 0.0152 mV (n=1). Due to the lack of recording electrodes, it was not possible to record from more than one area simultaneously.

The first activity to appear in the MEC, layer III/IV, were seizure-like events (SLEs), as illustrated in **Figure 21**, middle trace. These consisted of a negative potential shift superimposed by high frequency, small-amplitude oscillations, field potential transients (tonic-like period) followed by a period in which clonic-like afterdischarges occurred. SLEs had a frequency of 6 ± 1 per 15 min (0.0075 ± 0.0008660 Hz, n=4), could last up to 64 s (46.800 ± 7.154 s, n=4) and exhibited a mean amplitude of 2.241 ± 0.3933 mV (n=4).

After 2 to 3 hours exposure to Mg^{2+}-free ACSF, SLEs were eventually replaced by a state where only short-lasting, high frequency discharges recurred. This transition usually occurs by an increase in frequency of the tonic clonic SLEs that gradually progresses to the state of recurrent tonic episodes (data not shown).

LRDs developed in the MEC consisting of negative field potential transients with duration of 1–3 s (2.796 ± 4.038 s, n=38) and a frequency of 16 ± 3 *per min* (0.2597 ± 0.04449 Hz, n=38). Although not tested in our laboratory it is described that this activity is pharmacoresistant to the standard anticonvulsants (Dreier, et al. 1998). As so it can serve as an *in vitro* model for pharmacoresistant epileptiform activity. LRDs displayed a mean amplitude of 1.111 ± 0.06615 mV (n=38).

These discharges are also reminiscent in frequency and morphology to electrographic activity in the EEG during later stages of status epilepticus both in animal and humans (Dreier and Heinemann 1991).

5.2.2 Epileptiform activity modifies glycine receptor mRNA levels

A transcript expression analysis was carried out in order to thoroughly study the effect of pharmacoresistant epileptic activity, mimicked *in vitro* by free Mg^{2+} induced LRDs, in the glycinergic transmission effectors. Specifically, mRNA expression of GlyR subunits (α1, α2, α3 and β) and glycine transporters 1 and 2 (GlyT1-2) in combined hippocampal-entorhinal slices exposed to free Mg^{2+} ACSF or regular ACSF was studied by RT-qPCR with specific oligonucleotide primers.

No PCR products were detected using cDNA synthesized in the absence of reverse transcriptase (–RT control) which ensured that amplification did not arise from contaminating genomic DNA. Furthermore, negative controls showed no signal amplification, which implies absence of genomic DNA, external contamination or other factors that could originate a non-specific increase in the fluorescence signal (data not shown).

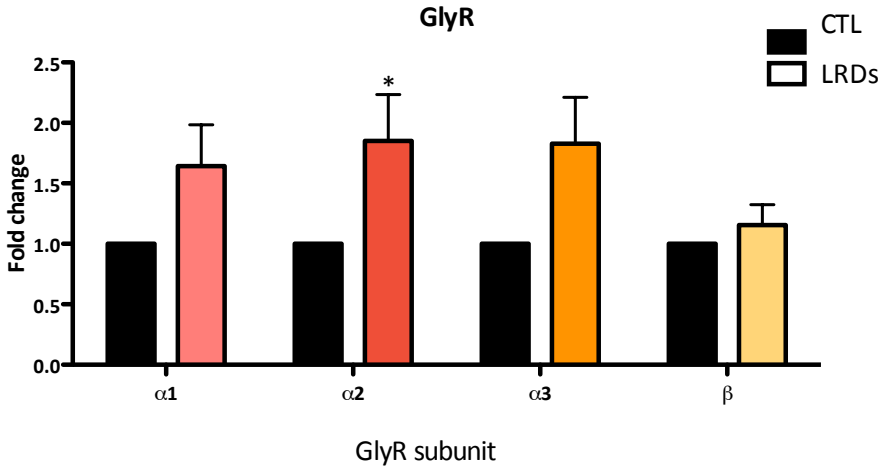

Figure 22 Transcript expression profile of glycine receptor (GlyR) subunits α1-3 and β. Composition analysis of GlyR subunit mRNAs in control (CTL) and free Mg^{2+} induced late recurrent discharges (LRDs) in combined hippocampal-entorhinal slices by relative qPCR. All values are mean ± SEM. n=6 *p < 0.05, paired t-student.

Glycine receptor subunits mRNA levels exhibited a general trend to be increased in slices displaying LRDs in respect to control slices (**Figure 22**).

Glycine receptor α2 subunit in particular, showed significant increase of 1.136 ± 0.3157 fold (n=6, p<0.05) associated with the epileptic phenotype.

Although not statistically significant, a substantial increase in α3 subunit transcript was also observed (1.006 ± 0.4154, n=6, p=0.0726) in the "epileptic" slices. The mRNA expression of the remaining subunits, α1 and β, tended to be increased but no significance was shown, p=0.1209 and p=0.4011, respectively.

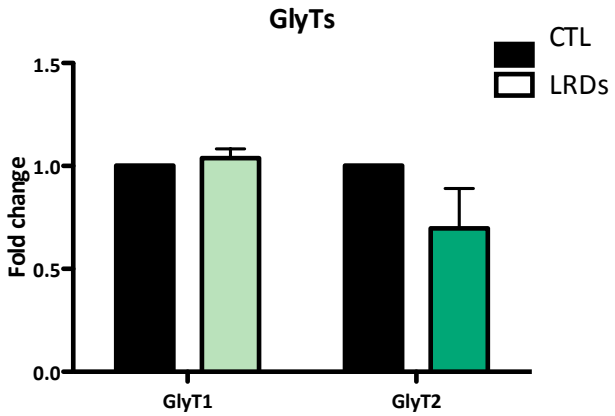

Figure 23 Transcript expression profile of glycine transporters 1 and 2 (GlyT1 and GlyT2). Composition analysis of GlyT1 and GlyT2 mRNAs in control (CTL) and free Mg^{2+} induced late recurrent discharges (LRDs) in combined hippocampal-entorhinal slices by relative qPCR. All values are mean ± SEM. n=6 (GlyT1), n=3 (GlyT2).

Glycine transporters transcript expression was also addressed, as shown in **Figure 23**. GlyT1 transcript levels were not altered by the occurrence of LRDS in combined hippocampal-entorhinal

slices. Conversely GlyT2 transcript profile revealed that slices exhibiting epileptiform discharges appear to have lower mRNA levels (0.3033 ± 0.1943, n=3, p=0.2588), when compared to control slices.

5.2.3 Protein expression pattern in combined hippocampal-entorhinal slices exhibiting late recurrent discharges (LRDs)

Western blot analysis, as a relative measure of protein expression, provides the protein composition in the system of choice. As epilepsy is thought to be related to an imbalance between excitation and inhibition, both excitatory and inhibitory transmission mediators were evaluated.

To assess total GlyR protein expression in combined hippocampal-entorhinal slices, a GlyR specific antibody (mAb4a) was used for western blot analysis (Pfeiffer, et al. 1984). mAb4a antibody identified a double band of 48–49 kDa, which corresponds to the molecular weight of GlyR α1 and α2 subunits (**Figure 24**, right panel). This double band pattern was consistently obtained in every blot, however most reports describe a single band (Danglot, et al. 2004). For comparison and positive control, spinal cord homogenates were also analysed (data not shown).

Densitometry analysis of western blots, shown in **Figure 24**, revealed no significant changes regarding GlyR protein levels. However an increasing tendency of the α2 subunit is evident (0.170 ± 0.1570, n=6, p=0.3283) in slices displaying LRDs.

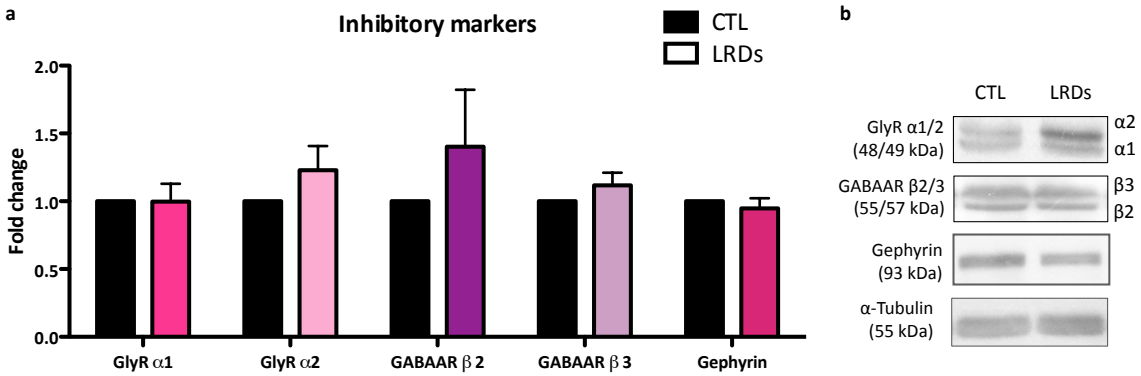

Figure 24 Expression of inhibitory markers in control slices and slices exhibiting free Mg^{2+} induced late recurrent discharges (LRDs). (a) Densitometry analysis of western blots. (b) Representative western blots obtained from control (CTL) slices (left lane) and from slices exhibiting LRDs (right lane). α-tubulin was used as a loading control (bottom lanes). Values are average GlyRα1/2, $GABA_AR$ β2/3 and Gephyrin (n=6) immunoreactivity, normalized to α-tubulin. * $p<0.05$; two-tailed paired Student's t-test.

Concerning $GABA_A$ receptor β2 and β3 subunits, which are known to regulate receptor trafficking, membrane insertion and surface stability (Michels and Moss 2007), no significant changes associated with LRDs onset were observed, even though a minor increasing trend was apparent (**Figure 24**).

Additionally, gephyrin immunoreactivity also remained unchanged in free Mg^{2+} perfused slices when compared to CTL slices. This post-synaptic protein plays an essential role in the recruitment of both inhibitory GlyR and $GABA_AR$ (Fritschy, et al. 2008).

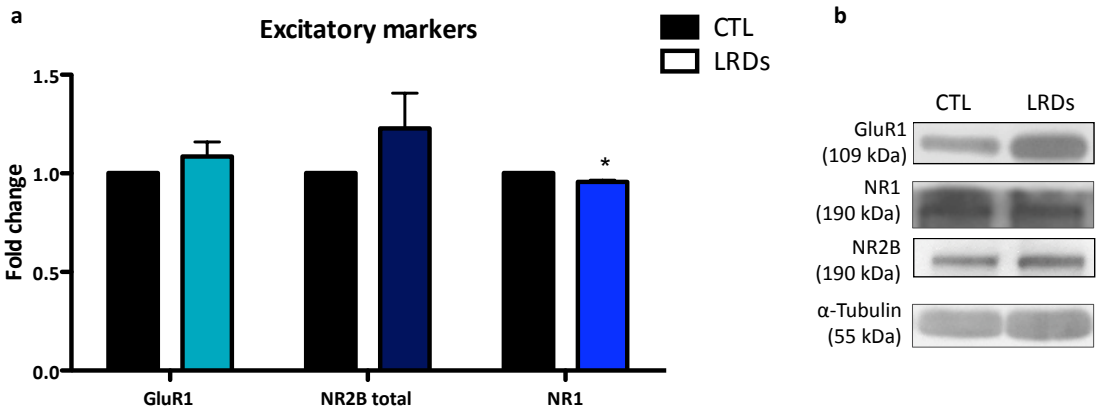

Figure 25 Expression of excitatory markers in control slices and slices exhibiting free Mg^{2+} induced late recurrent discharges (LRDs). (a) Densitometry analysis of western blots. (b) Representative western blots obtained from control (CTL) slices (left lane) and from slices exhibiting LRDs (right lane). α-tubulin was used as a loading control (bottom lanes). Values are average GluR1, NR2B total (n=6) and NR1 (n=3) immunoreactivity, normalized to α-tubulin. * $p<0.05$; two-tailed paired Student's t-test.

Besides inhibitory transmission related proteins, excitatory receptors were evaluated, namely two main glutamate receptor families, AMPA and NMDA receptors (see **Figure 25**), which play a pivotal role in the regulation of synaptic function and neuronal communication in the CNS.

Regarding, GluR1-containing AMPAR, which are predominantly located extrasynaptically in CA1 pyramidal neurons (Andràsfalvy, et al. 2003), no significant difference was found between CTL and LRDs conditions.

Moreover, NR2B subunit, that is almost exclusively found in extrasynaptic NMDAR (Köhr 2006), did not sustain any expression variation associated with epileptiform activity.

In contrast, glycine-binding NR1 subunit protein levels were significantly lower in slices that exhibited the epileptic phenotype (0.0433 ± 0.00882, n=3, $p<0.05$), as shown in **Figure 25**. The significance may dissolve with more experiments, since the difference between means is reduced.

Lastly, densitometry analysis for synaptic vesicle membrane protein, synaptophysin I, revealed no significant difference (**Figure 26**). Notwithstanding, a three hours period was probably insufficient to show any signs of synapse formation or elimination.

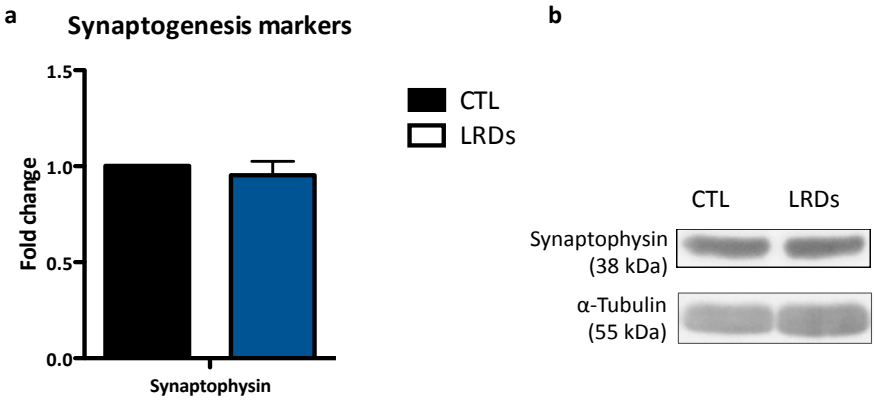

Figure 26 Expression of synaptogenesis marker in control slices and slices exhibiting free Mg^{2+} induced late recurrent discharges (LRDs). (a) Densitometry analysis of western blots. (b) Representative western blots obtained from control (CTL) slices (left lane) and from slices exhibiting LRDs (right lane). α-tubulin was used as a loading control (bottom lanes). Values are average synaptophysin (n=6) immunoreactivity, normalized to α-tubulin.

6 DISCUSSION

6.1 Hippocampal neuronal culture model of epileptiform discharges

Neuronal cultures possess engaging attributes, since they are far simpler than living tissue but are still able to preserve basic neuronal properties (Kaech and Banker 2006). Although the intrinsic circuitry properties of neuronal cultures have not been extensively studied, it is known that cultured neurons tend to have a bursting behaviour (Dichter and Pollard 2006). DeLorenzo and colleagues took advantage of this synchronous activation and enhanced it by exposing mixed astroglial/neuronal cultures to free Mg^{2+} solution (Sombati and DeLorenzo 1995).

In the attempt of establishing this system, one main methodological modification was employed. Primary hippocampal neuronal cultures were used since one aimed to analyze the neuronal expression pattern associated with the epileptic-like phenotype.

Two exposure periods to free Mg^{2+}, 30 min and 1 hour, were applied. Even though the 1-hour treatment was able to induce epileptiform discharges in about 20% of the recorded neurons, 1.6 times more than 30 min exposure, none of the exposure times induced permanent changes at network level consistent with the 90% efficiency described in the literature (Sombati and DeLorenzo 1995; DeLorenzo, et al. 1998).

The epileptiform discharges exhibited different electrographic features when compared to the SREDs, typically associated with the AE model. SREDs, which are spontaneous recurrent electrographic seizure-like discharges, have durations of 1 to 2 min and occur at frequencies of up to 2–4 episodes every hour, and are intercalated by interictal discharges (Blair, et al. 2006). Instead, the activity recorded resembles the epileptiform bursts described in the *status epilepticus* (SE) model also developed by the DeLorenzo's group. This model encompasses the time frame immediately after and the 9 hours following the free Mg^{2+} treatment. Afterward discharges frequency start to decrease and the activity evolves to SREDs.

Epileptiform discharges obtained in the present study had duration amplitude and overall waveform consistent with the SE discharges, which are characterized by repetitive and continuous burst discharges. Each burst was comprised of multiple spikes overlaying a depolarization shift comparable to those observed *in vivo* during SE (Deshpande, et al. 2008).

Regarding the frequency parameters, the epileptiform activity obtained in this work had far less events per second, around 10 times less (≈0.3 Hz in 1 hour free Mg^{2+} exposure), than the frequency described in the literature, which was greater than 3 Hz. This discrepancy may be accounted by the fact that recordings were performed at day 5 after free Mg^{2+} treatment, time point by which one would expect the transition to SREDs.

This observation reflects perhaps that the hippocampal neurons in culture were not able to endure the long-lasting plasticity changes associated with the development of SREDs.

Alongside the fact that resting membrane potentials recorded, from neurons treated for both 30 min (-27.57 ± 1.584 mV) and 1 hour (-31.14 ± 2.656 mV), were more depolarized when compared to -65 to -50 mV, reported in the literature (Sombati and DeLorenzo 1995). The resting membrane potentials data provides by itself a measure of the overall condition of the cultures, i.e. the functional and network "fitness" of the neurons. Thus, the values obtained corroborated the visual general evaluation of the cultures, which started to deteriorate at day 7, evidenced by neuronal aggregates and less 3D looking soma in light phase microscopy.

One may then speculate that the underlying health problems in the primary hippocampal cultures exacerbated and intensified subsequent interventions in the culture, specifically the effect of the free Mg^{2+} treatment.

Furthermore, it is described that SE causes neuronal death in a time-dependent manner whereas SREDs do not. Particularly, cell death increases from approximately 10–15% after 3 h of continuous high-frequency epileptiform discharges up to 80% after 12 h of exposure to free Mg^{2+} (Deshpande, et al. 2007). This neuronal death was proven to be dependent on extracellular Ca^{2+} influx NMDAR-mediated, and following neurotoxic signalling cascades (Deshpande, et al. 2008).

As so, the neuronal death resulting from SE-related excitotoxicity was probably aggravated by already fragile neurons, and prevented the plastic transition required for neurons to undergo to a non-neurotoxic state of permanent SREDs. This may provide an explanation why, although attempted, 2 and 3 hours exposures (the latter being referenced as the optimal exposure time in the literature), did not successfully induce SREDs but rather caused extensive neuronal death.

Primary causes of unhealthy cultures were found to be related to the glass coverslips used in addition to suboptimal coating. In fact, it was not possible to generate highly viable cultures for a few months.

The inefficiency in implementing this *in vitro* model of epileptiform discharges in cultured cells may have been also partially influenced by the absence of 2-week old glial feeder layer, since astrocytes are essential in the regulation of extracellular levels of ions and neurotransmitters (Girardi, et al. 2004) and have been shown to have a protective role in glutamate-mediated excitotoxicity, not only due to uptake mechanisms but also by releasing protective factors (reviewed in Allaman, et al. 2011). Given that, the glial layer may be a critical prerequisite in the model, in order to ensure that neurons are capable of overcoming the excitotoxicity promoted by the initial SE insult.

Despite the considerations mentioned above, molecular expression data regarding synaptophysin protein levels is in accordance with previous reports. Cultured neurons did exhibit increasing

levels of synaptophysin during development, which is associated with synapse formation. This expression pattern has been observed both *in vitro* - i.e. in culture - (Rao, et al. 1998), and *in vivo* experiments (Grabs, et al. 1994).

Concomitantly, AMPA subunit, GluR1, displayed increasing expression throughout the culture's development. Pickard and colleagues also observed, in hippocampal neurons, that total GluR1-4 increased from day 3 to 10 and was sustained throughout the rest of the culture (Pickard, et al. 2000). This is consistent with the knowledge that at developmentally early stages many excitatory synapses are thought to be postsynaptically "silent". At this time point there is a large proportion of synapses containing only NMDAR, which later in development acquire AMPA receptors (Wu, et al. 1996).

Although *in vivo* data from the spinal cord demonstrates that gephyrin protein levels increased progressively with neuronal development (Colin, et al. 1998) and GlyR expression in rat hippocampal neurons achieves a maximum at day 7 postnatal, followed by reduction and stabilization in adulthood (Aroeira, et al. 2011), no statistically significant changes were obtained concerning the expression levels of the inhibitory postsynaptic proteins, gephyrin and GlyR, in the hippocampal cultures.

Regarding the effect of the treatment in the expression of the different proteins accessed, no conclusions can be drawn, since no difference was found between experimental and control conditions at the same time point (15 DIV).

Altogether, it was not attainable to successfully implement the *in vitro* cell model of epileptiform activity due to considerable decay in cultures. Ergo, it was not possible to continue this line of investigation and an alternative approach was pursued.

6.2 *In vitro* model of epileptiform activity in combined hippocampal-entorhinal cortex slices

The present study allowed the profiling of the expression pattern of glycinergic transmission-related markers associated with epileptiform activity in acute combined slices of hippocampus and entorhinal cortex.

The model allows the induction of different patterns of epileptiform activity, by lowering the extracellular Mg^{2+} concentration to nominally zero, through omission of Mg_2SO_4 from the ACSF. CA1 high-frequency positive going short voltage shifts were recorded and have been described as RSDs. Despite the fact that a single recording was performed in the CA1, the frequency, amplitude and duration of the events obtained were in agreement with what has been previously reported (Dreier and Heinemann 1991). RSDs typically display a frequency of 5-33 events/min and can last

from 60 to 150 ms. RSDs, although not measured in this work, are also reported to occur in CA3, usually in a synchronized fashion with CA1 (Behr and Heinemann 1996).

The first signs of epileptiform activity in the MEC were SLEs. These typically exhibit durations of 13 to 88s and amplitudes up to 4.3 mV, which fall within the range obtained.

Besides being reminiscent of electrographic activity in tonic-clonic seizures, SLEs obtained in free-Mg^{2+} conditions also enclose the same pharmacologic properties as seizures induced *in vivo*, since they are sensitive to routinely used anticonvulsants (e.g. benzodiazepines, barbiturates, carbamazepine, phenytoin and valproate) in clinically relevant concentrations (Zhang, et al. 1995).

Upon prolonged exposure to Mg^{2+} free ACSF the SLEs changed to a characteristic pattern of short-lasting high-frequency negative potential shifts reminiscent of electrographic activity, which can be observed during prolonged *status epilepticus*, LRDs. Spontaneous extracellular field potentials revealed that the LRDs obtained in this work possessed electrographic features comparable to those described in the literature - i.e. duration of 1–3 s and a frequency of 14 ± 3 *per* min - (Dreier and Heinemann, 1991; Kirchner, et al. 2003).

Conversely to SLEs, LRDs have been reported to be resistant to all clinically employed anticonvulsants and therefore may be qualified as a model of acute pharmacoresistant epilepsy (Zhang et al., 1995). Previous work has shown that the pattern of pharmacoresistant LRDs in the entorhinal cortex remains stable for several hours (Dreier and Heinemann, 1990).

However, application of GABA or GABA-uptake inhibitors can suppress LRD activity, with reappearance of SLEs, which may suggest that loss of GABA function is involved in this activity pattern (Pfeiffer, et al. 1996).

As previously mentioned LRDs may be considered an experimental model of drug-resistant epilepsy, due to its pharmacological properties, especially useful when trying to understand the neuronal mechanisms underlying pharmacoresistance and testing new therapeutic approaches.

Nevertheless, the cellular basis of pharmacoresistance has so far remained unclear. Three main general hypotheses have been proposed: (1) Disease related mechanisms, which might include modifications in drug targets; (2) Genetic variations, namely polymorphisms in drug transporters; (3) Drug-related mechanisms, such as tolerance, which may reduce AEDs efficacy (Wahab, et al. 2009).

In the current study an elevated concentration of K^+ (5 mM) was applied in combination with the free Mg^{2+} condition. However, this should not be considered a free Mg^2/high K^+ model, since high K^+ models usually refer to concentrations above 7 mM (Heinemann, et al. 2006). In the model of epileptiform activity explored in this work the elevated extracellular potassium depolarizes neuronal membranes, which primes the biological network for activation, and the low extracellular magnesium concentration reduces Mg^{2+} blockade upon NMDAR and Mg^{2+}-sensitive

Ca^{2+} channels, increasing network susceptibility to depolarizing influences, as well as decreasing membrane charge-screening effects (Dreier and Heinemann 1991). As a result, elevation of K^+ concentration allowed for a more consistent and efficient induction of epileptiform activity.
Interestingly, in chronically epileptic tissue (e.g. human epileptic tissue) it is not possible to induce epileptiform activity with low Mg^{2+} protocol. The mechanism implicated still remains elusive, but it raises the possibility that adaptive homeostatic plastic changes develop in chronically epileptic tissue, which may prevents recurrent occurrence of seizures (Heinemann, et al. 2006).
Another intriguing characteristic of SLEs and LRDs concerns the fact that these types of activity only spread to the CA1 and CA3 by removing GABAergic inhibition, even though connectivity between EC and DG/CA in the expanded slice is preserved. This observation along with the observation that in kindled rats (i.e. chronic epileptic tissue) propagation of free Mg^{2+}-induced epileptiform activity to the hippocampus is facilitated, probably due to loss of inhibition, supports the "filtering function" of the DG (Dreier and Heinemann 1991).

As an attempt to understand the role of glycinergic transmission in hyperexcitabily conditions, a molecular analysis was conducted. GlyR subunits (α1-3 and β) mRNA levels were assessed and revealed a significant increase in α2 subunit, as well as an evident elevation in α3 transcript levels. Up-regulation of α2 and α3 GlyR subunits has indeed been reported in pharmacoresistant TLE patients. Specifically, high affinity isoforms $\alpha2^{P192L}$ and $\alpha3^{P185L}$, which can be effectively activated at very low concentrations of glycine (e.g. 300 nM in the case of $\alpha3^{P185L}$) (Eichler, et al. 2008).
Despite the large body of literature reporting the GlyR-mediated anticonvulsant effect of glycine, Eichler and colleagues' study suggests that GlyR may play opposite role in chronic epilepsy (Eichler, et al. 2008).
RNA-edited GlyR variants arise from a single proline-to-leucine substitution at the position 192 and 185 of the mature GlyR α2 and α3 protein respectively. This rearrangement causes a conformation change in the GlyR tertiary structure, which generates an increased affinity (EC_{50}) for GlyR agonists (ha-GlyR). The expression of these ha-GlyR variants was found to be inversely correlated to KCC2 expression in TLE patients. The down-regulation of KCC2, a K^+/Cl^- cotransporter, is associated with high intracellular chloride equilibrium potential, which has also been described in TLE patients (Palma, et al. 2006).
Since under most physiological conditions, glycine concentration in cerebrospinal fluid has been estimated to be in the low micromolar range (Westergren, et al. 1994) and hippocampal GlyR are preferentially non-synaptically located (Aroeira, et al. 2011), haGlyRs, are functionally well adapted for "translation of hippocampal ambient glycine into tonic glycinergic inhibition" (Eichler,

et al. 2008). Furthermore, glycine (Lasley 1991) as well as taurine (Sherwin 1999) concentration has been described to increase upon seizure activity.

Therefore, long lasting ha-GlyR activation (i.e. opening of the Cl^- channels) causes an increase in the resting conductance and increase input resistance. In line with Ohm's law, $\Delta V=RI$, "the postsynaptic potential induced by the same synaptic current would be reduced, resulting in depression of both inhibitory and excitatory transmission" – i.e. shunting process (Legendre, et al. 2009; Xu and Gong 2010). In this context, activity deprivation elicits up-regulation of Glu/GABA ratio, which is reminiscent of TLE pathology (Loup, et al. 2000; Legendre, et al. 2009).

Altogether, these data points toward a homeostatic but pathological driven compensatory mechanism involving of GlyR in TLE histopathology.

In addition, immunohistological analysis of subcellular location of α3-GlyR revealed that the long splice variant (α3L) is preferentially located at glutamatergic synapses and the short (α3K) is adjacent to GABAergic nerve endings. In TLE patients, down-regulation of α3L-GlyR and up-regulation of α3K-GlyR was reported. In context high chloride equilibrium potential, these circumstances may decrease inhibitory action on glutamatergic synapses, concomitantly to an increase in glycinergic current at depolarizing GABAergic neuronal terminals, adding to the pathological mechanism described above (Eichler, et al. 2009; Legendre, et al. 2009).

Taking into account the theoretical frame of reference cited it would be of great interest to assess the ha-GlyR isoforms mRNA levels as well as KCC2 expression in the free Mg^{2+} model in acute slices. This analysis would determine if a similar mechanism is occurring even in acute conditions.

On the other hand, there is convincing evidence reported since 1980's regarding the antiepileptic activity of glycine. Systemically administered glycine has been shown to reduce seizures in several models. Namely in seizures induced by MPA or by auditory stimuli in seizure-prone DBA/2 mice (Toth and Lajtha 1984; Seiler and Sarhan 1984). Moreover, glycine potentiates the anticonvulsant actions of clinically used anticonvulsants, such as phenobarbital and carbamazepine (Peterson 1986; Peterson, et al. 1990). Glycine also has a synergetic effect when administered in conjunction diazepam in seizures induced by amygdala kindling (Peterson 1986) and by electroshock (Peterson and Frye 1987).

Additionally, milacemide, a pro-glycine drug, was reported to suppress seizures in animal models and to have antiepileptic activity in human patients (van Dorsser, et al. 1983). Although it never reached the market it exemplifies the potential relevance of GlyR targeting designed drugs. More recently, studies on the mechanism of action of the AED levetiracetam suggest that its antiepileptic effects may be partly due to acting upon GlyR (Rigo, et al. 2002).

Taking into account the evidence described above, it might also be argued that local accumulation of glycine, either by reverse transport in glial cells (Roux and Supplisson 2000) or spillover to extrasynaptic sites, can activate functional GlyRs and might exert a non-pathological inhibitory effect (Chen, et al. 2011).

Apparently contradictory data stresses the fact that the role of glycinergic transmission in TLE is yet to be completely deciphered. Nevertheless, glycine, or glycine derivates should not be discarded as a potential pharmacological target in epilepsy disorders. At least as co-adjuvant therapy, allowing the reduction of AED dosage and consequently its side effects.

Protein expression analysis seams to corroborate the mRNA findings since an increase in GlyR α2 was patent, although not significant.

Even though a double band pattern in western blot is not usually associated with GlyR, it was found in hypothalamic supraoptic neurons, specifically a multiple band pattern ranging from 48 to 50 kDa, which correspond to GlyR subunits (Deleuze, et al. 2005). The better definition obtained in the present assay was probably due to the secondary antibody, given that it was the only modification when compared to cultures' experiments, in which only a single band was visible.

Regarding GlyT transcript expression, a minor non-significant decrease in GlyT2 was observed. GlyT2 mutations have been associated to hyperexcitability disorders such as hyperekplexia. Although at first glance it may be counterintuitive, GlyT2 down-regulation exerts an excitatory effect, since its main function is to replenish the presynaptic glycine pool in order to refill the vesicles. Even though at first GlyT2 decrease may exert inhibitory actions due to accumulation of extracellular glycine, depletion of presynaptic vesicles will eventually cause a deficiency in glycine (Harvey, et al. 2008).

In relation to GlyT1 transcript assessment no effect was observed. Nevertheless, compelling evidence has emerged regarding GlyT1 as potential pharmacological target in epilepsy treatment. A study by Kalinichev and colleagues revealed that some GlyT1 antagonists, such as SB-710622 and GSK931145, exhibit an anticonvulsant effect in electroshock-induced seizures in rat (Kalinichev, et al. 2010).

It is extensively reported that GABAergic transmission is altered in epileptic conditions, even so no significant correlation was observed related to $GABA_AR$ β subunit. Subunit expression and composition alterations have been documented in human and in animal models. Specifically anatomical studies show a reduction in the co-localization of the β2/β3 and α2 subunits of $GABA_AR$ with the presynaptic marker synaptophysin and an increase in intracellular accumulation

(associated with β3 subunit dephosphorylation) in dentate granule cells and other hippocampal neurons with SE (Naylor, et al. 2005).

In contrast, it has also been shown an up-regulation of $GABA_AR$ (α1) in the DG of human patients with TLE and hippocampal sclerosis. Despite DG granule cell loss in these patients, the surviving neurons exhibit hyperactive GABAergic synapses as a way of copping with overexcitation by increasing their sensitivity to inhibition (Loup 2006).

The study of other $GABA_AR$ subunits in the model would be valuable in order to understand the molecular changes in GABAergic transmission underlying free Mg^{2+} induced epileptiform activity.

Regarding gephyrin expression, no statistically significant trend was obtained although a slight decrease was observed. However, it is not surprising that a decrease in gephyrin expression was reported (Förstera, et al. 2010) in the *Cornu ammonis*, since gephyrin controls the number of postsynaptic α2 and γ2 containing-$GABA_AR$, as well as β containing-GlyR, due to the selective loss of inhibitory interneurons. Moreover, abnormally spliced gephyrin variants were indentified in patients with interactable TLE. These revealed deficits in oligomerization and reduced the gephyrin and $GABA_AR$ α2 in the postsynaptic density (Förstera, et al. 2010).

Drug-refractory TLE patients also exhibited a downregulation of gephyrin in the entorhinal cortex (Fang, et al. 2011). This observation emphasises the role of the EC in TLE, which has been increasingly highlighted in the literature. Mesial TLE patients often display shrinkage of the entorhinal cortex, which has been attributed to neuronal loss in medial entorhinal cortex layer III (MEC-III) (Du, et al. 1993). Specifically, it has been shown that enhanced excitability in CA1 does not relate to inhibitory cell loss in layer III but rather due to disrupted flow of information, since in TLE condition seizures may propagate to the hippocampus via the temporoammonic (MEC to CA1) pathway thereby bypassing the classic trisynaptic hippocampal loop (Wozny, et al. 2005).

Considering the fact that NMDAR activity plays a major role in neuronal excitation in the CNS, many investigators have evaluated the possible alterations of NMDAR in epilepsy. NMDAR may be involved in seizure-induced excitotoxic cell death in specific neuronal populations, reason why many NMDAR antagonists have anticonvulsant or protective activity (Platt 2007).

In our study, a minor but significant reduction in NR1 subunit was found. Bayer et al. in 1995, by using non-radioactive hybridization methods, demonstrated that *in situ* hippocampal specimens of patients with chronic temporal lobe epilepsy showed a loss of NR1-positive cells (Bayer, et al. 1995). The same pattern was observed in KA-induced model of limbic seizures in rats in CA1, only 3h after KA injection, and CA3 at 72 h after drug injection (Lason, et al. 1997). In both studies, down-regulation of NR1 is attributed to pyramidal cell loss.

Furthermore, autopsies of sclerotic hippocampi from TLE patients revealed increased AMPA GluR1 and NMDAR2 mRNA expression, in the *stratum granulosum* (Mathern, et al. 1997).

Alterations in hippocampal AMPAR and NMDAR subunit composition could modify the functional properties of glutamate receptors, and contribute to hyperexcitability and/or protect neurons from chronic seizure-related excitotoxicity. For example, heteromeric NMDAR containing NR2 subunits may exhibit less glutamate-mediated potential to open the channel, however once opened, due to longer decay, it may contribute to synchronization. Additionally, if there is a higher number of homomeric GluR1 relatively to GluR2-contaning AMPAR, an increase in hyperexcitability may occur caused by an elevation in Ca^{2+} permeability (reviewed in Ghasemi and Schachter 2011).

Finally, synaptophysin did not show any change associated with the epileptic phenotype. Still, human specimens resected from intractable TLE patients show a significant synaptic loss, with a marked decrement of synaptic immunostaining present in fields CA1 and CA4 that are highly correlated with hippocampal sclerosis grade (Looney, et al. 1999).

Evaluation of neuronal death represents another important parameter to further characterize and comprehend the free Mg^{2+} -induced epileptiform activity in combined Hip-EC slices.

The intricate network and its several "participants" - neurotransmitters and synaptic proteins – along with its relations, mirror the complexity of such phenomena, i.e. epilepsy. Studying the mechanisms that underlie epileptiform activity, even in simplified system as the acute slice, still compromises great complexity, as so further study of the molecular mechanisms underlying 'epileptic' phenotype in the free Mg^{2+} model in Hip-EC slice.

6.2.1 Methodological considerations

The development of the brain slice was a landmark in the discipline of neuroscience. The technique by which slices are prepared, cut, stored and recorded can determine not only the tissue's viability but also the validity and applicability of the results obtained from the preparation (Bernard 2006).

Three main advantages arise from using acute slices: (1) Slices are thick enough to maintain the network circuitry. Usually slices are no more than 400 µm thick, which ensures viability *in vitro* for up to 12 hours; (2) Concurrently, slices are much simpler than *in vivo* preparations, which allows an insight into the complexity of a given brain area, such as the extensively studied hippocampus. This knowledge of the hippocampal physiological and structural properties also facilitates experimental design as well as interpretation of the results; (3) Technical approaches can be easily

applied, from visually guided positioning of stimulation and recording electrodes in electrophysiology, to molecular and imaging procedures (Bernard 2006).

When implementing an epileptic activity model in acute slices a few specific considerations have to be taken into account. Firstly it is imperative to consider the age of the animal from which the slice is prepared. Rats 5 to 6 weeks old are regarded as adults. Prior to this age significant developmental changes are still taking place. Especially important is the fact that early in development both GABA and glycine act as excitatory neurotransmitters (Ben Ari 2002).

Another important issue concerns the slice itself in this particular case, since one aimed to study TLE-like conditions a combined hippocampal-EC slice was chosen due to the critical involvement of the EC in epileptiform activity occurrence. The preserved extrinsic connectivity facilitates the induction and allows for the recording of different types of activity.

The ACSF composition is similar from laboratory to laboratory. Ca^{2+}, Mg^{2+} and K^{+} concentrations must be carefully adjusted because small variations in concentrations of these ions have marked effects on neuronal activity. Particularly important is the Ca^{2+}. Extracellular Ca^{2+} concentration in vivo is about 1.2 mM, which is mimicked in slices by 1.6 mM, since the difference is due to the chelating effect of HCO^{3-} on Ca^{2+}.

One of the key factors influencing the induction of epileptiform discharges in acute slices is the recording chamber used. Although it has been shown that pre-incubation in interface improves slices' viability, in the current layout of the laboratory was not possible. So, slices were only transferred to the interface chamber for recordings. The Haas chamber, where the slices are set on the floor of the chamber, provides mechanical stability. Extracellular space in this chamber is reduced and epileptiform discharges are more easily induced. The oxygen supply is also more efficient when compared to submerged conditions, since it is supplied through gas diffusion of O_2 saturated atmosphere.

Temperature is another critical parameter. Not only recordings should be made at physiological temperatures to preserve the networks' biophysical properties but especially because it is very difficult to induce epileptiform activity below 33ºC (reviewed in Heinemann, et al. 2006).

Despite the technical benefits of using an acute model, one should always keep in mind that some drawbacks must be taken into account, in particular regarding extrapolations from *in vitro* data to *in vivo* or clinical condition.

7 GENERAL CONCLUSIONS

In vitro models of epileptiform activity are valuable tools in epilepsy research. The main findings of this work were obtained by studying two distinct in vitro models of epileptiform activity. The neuronal culture model was not successfully established due to technical constrains and a more physiological and complex system in acute hippocampal-entorhinal cortex slices was therefore pursued. The acute combined hippocampal-entorhinal cortex slice model proved to be highly versatile, allowing the application of different molecular techniques. Reducing the extracellular Mg^{2+} was able to induce different patterns of epileptiform activity, namely LRDs, in a reproducible way. LRDs have particular interest, since they are not sensitive to standard anticonvulsants.

Although LRDs are considered an acute model of pharmacoresistant epileptiform discharges, it was still possible to mimic some of the pathophysiological features found in chronic models of TLE. Specifically, an increase in mRNA levels of glycine receptor α2 and α3 subunits, which can be found in human TLE patients. Furthermore, the LRD phenotype also elicited molecular changes related to excitatory NMDA subunit NR1. Evidence further indicates that a compensatory pathological mechanism might occur during epileptiform activity involving glycinergic transmission effectors.

The characterization of this model will allow further understanding of the role of glycinergic transmission in hyperexcitability disorders, such as epilepsy.

In the future, to a more comprehensive understanding of this model, immunohistochemical studies should be carried. These will allow studying and determining the changes in the subcellular localization of glycinergic-related proteins associated with the epileptic phenotype.

8 ACKNOWLEDGMENTS

À mãe e ao pai, pelo amor e apoio incondicional. Por acreditarem em mim principalmente quando eu começava a deixar de o fazer, por me fazerem sentir que tenho sempre o vosso colo, cada vez menos literal mas sempre emocional. Aos meus avós, esta tese parece pouco para agradecer todo o apoio que me dão, e mesmo juntando a de doutoramento que há-de vir nunca conseguirei mostrar-vos o quão gosto de vocês, por isso continuarei a fazê-lo todos os dias. Ao Jorge, porque mesmo longe é uma presença constante, que me deixa ser eu e me faz querer ser melhor. A todos os meus amigos, vocês são mesmo muitos e apesar de querer fugir ao típico, vocês sabem quem são, também sabem que nestas coisas não temos caracteres suficientes para o agradecimento devido a todos e cada um pela paciência e apoio que me deram, por aguentarem as manias e desesperos.

À minha orientadora, Dr. Cláudia Valente, sem a qual este trabalho não teria sido possível. Obrigado por me mostrares que havia sempre solução, pelo espírito entusiasta contagiante que fazia crer que o amanhã iria sempre ser melhor. Por veres sempre primeiro a pessoa e depois a aluna. Obrigada pela paciência inesgotável e pela confiança depositada que espero ser merecedora.

Gostaria de agradecer ao Professor Doutor Joaquim Ribeiro e à Professora Doutora Ana Sebastião pela oportunidade de realizar o trabalho científico no seu laboratório.

Não posso deixar de agradecer a todos no laboratório, em especial a.. Ah, não posso, vocês são muitos e depois ficam aborrecidos e a pensar que saio daí com preferidos! Tenho, no entanto, que agradecer ao Diogo que me ensinou como lidar com o patch clamp e todos os seus truques.

Gostaria de agradecer ao Dr. Uwe Heinemann por me acolher no seu laboratório e pelo conhecimento imprescindível ao sucesso deste trabalho.

9 BIBLIOGRAPHY

Allaman, I., Bélanger, M., & Magistretti, P. J. (2011). Astrocyte-neuron metabolic relationships: for better and for worse. *Trends Neuroscience , 34* (2), 76-87.

Andersen, P., Bliss, T. V., & Skerede, K. K. (1971b). Lamellar organization of hippocampal excitatory pathways. *Exp Brain Research , 13*, 222-238.

Andersen, P., Bliss, T. V., & Skerede, K. K. (1971a). Unit analysis of nit analysis of hippocampal population spikes. *Expl Brain Research , 13*, 208-221.

Andersen, P., Morris, R., Amaral, D., Bliss, T., & O'Keefe, J. (2007). *The Hippocampus Book.* New York, New York, USA: Oxford University Press.

Anderson, W. W., & Collingridge, G. L. (2007). Capabilities of the WinLTP data acquisition program extending beyond basic LTP experimental functions. *Journal of Neuroscience Methods* (162), 346-356.

Andràsfalvy, B. K., Smith, M. A., Borchardt, T., Sprengel, R., & Magee, J. C. (2003). Impaired regulation of synaptic strength in hippocampal neurons from GluR1-deficient mice. *Journal of Physiology , 552*, 35-45.

Aprison, M. H., & Werman, R. (1965). The distribution of glycine in cat spinal cord and roots. *Life Sciences, 4*, 2075–83.

Aroeira, R. I., Ribeiro, J. A., Sebastião, A. M., & Valente, C. C. (2011). Age-related changes of glycine receptor at the rat hippocampus: from the embryo to the adult. *Journal of Neurochemistry , 118* (3), 339-353.

Böhme, I., & Lüddens, H. (2001). The Inhibitory Neural Circuitry as Target of Antiepileptic Drugs. *Current Medicinal Chemistry , 8*, 1257-1274.

Babb, T. L., & Pretorius, J. K. (1993). Pathological substrates in epilepsy. In W. ER, *The treatment of epilepsy* (pp. 55-70). Philadelphia: Lea and Fibiger.

Ballanyi, K. (1999). Chapter 9: In Vitro Preparations. In U. Windhorst, & H. Johansson, *Modern techniques in neuroscience research* (pp. 307-326). Berlin ; Heidelberg ; New York : Springer.

Baltimore, D. (1970). RNA-dependent DNA polymerization in virions of RNA tumor viruses. *Nature , 226*, 1209–11.

Bayer, T. A., Wiestler, O. D., & Wolf, H. K. (1995). Hippocampal loss of N-methyl-D-aspartate receptor subunit 1 mRNA in chronic temporal lobe epilepsy. *Acta Neuropathol , 89*, 446–450.

Behr, J., & Heinemann, U. (1996). Low Mg2+ induced epileptiform activity in the subiculum before and after disconnection from rat hippocampal and entorhinal cortex slices. *Neuroscience Letters , 205* (1), 25-28.

Ben Ari, Y. (2002). Excitatory actions of GABAduring development: the nature of the nurture. *Nature Reviews Neuroscience , 3*, 728–739.

Ben-Ari, Y. (1985). Limbic seizure and brain damage produced by kainic acid: mechanisms and relevance to human temporal lobe epilepsy. *Neuroscience , 14*, 375-403.

Bernard, C. (2006). Hippocampal Slices: Designing and Interpreting Studies in Epilepsy Research. In A. Pitkanen, P. P. Schwartzkroin, & S. L. Moshé, *Models of Seizures and Epilepsy* (pp. 59-71). London: Elsevier.

Bernstein, J. (1868). Ueber den zeitlichen Verlauf der negativen Schwankung des Nervenstroms. *Pflügers Archiv , 1*, 173-207.

Bernstein, J. (1902). Untersuchungen zur Thermodynamik der bioelektrischen Ströme I. *Pflügers Arch Gesamte Physiol Menschen Tiere* (92), 521-562.

Betz, H., & Laube, B. (2006). Glycine receptors: recent insights into their structural organization and functional diversity. *J Neurochemistry , 97*, 1600-10.

Blair, R. E., Deshpande, L. S., Sombati, S., Falenski, K. W., Martin, B. R., & DeLorenzo, R. J. (2006). Activation of the cannabinoid type-1 receptor mediates the anticonvulsant properties of cannabinoids in the hippocampal neuronal culture models of acquired epilepsy and status epilepticus. *Journal of Pharmacology and Experimental Therapeutics , 317* (3), 1072-78.

Blair, R. E., Laxmikant, D. S., Sombati, S., Elphick, M. R., Martin, B. R., & DeLorenzo, R. J. (2009). Prolonged exposure to WIN55,212-2 causes downregulation of the CB1 receptor and the development of tolerance to its anticonvulsant effects in the hippocampal neuronal culture model of acquired epilepsy. *Neuropharmacology* (57), 208-218.

Bowery, N. G., & Smart, T. G. (2006). GABA and glycine as neurotransmitters: a brief history. *British Journal of Pharmacology , 147*, 109-119.

Bradford, M. M. (1976). A Rapid and Sensitive Method for the Quantitation of Microgram Quantities of Protein Utilizing the Principle of Protein-Dye Binding. *Analytical Biochemistry* (72), 248-254.

Briellmann, R. S., Kalnins, R. M., Berkovic, S. F., & Jackson, G. D. (2002). Hippocampal pathology in refractory temporal lobe epilepsy: T2-weighted signal change reflects dentate gliosis. *Neurology , 58* (2), 265-271.

Brock, T. D., & Freeze, H. (1969). Thermus aquaticus gen. n. and sp. n., a nonsporulating extreme thermophile. *Journal of Bacteriology , 98* (1), 289-297.

Browne, T. R., & Holmes, G. L. (2003). *Handbook of epilepsy* (3rd ed.). Philadelphia: Lippincott Williams & Wilkins.

Burnette, W. N. (1981). "Western blotting": electrophoretic transfer of proteins from sodium dodecyl sulfate--polyacrylamide gels to unmodified nitrocellulose and radiographic detection with antibody and radioiodinated protein A. *Analytical Biochemistry* (112), 195-203.

Cajal, S. R. (1909). Histologie du système nerveux central de l´homme et des vertébrés. *Maloine Editeurs, Paris.*

Canto, C. B., Wouterlood, F. G., & Witter, M. P. (2008). What Does the Anatomical Organization of the Entorhinal Cortex Tell Us? *Neural Plasticity , 2008*, 1-18.

Carruthers-Jones, D. I., & Gelder, N. M. (1978). Influence of taurine dosage on cobalt epilepsy in mice. *Neurochemical Research , 3* (1), 115-123.

Carter, M., & Shieh, J. (2010). *Guide to Reasearch Tecniques in neuroscience.* Oxford: Academic Press.

Cell Signaling Technology. (2011). *www.cellsignal.com*. Retrieved 11 9, 2011 from http://www.cellsignal.com/products/7072.html

Chattipakorn, S. C., & McMahon, L. L. (2002). Pharmacological characterization of glycine- gated chloride currents recorded in rat hippocampal slices. *J Neurophysiol , 87*, 1515-25.

Chattipakorn, S. C., & McMahon, L. L. (2003). Strychnine-sensitive glycine receptors depress hyperexcitability in rat dentate gyrus. *J Neurophysiol , 89*, 1339-42.

Chen, R. Q., Wang, S. H., Yoa, W., Wang, J. J., Ji, F., Yan, J. Z., et al. (2011). Role of glycine receptors in glycine-induced LTD in hippocampal CA1 pyramidal neurons. *Neuropsychopharmacology , 39* (9), 1948-58.

Cherubini, E., Bernardi, G., Stanzione, P., Marciani, M. G., & Mercuri, N. (1981). The action of glycine on rat epileptic foci. *Neuroscienses Letters , 21* (1), 93-97.

Chien, A., Edgar, D. B., & Trela, J. M. (1976). Deoxyribonucleic acid polymerase from the extreme thermophile Thermus aquaticus. *Journal of Bacteriology , 127* (3), 1550-57.

Cole, K. S. (1949). Dynamic electrical characteristics of the squid axon membrane. *Arch Sci Physiol 3: , 3*, 253–258.

Colin, I., Rostaing, P., Augustin, A., & Triller, A. (1998). Localization of components of glycinergic synapses during rat spinal cord development. *J Comparative Neurolology , 398* (3), 359-372.

Collingridge, G. L. (1995). The brain slice preparation: a tribute to the pioneer Henry Mcllwain. *J Neuroscience Methods , 59*, 5-9.

Commission on Classification and Terminology of the International League Against Epilepsy. (1981). Proposal for revised clinical and electroencephalographic classification of epileptic seizures. *Epilepsia , 22*, 489-501.

Costa, A., & Antunes, L. (2010). *Handling and minor procedures of laboratory animals: Mice, Rats and Rabbits* (Série Didática. Ciências Aplicadas ed., Vol. 413). Vila Real, Portugal: SDB, UTAD.

Cragg, B. G., & Hamlyn, L. (1955). Action potentials of the pyramidal neurones in the hippocampus of the rabbit. *J Physiology , 129*, 608-627.

Cragg, B., & Hamlyn, L. H. (1957). Some commissural and septal connections of the hippocampus in the rabbit. A combined histological and electrical study. *J Physiology , 135*, 460-485.

Crawford, P. M., & Chadwick, D. W. (1987). GABA and amino acid concentrations in lumbar CSF in patients with treated and untreated epilepsy. *Epilepsy Research , 1* (6), 328-338.

Cubelos, B., Gimenez, C., & Zafra, F. (2005). Localization of the GLYT1 glycine transporter at glutamatergic synapses in the rat brain. *Cereb. Cortex , 15*, 448-459.

Curtis, D. R., & Watkins, J. C. (1960). The excitation and depression of spinal neurones by structurally related amino acids. *J. Neurochemistry , 6*, 117-141.

Czapiński, P., Blaszczyk, B., & Czuczwar, S. J. (2005). Mechanisms of Action of Antiepileptic Drugs. *Current Topics in Medicinal Chemistry , 5*, 3-14.

Danglot, L., Rostaing, P., Triller, A., & Bessis, A. (2004). Morphologically identified glycinergic synapses in the hippocampus. *Mol Cell Neurosciencee , 27*, 394-403.

Deleuze, C., Runquist, M., Orcel, H., Rabié, A., Dayanithi, G., Alonso, G., et al. (2005). Structural difference between heteromeric somatic and homomeric axonal glycine receptors in the hypothalamo-neurohypophysial system. *Neuroscience , 135* (2), 475-483.

DeLorenzo, R. J., Pal, S., & Sombati, S. (1998). Prolonged activation of the N-methyl-d-aspartate receptor-Ca2+ transduction pathway causes spontaneous recurrent epileptiform discharges in hippocampal neurons in culture. *Proc Natl Acad Sci , 95* (24), 14482-87.

DeLorenzo, R. J., Sun, D. A., & Deshpande, L. S. (2005). Cellular mechanisms underlying acquired epilepsy: The calcium hypothesis of the induction and maintainance of epilepsy. *Pharmacology and Therapeutics , 105* (3), 229-266.

Deshpande, L. S., Lou, J. K., Mian, A., Blair, R. E., Sombati, S., & DeLorenzo, R. J. (2007). In vitro status epilepticus but not spontaneous recurrent seizures cause cell death in cultured hippocampal neurons. *Epilepsy Research* (75), 171-179.

Deshpande, L. S., Lou, J. K., Mian, A., Blair, R. E., Sombati, S., Attkisson, E., et al. (2008). Time course and mechanism of hippocampal neuronal death in an in vitro model of status epilepticus: Role of NMDA receptor activation and NMDA dependent calcium entry. *Eur J Pharmacology , 583* (1), 73-83.

Dichter, M. A., & Pollard, J. (2006). Cell Culture Models for Studying Epilepsy. In A. Pitkanen, P. P. Schwartzkroin, & S. L. Moshé, *Models of Seizures and Epilepsy* (pp. 23-34). London, UK: Elsevier.

Dorak, M. T. (2006). *Real-time PCR - The BIOS Advanced Methods.* Abigdon: Taylor & Francis Group.

Dreier, J. P., & Heinemann, U. (1990). Late low magnesium-induced epileptiform activity in rat entorhinal cortex slices becomes insensitive to the anticonvulsant valproic acid. *Neuroscience Letters , 119*, 68-70.

Dreier, J. P., & Heinemann, U. (1991). Regional and time dependent variations of low Mg 2+ induced epileptiform activity in rat temporal cortex slices. *Experimental Brain Research , 87*, 581-596.

Dreier, J. P., Zhang, C. L., & Heinemann, U. (1998). Phenytoin, phenobarbital, and midazolam fail to stop status epilepticus-like activity induced by low magnesium in rat entorhinal slices, but can prevent its development. *Acta Neurol Scandinavica , 98* (3), 154-160.

du Bois-Reymond, E. (1848–1884). *Untersuchungen über thierische elektricität.* Berlin: Reimer.

Du, F., Whetsell, W. O., Abou-Khalil, B., Blumenkopf, B., Lothman, E. W., & Schwarcz, R. (1993). Preferential neuronal loss in layer III of the entorhinal cortex in patients with temporal lobe epilepsy. *Epilepsy Research , 16* (3), 223-233.

Dumoulin, A., Rostaing, P., Bedet, C., Levi, S., Isambert, M. F., Henry, J. P., et al. (1999). Presence of the vesicular inhibitory amino acid transporter in GABAergic and glycinergic synaptic terminal boutons. *J. Cell Sci. , 112* (6), 811-823.

Durlach, J. (1967). [Apropos of a case of the "epileptic" form of latent tetany due to a magnesium deficiency]. *Rev Neurol (Paris) , 117*, 189-196.

Edwards, F. A., & Konnerth, A. (1992). Patch clamping cells in sliced tissue preparations. . *Methods in Enzymology* (207), 208-222. .

Eichler, S. A., Förstera, B., Smolinsky, B., Jüttner, R., Lehmann, T. M., Fähling, M., et al. (2009). Splice-specific roles of glycine receptor α3 in the hippocampus. *European Journal of Neuroscience , 30* (6), 1077-91.

Eichler, S. A., Kirischuk, S., Juttner, R., Schafermeier, P. K., Legendre, P., Lehmann, T. N., et al. (2008). Glycinergic tonic inhibition of hippocampal neurons with depolarizing GABAergic transmission elicits histopathological signs of temporal lobe epilepsy. *J Cell Mol Medicine , 12*, 2848-66.

Engel, D., Endermann, U., Frahm, C., Heinemann, U., & Draguhn, A. (2000). Acute effects of g-vinyl-GABA on low-magnesium evoked epileptiform activity in vitro. *Epilepsy Research , 40*, 99-107.

Engel, J. J. (1996). Introduction to temporal lobe epilepsy. *Epilepsy Research , 26*, 141-150.

Engel, J. J., & Schwartzkroin, P. A. (2006). What Should Be Modeled? In A. Pitkanen, P. P. Schwartzkroin, & S. L. Moshé, *Models of Seizures and Epilepsy* (pp. 1-14). London, UK: Elsevier.

Engel, J. J., Pedley, T. A., Aicardi, J., & Dichter, M. A. (2008). *Epilepsy: A Comprehensive Textbook* (Vol. 2). Philadelphia: Lippincott Williams & Wilkins.

Eulenburg, V., Armsen, W., Betz, H., & Gomeza, J. (2005). Glycine transporters: essential regulators of neurotransmission. *TRENDS in Biochemical Sciences , 30* (6), 325-333.

Förstera, B., Belaidi, A. A., Jüttner, R., Bernert, C., Tsokos, M., Lehmann, T. N., et al. (2010). Irregular RNA splicing curtails postsynaptic gephyrin in the cornu ammonis of patients with epilepsy.. *Brain , 113*, 3778-94.

Fang, M., Shen, L., Yin, H., Pan, Y. M., Wang, L., Chen, D., et al. (2011). Downregulation of gephyrin in temporal lobe epilepsy neurons in humans and a rat model. *Synapse , 65* (10), 1006-14.

Faraday, M. (1834). On Electrical Decomposition. *Philosophical Transactions of the Royal Society , 124* (79).

Fath, T., Ke, Y. D., Gunning, P., Götz, J., & Ittner, L. M. (2008). Primary support cultures of hippocampal and substantia nigra neurons. *Nature Protocols* (4), 78-85.

Fisher, R. S., van Emde Boas, W., Blume, W., Elger, C., & Genton, P. (2005). Epileptic seizures and epilepsy: definitions proposed by the International League Against Epilepsy (ILAE) and the International Bureau for Epilepsy (IBE). *Epilepsia , 46* (4), 470–472.

Freund, T. E., & Buzsáki, G. (1996). Interneurons of the hippocampus. *Hippocampus , 6*, 347- 470.

Friauf, E., Hammerschmidt, B., & Kirsch, J. (1997). Development of adult-type inhibitory glycine receptors in the central auditory system of rats. *J Comp Neurology , 385* (1), 117-134.

Fritschy, J. M., Harvey, R. J., & Schwarz, G. (2008). Gephyrin: where do we stand, where do we go? *Trends Neuroscience , 31* (5), 257-264.

Fritschy, J. M., Kiener, T., Bouilleret, V., & Loup, F. (1999). GABAergic neurons and GABA(A)-receptors in temporal lobe epilepsy. *Neurochem. Int. , 34*, 435-445.

Galvani, L. (1971). De viribus electricitatis in motu musculari commentarius. *Bon Sci Art Inst Acad Comm , 7*, 363–418.

Galvani, L. (1841). Opere edite ed inedite del Professore Luigi Galvani raccolte e pubblicate dall´Accademia delle Science dell´Istituto di Bologna. Dall´Olmo, Bologna.

GE Healthcare. (2011). *GE Healthcare - Western Blotting Principles and Methods.* Retrieved November 5, 2011 from GE Healthcare Life Sciences: http://www.gelifesciences.com/Aptrix/upp00919.nsf/Content/LD_497901435-A543

Gershoni, J. M., & Palade, G. E. (1983). Protein blotting: principles and applications. *Analytical Biochemistry* (131), 1-15.

Ghasemi, M., & Schachter, S. C. (2011). The NMDA receptor complex as a therapeutic target in epilepsy: a review. *Epilepsy & Behavior , 22*, 617-640.

Gibb, A. J., & Edwards, F. A. (2006). Patch clamp recording from cells in sliced tissues. *Microelectrode Techniques The Plymouth Workshop (2006)* , 255-274.

Girardi, E., Ramos, A. J., Vanore, G., & Brusco, A. (2004). Astrocytic Response in Hippocampus and Cerebral Cortex in an Experimental Epilepsy Model. *Neurochemical Research , 29* (2), 371–377.

Gomeza, J., Ohno, K., Hulsmann, S., Armsen, W., Eulenburg, V., Richter, D. W., et al. (2003). Deletion of the mouse glycine transporter 2 results in a hyperekplexia phenotype and postnatal lethality. *Neuron , 40*, 797-806.

Goodman, J. H. (1998). Experimental Models of Status Epilepticus. In S. L. Peterson, & T. E. Albertson, *Neuropharmacology Methods in Epilepsy Research.* New York: CRC Press .

Grabs, D., Bergmann, M., Schuster, T., Fox, P. A., Brich, M., & Gratz, M. (1994). Differential Expression of Synaptophysin and Synaptoporin During Pre- and Postnatal Development of the Rat Hippocampal Network. *European Journal of Neuroscience , 6*, 1745-71.

Graham, D., Pfeiffer, F., & Betz, H. (1983). Photoaffinity labelling of the glycine receptor of rat spinal cord. *Eur. J. Biochemistry , 131*, 519-525.

Harvey, R. J., Carta, E., Pearce, B. R., Chung, S.-K., Supplisson, S., Ress, M. I., et al. (2008). A Critical Role for Glycine Transporters in Hyperexcitability Disorders. *Front Mol Neuroscience , 1* (1).

Heinemann, U., Kann, O., & Schuchma, S. (2006). An Overview of In Vitro Seizure Models in Acute and Organotypic Slices. In A. Pitkanen, P. P. Schwartzkroin, & S. L. Moshé, *Models of Seizures and Epilepsy* (pp. 35-44). London, UK: Elsevier.

Helmholtz, H. (1850). Note sur la vitesse de propagation de l'agent nerveux dans les nerfs rachidiens. *Comptes Rendus Académie des Sciences (Paris)* (30), 204-206.

Hernandes, M. S., & Tronco, L. R. (2009). Glycine as a neurotransmitter in the forebrain: a short review. *J Neural Transm , 116*, 1551-60.

Higuchi, R., Dollinger, G., Walsh, P. S., & Griffith, R. (1992). Simultaneous amplification and detection of specific DNA sequences. *Biotechnology , 10* (4), 413-417.

Higuchi, R., Fockler, C., Dollinger, G., & Watson, R. (1993). Kinetic PCR analysis: real-time monitoring of DNA amplification reactions. *Biotechnology , 11* (9), 1026-30.

Hodgkin, A. L., & Huxley, A. F. (1939). Action potentials recorded from inside a nerve fibre. *Nature* (144), 710–711.

Hopkin, J. M., & Neal, M. J. (1970). The release of 14C-glycine from electrically stimulated rat spinal cord slices. *Br. J. Pharmacology , 40*, 136-138.

Johnston, D., & Miao-Sin Wu, S. (1995). *Foundations of Cellular Neurophysiology.* Cambridge: MIT Press.

Köhr, G. (2006). NMDA receptor function: subunit composition versus spatial distribution. *Cell Tissue Research , 326*, 439-446.

Kälviäinen, R., & Salmenperä, T. (2002). Do recurrent seizures cause neuronal damage? A series of studies with MRI volumetry in adults with partial epilepsy. *Prog Brain Research , 135*, 279-295.

Kaech, S., & Banker, G. (2006). Culturing hippocampal neurons. *Nature Protocols* (1(5)), 2406-15.

Kalinichev, M., Starr, K. R., Teague, S., Bradford, A. M., Porter, R. A., & Herdon, H. J. (2010). Glycine transporter 1 (GlyT1) inhibitors exhibit anticonvulsant properties in the rat maximal electroshock threshold (MEST) test. *Brain Research , 1331* (17), 105-113.

Kirchner, A., Breustedt, J., Rosche, B., Heinemann, U. F., & Schmieden, V. (2003). Effects of taurine and glycine on epileptiform activity induced by removal of Mg2+ in combined rat entorhinal cortex-hippocampal slices. *Epilepsia , 44*, 1145-52.

Kirsch, J. (2006). Glycinergic transmission. *Cell Tissue Research , 326*, 535-540.

Kleppe, K., Ohtsuka, E., Kleppe, R., Molineux, I., & Khorana, H. G. (1971). Studies on polynucleotides. XCVI. Repair replications of short synthetic DNA's as catalyzed by DNA polymerases. *Journal of Molecular Biology , 56* (2), 341-361.

Laemmli, U. K. (1970). Cleavage of structural proteins during the assembly of the head of bacteriophage T4. *Nature* (227), 680-685.

Lasley, S. M. (1991). Roles of neurotransmitter amino acids in seizure severity and experience in the genetically epilepsy-prone rat. *Brain Res , 560*, 63-70.

Lason, W., Turchan, J., Przewlocki, R., Machelska, H., Labuz, D., & Przewlocka, B. (1997). Effects of pilocarpine and kainate-induced seizures on N-methyl-D-aspartate receptor gene expression in the rat hippocampus. *Neuroscience* , 997–1004.

Legendre, P. (2001). The glycinergic inhibitory synapse. *Cell. Mol. Life Sci. , 58*, 760–793.

Legendre, p., Förstera, B., Jüttner, R., & Meier, J. C. (2009). Glycine receptors caught between genome and proteome – functional implications of RNA editing and splicing. *Frontiers in Molecular Neuroscience , 2*, 23.

Lein, P. J., Barnhart, C. D., & Pessah, I. N. (2011). Acute Hippocampal Slice Preparation and Hippocampal Slice Cultures. In L. G. Costa, G. Giordano, & M. Guiz, *In Vitro Neurotoxicology : Methods and Protocols* (Vol. 758, pp. 115-134). New York: Humana - Springer .

Leinco. (2011). *www.leinco.com*. Retrieved 11 6, 2011 from http://www.leinco.com/general_wb

Leung, L.-W. S. (1991). Field Potentials in the Central Nervous System Recording, Analysis,and Modeling. *Neuromethods - Neurophysiological Techniques , 15*, 277-312.

Lewis, T. M., Schofield, P. R., & McClellan, A. M. (2003). Kinetic determinants of agonist action at the recombinant human glycine receptor. *J Physiol. : , 549* (2), 361-374.

Li, Y., & Xu, T. L. (2002). State-dependent cross-inhibition between anionic GABA(A) and glycine ionotropic receptors in rat hippocampal CA1 neurons. *Neuroreport , 13*, 223-226.

Lipton, P. (1985). Chapter 3: Brain Slices. In A. A. Boulton, & G. B. Baker, *General Neurochemical Techniques* (Vol. 1, pp. 69-115). Clifton, NJ: Humana Press.

Logan, J., Edwards, K., & Saunder, N. (2009). *Real-time PCR: current technology and applications.* Norfolk: Caister Academic Press.

Looney MR, D. F. (1999). Synaptophysin immunoreactivity in temporal lobe epilepsy-associated hippocampal sclerosis . *Acta Neuropathol , 98* (2), 179-185.

Lopes da Silva, F. H., Witter, M. P., Boeijinga, P. H., & Lohman, A. H. (1990). Anatomic Organization and Physiology of the limbic cortex. *Physiology Rev , 70*, 453-511.

Lorento de Nó, R. (1947b). A study of nerve physiology. *Studies from Rockfeller Institute , 132*.

Lorento de Nó, R. (1947a). Action potential of the motor neurones of hypoglossus nucleus. *J cell Com Physiology , 29*, 207-287.

Loup, F. (2006). GABAA Receptors in Human Temporal Lobe Epilepsy. *Epileptologie , 23*, 187 – 194.

Loup, F., Wieser, H. G., Yonekawa, Y., Aguzzi, A., & Fritschy, J. M. (2000). Selective alterations in GABAA receptor subtypes in human temporal lobe epilepsy. *J Neuroscience , 20*, 5401-19.

Lowry, O. H., Rosebrough, N. J., Farr, A. L., & Randall, R. J. (1951). Protein Measurement with the Folin Phenol Reagent. *Journal of Biological Chemistry* (193), 265-275.

Luttman, W., Bratke, K., Küpper, M., & Myrtek, D. (2006). *Immunology. The experimenter series.* Oxford: Academic Press.

Lux, H. D., Heinemann, U., & Dietzel, I. (1986). Ionic changes and alterations in the size of the extracellular space during epileptic activity. In A. V. Delgado-Escueta, A. A. Ward, D. M. Woodbury, & R. J. Porter, *Advances in Neurology: Basic Mechanisms of the Epilepsies: Molecular and Cellular Approaches* (pp. 619-639). New York: Raven Press.

Mangan, P. S., & Kapur, J. (2004). Factors underlying bursting behavior in a network of cultured hippocampal neurons exposed to zero magnesium. *J. Neurophysiology , 91*, 946-957.

Mathern GW, P. J. (1997). Human hippocampal AMPA and NMDA mRNA levels in temporal lobe epilepsy patients. *Brain , 120*, 1937-59.

Meier, J., Vannier, C., Serge, A., Triller, A., & Choquet, D. (2001). Fast and reversible trapping of surface glycine receptors by gephyrin. *Nature Neuroscience , 4*, 253-60.

Michels, G., & Moss, S. J. (2007). GABAA receptors: properties and trafficking. *Crit Rev Biochem Mol Biol , 42* (1), 3-14.

Mitchell, S. J., & Silver, R. A. (2003). Shunting inhibition modulates neuronal gain during synaptic excitation. *Neuron , 38*, 433-445.

Mody, I., De Koninck, Y., Otis, T. S., & Soltesz, I. (1994). Bridging the cleft at GABA synapses in the brain. *Trends Neuroscience , 17*, 517-25.

Mody, I., Lambert, J. D., & Heinemann, U. (1987). Low extracellular magnesium induces epileptiform activity and spreading depression in rat hippocampal slices. *J Neurophysiology , 57*, 869-888.

Mori, M., Gähwiler, B. H., & Gerber, U. (2002). b-Alanine and taurine as endogenous agonists at glycine receptors in rat hippocampus in vitro. *Journal of Physiology , 539.1*, 191-200.

Moss, S. J., & Smart, T. G. (2001). Constructing inhibitory synapses. *Nature Reviews Neuroscience , 2*, 240-250.

Mothet, J. P., Parent, A. T., Wolosker, H., Brady Jr, R. O., Linden, D. J., Ferris, C. D., et al. (2000). D-serine is an endogenous ligand for the glycine site of the N-methyl-D-aspartate receptor. *Proc. Natl. Acad. Sci. , 97*, 4926-31.

Mullis, K. B., & Faloona, F. A. (1987). Specific synthesis of DNA in vitro via a polymerase-catalyzed chain reaction. *Methods Enzymolology , 155*, 335-350.

Najam, I., Möder, G., & Janigro, D. (2006). Mechanisms of epileptogenesis and experimental models of seizures. In E. Wyllie, *The Treatment Of Epilepsy: Principles & Practice* (2nd ed., pp. 91-101). Baltimore: Lippincott Williams & Wilkins.

Naylor, D. E., Liu, H., & Wasterlain, C. G. (2005). Trafficking of GABAA Receptors, Loss of Inhibition, and a Mechanism for Pharmacoresistance in Status Epilepticus. *Journal of Neuroscience , 25* (34), 7724-33.

Nolan, T., Hands, R. E., & Bustin, S. A. (2006). Quantification of mRNA using real-time RT-PCR. *Nature Protocols , 1* (3), 1559-82.

Nong, Y., Huang, Y. Q., Ju, W., Kalia, L. V., Ahmadian, G., Wang, Y. T., et al. (2003). Glycine binding primes NMDA receptor internalization. . *Nature , 422*, 302-307.

Overton, C. E. (1902). Beiträge zur allgemeinen Muskel- und Nervenphysiologie. II. Mittheilung. Ueber die Unentbehrlichkeit von Natrium- (oder Litium-) Ionen für den Contractionsact des Muskels. *Pflügers Archiv* (92), 346-380.

Palma, E., Amici, M., Sobrero, F., Spinelli, G., Di Angelantonio, S., Ragozzino, D., et al. (2006). Anomalous levels of Cl- transporters in the hippocampal subiculum from temporal lobe epilepsy patients make GABA excitatory. *Proc Natl Acad Sci , 103* (2), 8465-68.

Pelt-Verkuil, E. v., Belkum, A. v., & Hays, J. P. (2008). *Principles and technical aspects of PCR amplification.* Rotterdam: Springer.

Peterson, G. L. (1979). Review of the folin phenol protein quantitation method of Lowry, Rosebrough, Farr and Randall. *Anal. Biochem.* (100), 201-220.

Peterson, S. L. (1986). Glycine potentiates the anticonvulsant action of diazepam and phenobarbital in kindled amygdaloid seizures of rats. *Neuropharmacology , 25*, 1359-63.

Peterson, S. L., & Frye, G. D. (1987). Glycine potentiates diazepam anticonvulsant activity in electroshock seizures of rats: possible sites of interaction in the brainstem. *Brain Research Bulletin , 18* (6), 715-721.

Peterson, S. L., Trzeciakowski, J. P., Frye, G. D., & Adams, H. R. (1990). Potentiation by glycine of anticonvulsant drugs in maximal electroshock seizures in rats. *Neuropharmacology , 29* (4), 399-409.

Pfaffl, M. W. (2001). A new mathematical model for relative quantification in real-time RT-PCR. *Nucleic Acids Research* (29), 2002-07.

Pfeiffer, F., Simler, R., Grenningloh, G., & Betz, H. (1984). .Monoclonal antibodies and peptide mapping reveal structural similarities between the subunits of the glycine receptor of rat spinal cord. *Proc. Natl Acad. Sci. , 81*, 7224-27.

Pfeiffer, M., Draguhn, A., Meierkord, H., & Heinemann, U. (1996). Effects of gamma-aminobutyric acid (GABA) agonists and GABA uptake inhibitors on pharmacosensitive and pharmacoresistant epileptiform activity in vitro. *Br J Pharmacology , 119* (3), 569-577.

Piccolino, M. (1998). Animal electricity and the birth of electrophysiology: the legacy of Luigi Galvani. *Brain Research Bulletin* (46).

Pickard, L., Noël, J., Henley, J. M., Collingridge, G. L., & Molnar, E. (2000). Developmental Changes in Synaptic AMPA and NMDA Receptor Distribution and AMPA Receptor Subunit Composition in Living Hippocampal Neurons. (21, Ed.) *Journal of Neuroscience* , 7922-3120.

Pitkänen, A., & Sutula, T. T. (2002). Is epilepsy a progressive disorder? Prospects for new therapeutic approaches in temporal-lobe epilepsy. *Lancet Neurology , 1*, 173-181.

Platt, S. R. (2007). The role of glutamate in central nervous system health and disease – A review. *The Veterinary Journal , 173*, 278-286.

Poulter, M. O., Brown, L. A., Tynan, S., Willick, G., William, R., & McIntyre, D. C. (2000). Differential expression of alpha1, alpha2, alpha3, and alpha5 GABAA receptor subunits in seizure-prone and seizure-resistant rat models of temporal lobe epilepsy. *J Neuroscience , 19*, 4654-61.

Purves, D. (2004). Overview 69 Neurotransmitters and Their Receptors. In D. Purves, G. J. Augustine, D. Fitzpatrick, W. C. Hall, A. S. LaMantia, & J. O. McNamara, *Neuroscience* (pp. 129-140). Sunderland: Sinauer Associates Inc.

Qiagen. (2004, January). *Qiagen - Brochures and application guides.* Retrieved February 2012 from Qiagen - Sample & Assay Technologies: http://www.qiagen.com/literature/brochures/category.aspx?ID=234

Rao, A., Kim, E., Sheng, M., & Craig, A. M. (1998). Heterogeneity in the Molecular Composition of Excitatory Postsynaptic Sites during Development of Hippocampal Neurons in Culture. *Journal of Neuroscience , 18* (4), 1217-29.

Raymond, S., & Weintraub, L. (1959). Acrylamide Gel as a Supporting Medium for Zone Electrophoresis. *Science , 130*, 711.

Reiter, M., & Pfaffl, M. W. (2011). RT-PCR Optimization Strategies. In S. Kennedy, *PCR Troubleshooting and Optimization: The Essential Guide* (pp. 97-118). Norfolk: Caister Academic Press.

Rho, J. M., & Sankar, R. (1999). The Pharmacologic Basis of Antiepileptic Drug Action. *Epilepsia , 40* (11), 1471-1483.

Rigo, J. M., Hans, G., Nguyen, L., Rocher, V., Belachew, S., Malgrange, B., et al. (2002). The anti-epileptic drug levetiracetam reverses the inhibition by negative allosteric modulators of neuronal GABA- and glycine-gated currents. *British J Pharmacology , 136* (5), 659-672.

Rogawski, M. A., & Löscher, W. (2004). The neurobiology of antiepileptic drugs. *Nature Reviews Neuroscience , 5*, 553-564.

Roux, M. J., & Supplisson, S. (2000). Neuronal and glial glycine transporters have different stoichiometries. *Neuron , 25*, 373-383.

Saiki, R. K., Gelfand, D. H., Stoffel, S., Scharf, S. J., Higuchi, R., Horn, G. T., et al. (1988). Primer-directed enzymatic amplification of DNA with a thermostable DNA polymerase. *Science , 239*, 487-491.

Saiki, R. K., Scharf, S. J., Faloona, F., Mullis, K. B., Horn, G. T., Erlich, H. A., et al. (1985). Enzymatic amplification of beta-globin genomic sequences and restriction site analysis for diagnosis of sickle cell anemia. *Science , 230*, 1350-54.

Sayin, U., Osting, S., Hagen, J., Rutecki, P., & Sutula, T. (2003). Spontaneous seizures and loss of axo-axonic and axo-somatic inhibition induced by repeated brief seizures in kindled rats. *J Neurosciences , 23*, 2759-68.

Seiler, N., & Sarhan, S. (1984). Synergistic anticonvulsant effects of GABA-T inhibitors and glycine. *Naunyn Schmiedebergs Arch Pharmacol , 326* (1), 49-57.

Sharma, A. K., Reams, R. Y., Jordan, W. H., Miller, M. A., Thacker, H. L., & Snyder, P. W. (2007). Mesial Temporal Lobe Epilepsy: Pathogenesis, Induced Rodent Models and Lesions. *Toxicologic Pathology , 35*, 984-999.

Sherwin, A. L. (1999). Neuroactive amino acids in focally epileptic human brain: a review. *Neurochemical Research , 24*, 1387-95.

Simeone, T. A. (2010). Mechanisms of Antiepileptic Drug Action. In ,. J. Rho, S. Raman, & C. E. Stafstrom, *Epilepsy Mechanisms, Models, and Translational Perspectives* (pp. 123-141). CRC Press.

Sirol, M. (1939). *Galvani et le galvanisme. Paris: Vigot Fre` res; 1939.* Paris: Vigot Frères.

Smith, P. K., Krohn, R. I., Hermanson, G. T., Mallia, A. K., Gartner, F. H., Provenzano, M. D., et al. (1985). Measurement of protein using bicinchoninic acid. *Analytical Biochemistry* (150), 76-85.

Sombati, S., & DeLorenzo, R. J. (1995). Recurrent spontaneous seizure activity in hippocampal neuronal networks in culture. *Journal of Neurophysiology , 4* (73), 1706-11.

Song, W., Chattipakorn, S. C., & McMahon, L. L. (2006). Glycine-Gated Chloride Channels Depress Synaptic Transmission in Rat Hippocampus. *J Neurophysiology , 95*, 2366-79.

Squire, L. R. (2003). *Fundamental Neuroscience* (Vol. 1). San Diego, California, USA: Elsevier Science.

Stafstrom, C. E. (2006). Epilepsy: a review of selected clinical syndromes and advances in basic science. *Journal of Cerebral Blood Flow & Metabolism , 26*, 983-1004.

Suter, K. J., Smith, B. N., & Dudek, F. E. (1999). Electrophysiological recording from brain slices. *Methods , 18*, 86-90.

Sutula, T., Cascino, G., Cavazos, J., Parada, I., & Ramirez, L. (1989). Mossy fiber synaptic reorganization in the epileptic human temporal lobe. *Ann Neurology , 26*, 321-330.

Swammerdam, J. (1758). *The book of nature (Biblia naturae).* London: Seyfert.

Swinyard, E. A. (1972). Electrically induced convulsions. In D. P. Purpura, J. K. Penry, D. Tower, D. M. Woodbury, & R. Walter, *Experimental Models of Epilepsy* (pp. 433–458). New York: Raven Press.

Temin, H. M., & Mitzutani, S. (1970). RNA-directed DNA polymerase in virions of Rous sarcoma virus. *Nature , 226*, 1211-13.

Thellin, O., Zorzi, W., Lakaye, B., De Borman, B., Coumans, B., Hennen, G., et al. (1999). Housekeeping genes as internal standards: use and limits. *Journal of Biotechnology , 75* (2-3), 291-295.

Tiselius, A. (1937). A new apparatus for electrophoretic analysis of colloidal mixtures. *Transactions of the Faraday Society , 33* (524).

Tiselius, A. (1930). The moving boundary method of studying the electrophoresis of proteins (Thesis). *Nova Acta Regiae Societatis Scientiarum Upsaliensis , 7* (4).

Toth, E., & Lajtha, A. (1984). Glycine potentiates the action of some anticonvulsant drugs in some seizure model. *Neurochem Research , 9* (12), 1711-18.

Towbin, H., Staehelin, T., & Gordon, J. (1979). Electrophoretic transfer of proteins from polyacrylamide gels to nitrocellulose sheets: procedure and some applications. *Proc Natl Acad Sci USA* (76), 4350-54.

Turski, W. A., Cavalheiro, E. A., Schwarz, M., Czuczwar, S. J., Kleinrok, Z., & Turski, L. (1983). Limbic seizures produced by pilocarpine in rats: behavioural, electroencephalographic and neuropathological study. *Behav Brain Research , 9*, 315-335.

van Dorsser, W., Barris, D., Cordi, A., & Roba, J. (1983). Anticonvulsant activity of milacemide. *Arch Int Pharmacodyn Ther , 266* (2), 239-249.

van Strien, N. M., Cappaert, N. L., & Witter, M. P. (2009). The anatomy of memory: an interactive overview of the parahippocampal-hippocampal network. *Nat Rev Neurosciences , 10* (4), 272-282.

VanGuilder, H. D., Vrana, K. E., & Freeman, W. M. (2008). Twenty-five years of quantitative PCR for gene expression analysis. *Biotechniques , 44* (5), 619-626.

Verkhratsky, A., Krishtal, O. A., & Petersen, O. H. (2006). From Galvani to patch clamp: the development of electrophysiology. *Pflugers Archiv* (453), 233-247.

Vesterberg, O. (1993). A short history of electrophoretic methods. *Electrophoresis* (14), 1243-49.

Wässle, H., Heinze, L., Ivanova, E., Majumdar, S., Weiss, J., Harvey, R. J., et al. (2009). Glycinergic transmission in the Mammalian retina. *Front Mol Neuroscience , 2* (6).

Wahab, A., Heinemann, U., & Albus, K. (2009). Effects of γ-aminobutyric acid (GABA) agonists and a GABA uptake inhibitor on pharmacoresistant seizure like events in organotypic hippocampal slice cultures. *Epilepsy Research , 86* (2), 113-123,.

Wang, T., & Kass, I. S. (1997). Preparation of Brain Slices. In R. C. Rayne, *Neurotransmitter Methods* (Vol. 72, pp. 1-14). Totowa, NJ : Humana Press Inc .

Werman, R. (1966). Criteria for identification of a central nervous system transmitter. *Comp. Biochem. Physiology , 18*, 745-766.

Westergren, I., Nystrom, B., Hamberger, A., Nordborg, C., & Johansson, B. B. (1994). Concentrations of amino acids in extracellular fluid after opening of the blood-brain barrier by intracarotid infusion of protamine sulfate. *J Neurochemistry , 62*, 159-165.

White, H. S. (2002). Animal models of epileptogenesis. *Neurology , 59*, S7-S14.

Wilson, K., & Walker, J. (2010). *Principles and Techniques of Biochemistry and Molecular Biology* (7th ed.). Cambridge: Cambridge University Press.

Witter, M. P., Wouterlood, F. G., Naber, P. A., & Van Haeften, T. (2000). Anatomical organization of the parahippocampal-hippocampal network. *Ann N Y Acad Sci , 911*, 1-24.

Wittwer, C. T., & Farrar, J. S. (2011). Magic in solution: an introduction and brief history of PCR. In S. Kennedy, *PCR Troubleshooting and Optimization: The Essential Guide* (pp. 1-22). Norfolk: Caister Academic Press.

World Health Organization. (2005). Atlas of epilepsy care in the world. *Programme for Neurological Diseases and Neurosciences* (pp. 15-26). Geneva: Depatemant of mental health and substance abuse.

World Health Organization. (2009, January). *Epilepsy: Factsheet*. Retrieved July 2010 from http://www.who.int/mediacentre/factsheets/fs999/en/

Wozny, C., Gabriel, S., Jandova, K., Schulze, K., Heinemann, U., & Behr, J. (2005). Entorhinal cortex entrains epileptiform activity in CA1 in pilocarpine-treated rats. *Neurobiology of Disease , 19*, 451 – 460.

Wu, G. Y., Malinow, R., & Cline, H. T. (1996). Maturation of a central glutamatergic synapse. *Science , 274*, 972-976.

Xu, T. L., & Gong, N. (2010). Glycine and glycine receptor signaling in hippocampal neurons: Diversity; function and regulation. *Progress in Neurobiology , 4*, 349-61.

Zafra, F., Aragon, C., Olivares, L., Danbolt, N. C., Gimenez, C., & Storm-Mathisen, J. (1995). Glycine Transporters Are Differentially Expressed among CNS Cells. *J. Neuroscience , 15*, 3952-69.

Zhang, C. L., Dreier, J. P., & Heinemann, U. (1995). Paroxysmal epileptiform discharges in temporal lobe slices after prolonged exposure to low magnesium are resistant to clinically used anticonvulsants. *Epilepsy Research , 20*, 105-111.

Zhang, L. H., Gong, N., Fei, D., Xu, L., & Xu, T. L. (2008). Glycine uptake regulates hippocampal network activity via glycine receptor-mediated tonic inhibition. *Neuropharmacology , 33*, 701-11.

10 APPENDIX

10.1 qPCR standard and melting curve analysis

The following figures illustrate qPCR standard and melting curves analysis for each analysed gene (actin, GlyRα1, GlyRα2, GlyRα3, GlyRβ, GlyT1 and GlyT2). 5-fold serial dilutions of the cDNA net solution were used to create a standard curve for each gene. As explained in section 3.3, the Pfaffl relative quantification method requires the crossing point (CP) determination indicated by the red line in the Normalized fluorescence vs. Cycle plot. The standard curves (panels b) were created by plotting CP vs. the log concentration of cDNA (ng/µL). The parameters calculated using the standard curve are indicated in panels c. Slope value (m) is required in order to calculate the amplification efficiency [E= 10^(-1/slope)] for the Pfaffl relative quantification method and should be included in the [3.1; 3.7] interval. E(Corbett) is a parameter determined by the software which is a measure of the overall efficiency of the reaction and should be included in the [0.85; 1.10] interval. R^2 gives a measure of the fitting of the linear regression and the linearity of the PCR assay. The assessment of the reaction specificity was also evaluated by melting curve analysis, represented in panels d. The visualisation of one single peak in the Derivate (dF/dt) vs. Temperature plot indicates a specific amplification of the targeted gene – actin. All plots were created using Corbett software (Corbett Life Science).

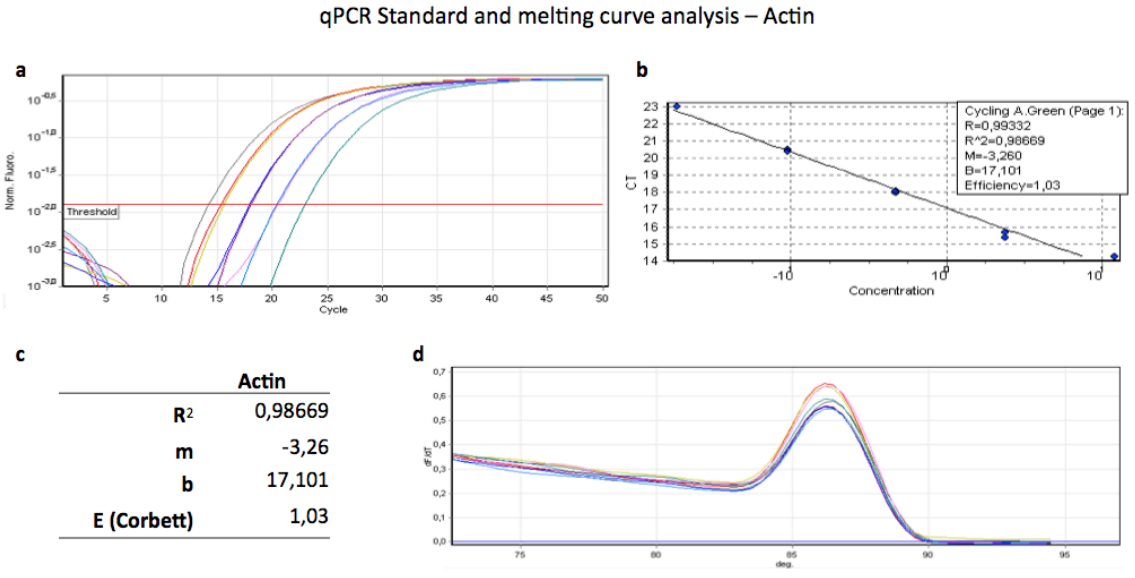

Figure 27 qPCR Standard and melting curves analysis for the actin gene - endogenous control. (a) PCR amplification plot for the actin gene. (b) Standard curve created by plotting CP vs. the log concentration of cDNA (ng/µL). (c) Parameters calculated using the standard curve. (d) Assessment of the reaction specificity by melting curve analysis. All plots were created using Corbett software (Corbett Life Science).

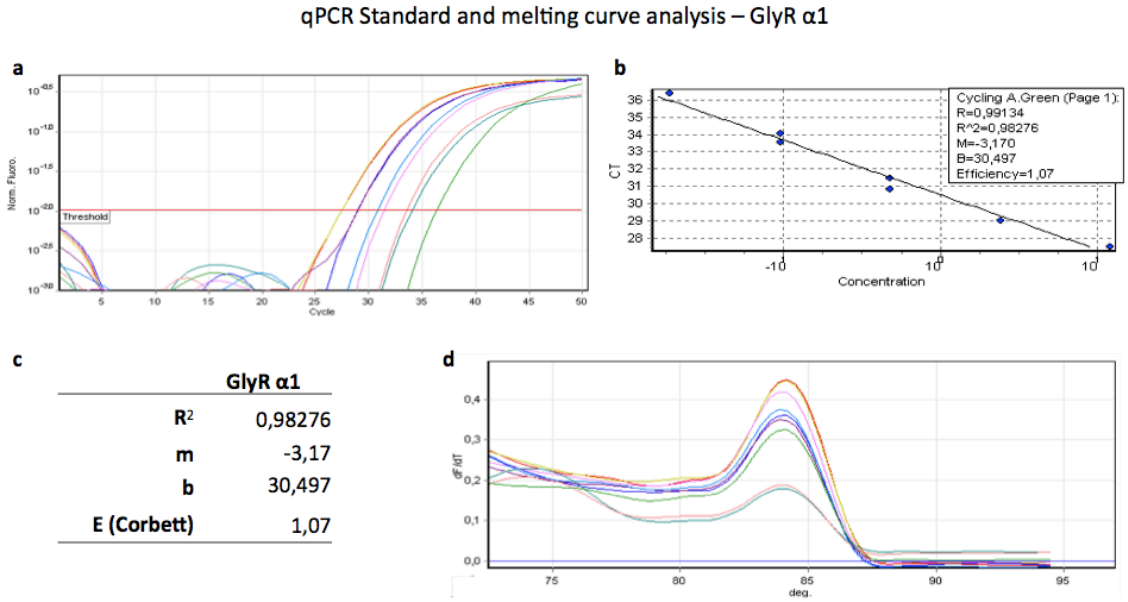

Figure 28 qPCR Standard and melting curves analysis for the glycine receptor subunit α1 (GlyR α1). (a) PCR amplification plot for the GlyR α1 gene. (b) Standard curve created by plotting CP vs. the log concentration of cDNA (ng/µL). (c) Parameters calculated using the standard curve. (d) Assessment of the reaction specificity by melting curve analysis. All plots were created using Corbett software (Corbett Life Science).

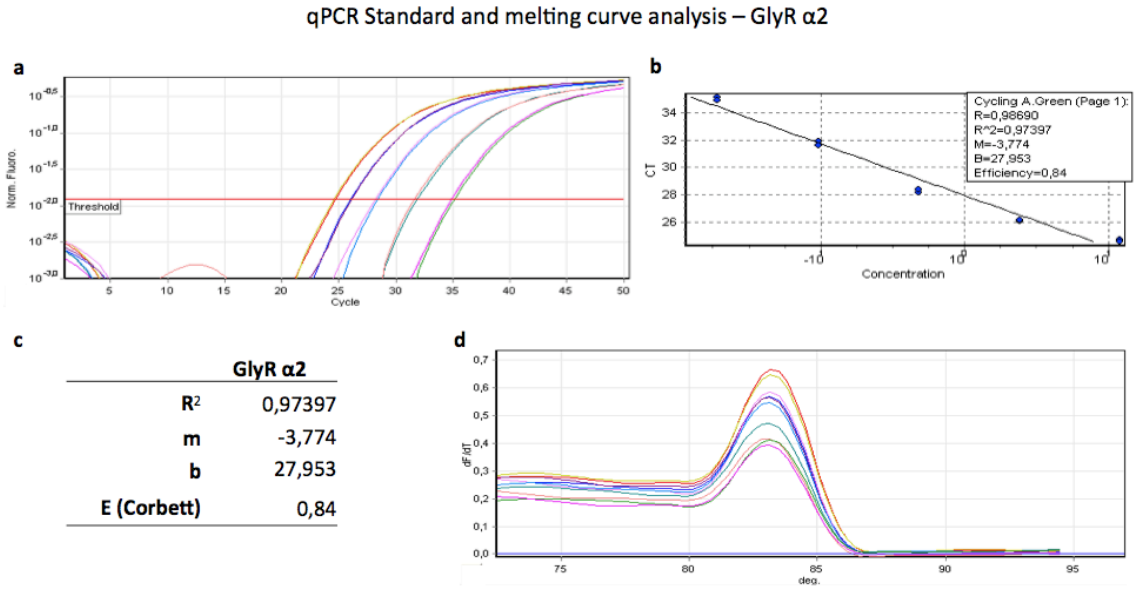

Figure 29 qPCR Standard and melting curves analysis for the glycine receptor subunit α2 (GlyR α2). (a) PCR amplification plot for the GlyR α2 gene. (b) Standard curve created by plotting CP vs. the log concentration of cDNA (ng/µL). (c) Parameters calculated using the standard curve. (d) Assessment of the reaction specificity by melting curve analysis. All plots were created using Corbett software (Corbett Life Science).

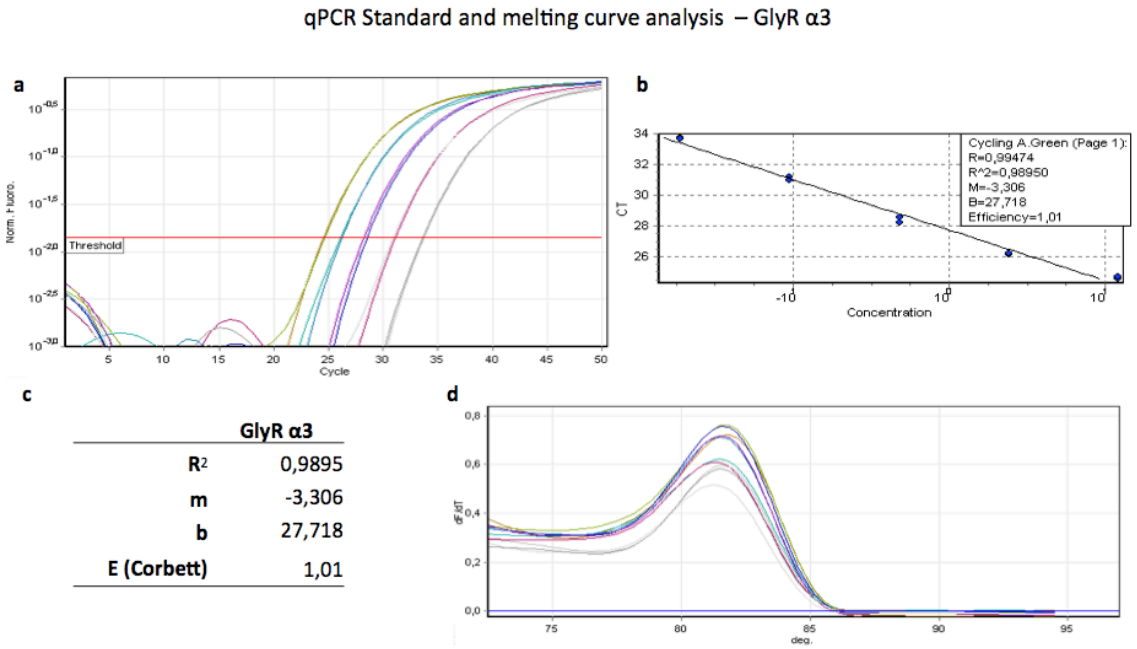

Figure 30 qPCR Standard and melting curves analysis for the glycine receptor subunit α3 (GlyR α3). (a) PCR amplification plot for the GlyR α3 gene. (b) Standard curve created by plotting CP vs. the log concentration of cDNA (ng/µL). (c) Parameters calculated using the standard curve. (d) Assessment of the reaction specificity by melting curve analysis. All plots were created using Corbett software (Corbett Life Science).

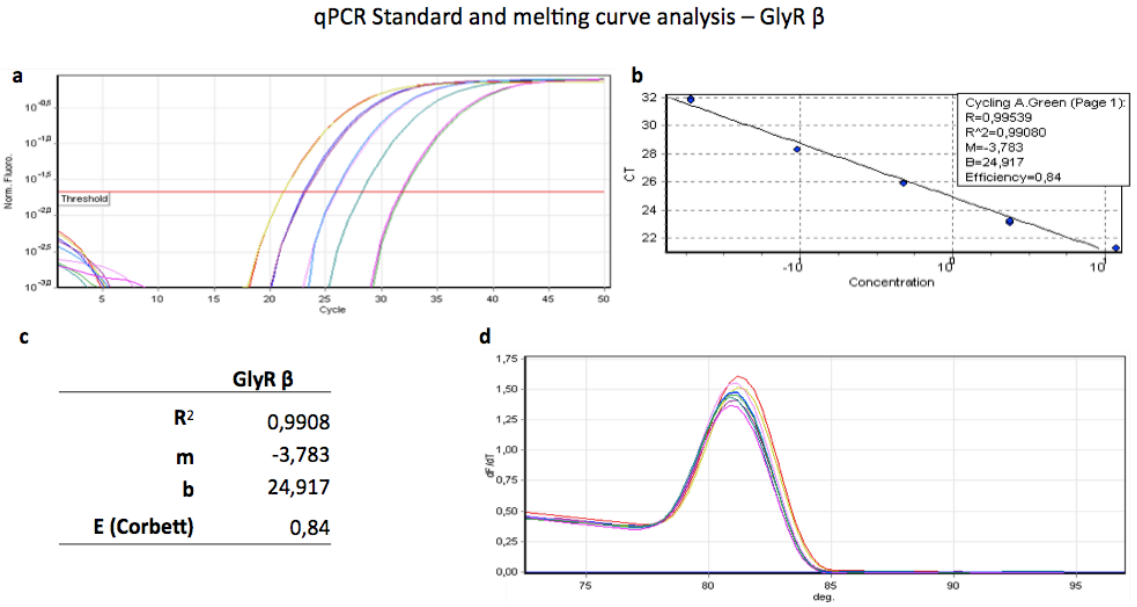

Figure 31 qPCR Standard and melting curves analysis for the glycine receptor subunit β (GlyR β). (a) PCR amplification plot for the GlyR β gene. (b) Standard curve created by plotting CP vs. the log concentration of cDNA (ng/µL). (c) Parameters calculated using the standard curve. (d) Assessment of the reaction specificity by melting curve analysis. All plots were created using Corbett software (Corbett Life Science).

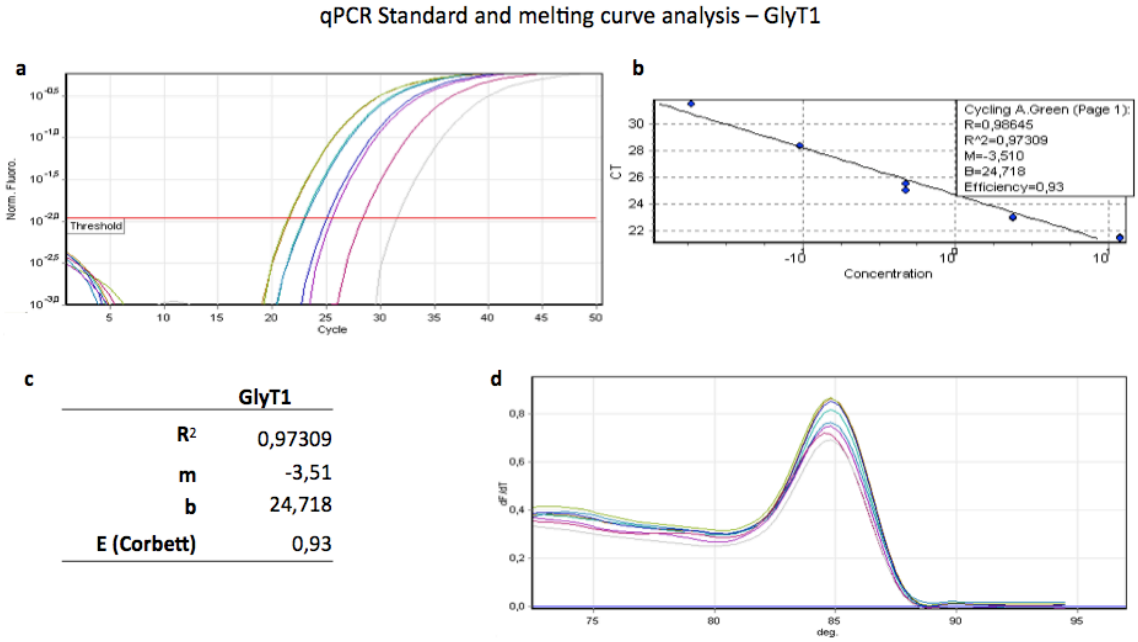

Figure 32 qPCR Standard and melting curves analysis for the glycine transporter 1 (GlyT1). (a) PCR amplification plot for the GlyT1 gene. (b) Standard curve created by plotting CP vs. the log concentration of cDNA (ng/µL). (c) Parameters calculated using the standard curve. (d) Assessment of the reaction specificity by melting curve analysis. All plots were created using Corbett software (Corbett Life Science).

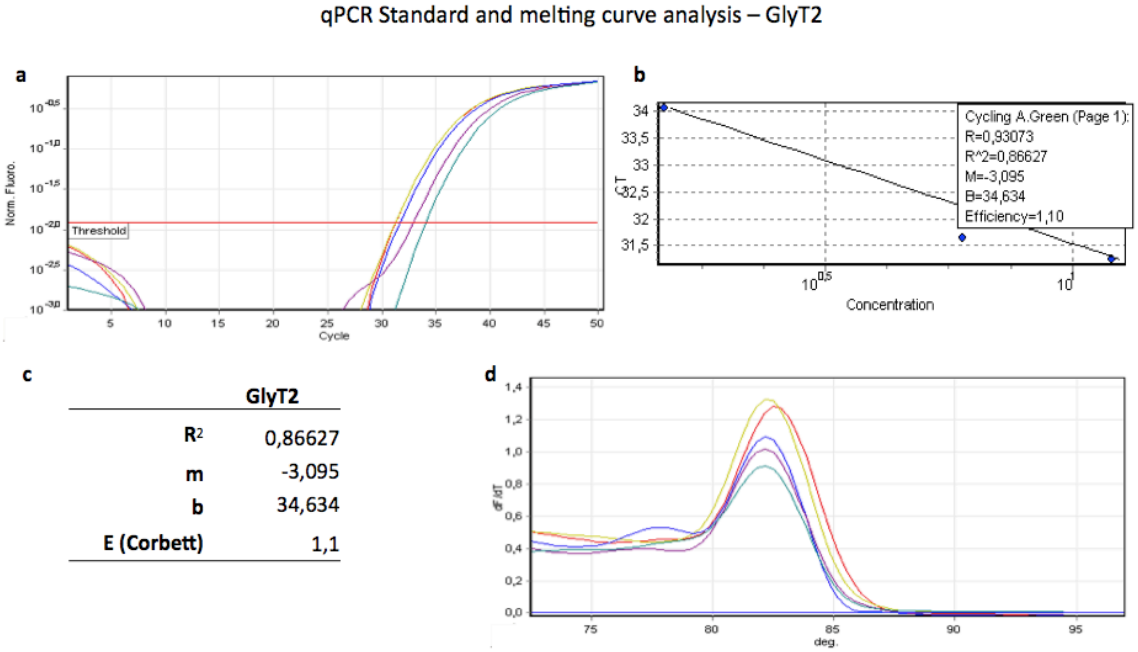

Figure 33 qPCR Standard and melting curves analysis for the glycine transporter 2 (GlyT2). (a) PCR amplification plot for the GlyT2 gene. (b) Standard curve created by plotting CP vs. the log concentration of cDNA (ng/µL). (c) Parameters calculated using the standard curve. (d) Assessment of the reaction specificity by melting curve analysis. All plots were created using Corbett software (Corbett Life Science).

10.2 Immunohistochemistry - Preliminary results

10.2.1 Immunohistochemistry protocol

Slices were washed with Phosphate Buffer Saline (PBS) (NaCl 137 mM, KCl 2.1 mM, KH_2PO_4 1.8 mM and $Na_2HPO_4.2H_2O$ 10 mM, at pH=7.40), and fixed with 4% paraformaldehyde (PFA) in PBS for 48h at 4°C. Afterward slices were dehydrated in 10% sucrose in PBS for 2 hours, followed by 20% sucrose in PBS for 2 hours and finally in 30% sucrose in PBS overnight (ON) at 4°C. Slices were then imbibed in Tissue Teck O.C.T. compound (Sakura Finetek, Japan) and frozen at -80°C.

Cutting protocol was carried out at -20°C in a cryostat, slices were cut at 20 µm each and placed in microscope slides (25x75x1.0 mm, Super Frost plus, VWR, Leuven) kept at -20°C.

A water-repelling circle was drawn around each slice using Dako Pen (Palex Medical SA, Barcelona), a hydrophobic paint that provides a barrier to liquids making it possible to reduce the amount of reagents used.

Slices were then incubated three times for 10 min in PBS, followed by permeabilization step with 1% Triton X-100 in PBS for 10 min at room temperature.

After blocking (6% BSA in PBST for 1 hour) slices were incubated with the primary antibodies (GFAP 1:500; NeuN 1:100 in 10% FBS in PBST), 4°C for 48 hours.

Extensive washes were then performed in PBS containing 0.1% Tween 20 (PBST), in which Tween 20 interacts with the antibody and facilitate the removal of nonspecific antibody binding.

Slices were incubated for 4h at room temperature with a goat anti-mouse or anti-rabbit secondary antibody conjugated to the fluorescent label Alexa Fluor 568 (1:400) or 488 (1:200) (Invitrogen) in 10% FBS in PBST.

Following three washes in PBST, for 10 min each, nuclei were stained with Hoechst Trihydrochloride Trihydrate 33342 (Invitrogen, 1:100) and the sections were mounted in Mowiol (Sigma, St. Louis, MO, USA).

The images were acquired with a frame size of 1024 x 1024 pixels on an inverted confocal laser scanning microscope (Zeiss LSM 710; Carl Zeiss AG, Weimar, Germany) using a PlanApochromat 20x objective (Carl Zeiss AG).

Hoechst fluorescence was detected with a 405 nm diode laser (25 mW nominal output) and a BP 420–480 nm filter. Alexa Fluor 488 fluorescence was detected using the 488 nm line of an Argon laser (25 mW nominal output). Alexa Fluor 568 was detected using a 561 nm DPSS laser (15 mW nominal output). The pinhole aperture was adjusted in each channel to achieve the same optical slice thickness for all channels. A series of optical sections were taken through the tissue slide (z-stack), and combined to create a ultra-sharp composite image, through a maximum intensity algorithm.

10.2.2 Results and brief comment

Glial proliferation is prominent in the sclerotic human hippocampus. In animal studies, upregulation of of glial-fibrillary acidic protein expression, as well as glial-cell hypertrophy and proliferation was reported. Alterations in glial functions, such as potassium buffering, pH regulation, transmitter uptake, and growth-factor production could have powerful effects on circuit excitability, which influences seizure susceptibility and progressive features of epilepsy (Pitkänen and Sutula 2002). DG is one of the hippocampal areas that have been shown to suffer neuronal loss and gliosis (Briellmann, et al. 2002)

One practical issue influenced the choice of antibodies to be used in this protocol. GFAP has a very clear staining and its use is common practice in the laboratory. So along with nuclei staining (NeuN and Hoechst), it was considered an adequate option to optimize the immunohistochemistry protocol.

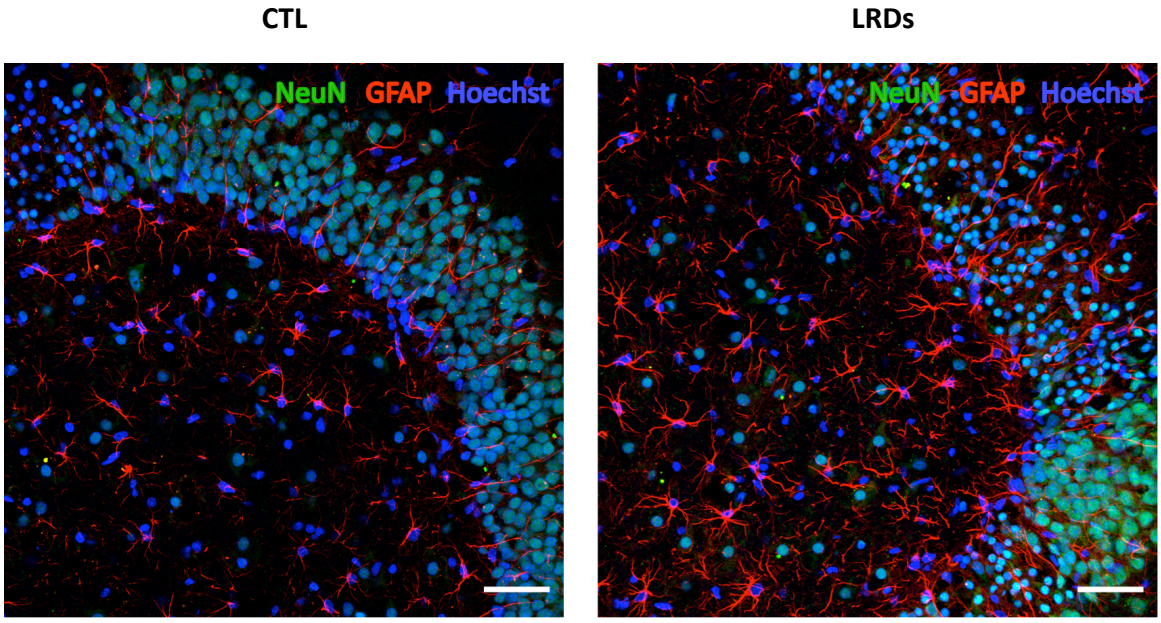

Figure 34 GFAP positive cells in hippocampus-entorhinal cortex combine slices. Triple detection astrocytic glial cells (GFAP 1:500), neuronal nuclei (NeuN 1:100) and nuclei (Hoechst 1:100) in rat hippocampus-entorhinal cortex combine slices in the denate gyrus region. Left image represents a control slice (CTL) while the image on the right displayed late recurrent discharges (LRDs). Confocal images were acquired with a 20X dry objective. Scale bars, 50 µm.

Although slices only underwent 3 to 4 hours of free Mg^{2+} ACSF exposure, epileptiform activity induction, even in acute conditions, seems (n=1) to trigger astrogliosis. It is rather striking the difference between control slices and slices displaying LRDs, both in astrocyte number and morphology.

This evidence correlates well with extensively reported astrocytic involvement in epilepsy pathophysiology.

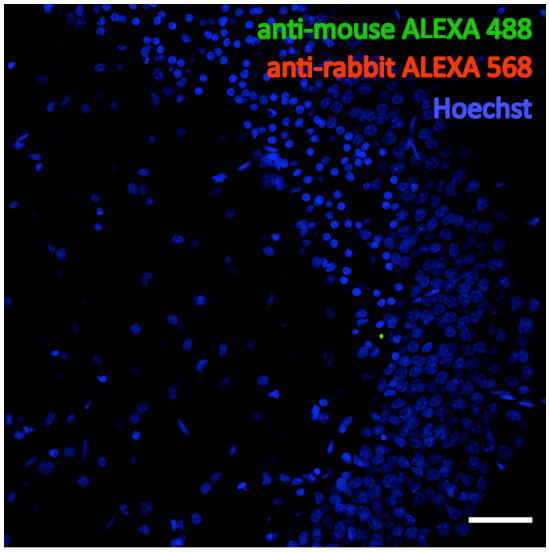

Figure 35 Negative control for immunohistochemistry in hippocampus-entorhinal cortex combine slices sections by confocal microscopy. No primary antibodies were added. The secondary fluorescent-labelled antibodies used were: goat anti-mouse-Alexa 488 (1:200) and goat anti-rabbit-Alexa 568 (1:400). Confocal images were acquired with a 20X dry objective. Scale bars, 50 µm.

This protocol will be particularly useful to evaluate the subcellular localization of other target markers, such as GlyR and $GABA_AR$ or even to evaluate neuronal death in slices recovered from the recording chamber.

The described immunohistochemistry protocol will also be applicable to other models, namely in organotypic slice cultures, which allow the evaluation of long-term effects.